UNIVERSITY OF ZULULAND

THE FLOW AND SEDIMENT DYNAMICS OF THE MLALAZI ESTUARY IN KWA-ZULU NATAL, SOUTH AFRICA

By: LV MMAKO

Student number: 200959289

November 2021

FINAL DISSERTATION

For the degree of MASTER OF SCIENCE

In the field of HYDROLOGY

With the title:

THE FLOW AND SEDIMENT DYNAMICS OF THE MLALAZI ESTUARY IN KWA-ZULU NATAL, SOUTH AFRICA

FACULTY OF SCIENCE AND AGRICULTURE

Candidate: LV MMAKO

Student number: 200959289

Supervisor

Prof B E Kelbe

Co-supervisors

Mr. B K Rawlins and Prof J J Simonis

November 2021

DECLARATION

I declare that **The flow and sediment dynamics of the Mlalazi Estuary in KwaZulu Natal of South Africa** is entirely my own work and that all the work of others or quoted have been indicated and acknowledged through a complete referencing and that I have not previously in its entirety or in part submitted it for obtaining any qualification.

Full names:		
Signed:	*Lesiba Vincent Mmako*	***Date: dd/mm/yyyy***
Signature:		*15/11/2021*

ACKNOWLEDGEMENTS

I would like to thank and give credit to the following personnel(s) who have played an important role in this master research project:

- Prof B.E. Kelbe for mentoring and providing the technical support. Prof Kelbe contributed heavily to this project by creating the Digital Elevation Model (DEM) for the estuary and floodplains, providing important references that contain historical data and assisted in setting up the hydraulic model.
- Mr B.K. Rawlins for providing the administration support and supervising this thesis.
- Prof J.J. Simonis for providing the administration and technical support.
- Mr K.J. Rasifudi for providing the flow and sediment data from the Mlalazi River using the Catchment (HEC –HMS) model(s).
- Dr R.H. Taylor and Mr S. Bachoo for providing the bathymetric data along the estuary channels using the Differential Global Positioning System (DGPS).
- Mr F. le Roux and the DWS survey team for providing the bathymetric data from the mouth until the Railway Bridge, using the ADP method.
- The Department of Water and Sanitation (DWS) for giving access to tidal data at W1T001 located at the mouth on the Mlalazi Estuary.
- Ezemvelo KZN Wildlife for providing access to water level logger measurement at the railway bridge.
- The Hydrological Research Unit (HRU) for installing the water level monitoring sites in the estuary.
- The Water Research Commission (WRC) for contributing financially and the DWS bursary unit for providing the logistic arrangements to the University of Zululand.
- My supervisor and mentor at work, Ms Z.T. Peteni-Kave, for giving me much needed technical advice and support. She also made sure that a road-worthy state vehicle was available for me to travel from Pretoria to the university and accommodation provided on my arrival.
- Lastly, my family for providing social support throughout this project, and almighty God for giving me strength to continue to push ahead.

ABSTRACT

The catchments and estuaries are fragile systems that are prone to serious degradation from many different anthropogenic impacts (e.g. flow abstraction/diversion, sand mining, soil erosion etc.). In South Africa, many of the anthropogenic impacts on estuarine systems are generally derived from subjective expert opinions that are not supported by hydrodynamic data (Rasifudi, 2019). River flow is one of the main factor that control the dynamics of many estuaries worldwide (Zhou *et al.*, 2014). It is important to understand the water flow depth, direction and velocity in estuaries since they affect and control the erosion, transport and deposition processes of alluvial sediment and nutrients.

The Mlalazi Estuary is one of the best conserved estuaries situated along the eastern shoreline of the Kwa-Zulu Natal Province of the Republic of South Africa (RSA). This Estuary is classified as a Temporarily Open/Closed Estuary (TOCE). There is limited observe hydrological data that can be use to improve the decision making process within the Mlalazi Estuary in future. Therefore, a numerical model is useful tool to derive best estimates of flow dynamics and sediment transport.

This study investigated the flow dynamics associated with fluvial events within the Mlalazi Estuary resulting from Q_{2yr}, Q_{10yr}, Q_{20yr}, Q_{50yr} and Q_{100yr} flood return periods. The hydraulic modelling software, HEC-RAS (version 5.0) flow model, aided by GIS (HEC-geoRAS), was used to obtain estimates of the flow velocity and water level (depth) within the Mlalazi Estuary and floodplain.

Available geometric data (DEM + bathymetry) was used to generate 174 river cross-section profiles at different interval spaces ranging from 60m to 200m along the Mlalazi Estuary. The Mlalazi run-off data simulated from the hydrologic model HEC-HMS (Rasifudi, 2019) was used as an upstream boundary condition. The model was calibrated and validated using the historical data from the 1987 flood survey and continuous water level data from monitoring sites established in 2015 by the Hydrological Research Unit of the University of Zululand. The hydraulic model gave satisfactory performance statistics for high flood events during calibration and validation periods. The model overestimated the Q_{2yr} stage and velocity event

in the upper estuary channel and underestimated the stage and velocity in the lower estuary channel. The simulated velocity and Hjulström-Sundborg diagram were used to analyse the fluvial sediments distribution in the estuary channel and floodplains. The inundation maps of different storm sizes revealed that erosion occurs mainly in the active estuary channel and deposition of alluvial sediment takes place on the floodplains.

The study concluded that a physically based, numerical flow model is best method for providing reliable estimates for hydrodynamic data and information in estuaries with limited observed data like the Mlalazi Estuary. The study will also provide essential flow information needed to set up the Mlalazi Mouth Model, which will help to determine the 'flow reserve' of the Mlalazi Estuary.

***Keywords*:** Hydrodynamics, Model calibration, Model validation, HEC-RAS and Mlalazi Estuary.

ABSTRAK

Die opvanggebiede en riviermondings is brose stelsels wat geneig is tot ernstige agteruitgang van verskillende antropogeniese impakte (bv. vloei-onttrekking/-afleiding, sandmynbou, gronderosie, ens.). In Suid-Afrika word baie van die antropogeniese impakte op riviermondingstelsels oor die algemeen afgelei van subjektiewe deskundige menings wat nie altyd deur die wetenskap ondersteun word nie (Rasifudi, 2019). Riviervloei is een van die hoof faktore wat die dinamika van baie riviermondings wêreldwyd beheer (Zhou et al., 2014). Dit is belangrik om die watervloeidiepte, rigting en snelheid in riviermondings te verstaan, aangesien dit die erosie, vervoer en afsettingsprosesse van alluviale sediment en voedingstowwe beïnvloed en beheer.

Die Mlalazi-riviermond is een van die bes bewaarde riviermondings wat langs die oostelike kuslyn van die Kwa-Zulu Natal Provinsie van die Republiek van Suid-Africa (RSA) geleë is. Hierdie riviermond word geklassifiseer as 'n tydelik oop/geslote riviermonding (TOCE). Daar is beperkte waargenome hidrologiese data wat gebruik kan word om die besluitnemingsproses in die Mlalazi-riviermond in die toekoms te verbeter. Daarom is 'n numeriese model 'n nuttige hulpmiddel om die beste skattings van vloeidinamika en sedimentvervoer af te lei.

Hierdie studie het die vloeidinamika ondersoek wat geassosieer word met fluviale gebeure binne die Mlalazi-riviermond wat voortspruit uit Q_{2jr}, Q_{10jr}, Q_{20jr}, Q_{50jr} en Q_{100jr} vloed-terugkeerperiodes. Die hidrouliese modelleringsagteware, HEC-RAS (weergawe 5.0) vloeimodel, aangehelp deur GIS (HEC-geoRAS), is gebruik om ramings van die vloeisnelheid en watervlak (diepte) binne die Mlalazi-riviermond en vloedvlakte te verkry.

Beskikbare geometriese data (DEM + batimetrie) is gebruik om 174 rivier-dwarssnitprofiele te genereer by verskillende intervalruimtes wat wissel van 60m tot 200m langs die Mlalazi-riviermond. Die Mlalazi-afloopdata gesimuleer vanaf die hidrologiese model HEC-HMS (Rasifudi, 2019) is as 'n stroomop-grenstoestand gebruik. Die model is gekalibreer en bekragtig deur gebruik te maak van die historiese data van die 1987-vloedopname en deurlopende watervlakdata van moniteringsterreine wat in 2015 deur die Hidrologiese Navorsingseenheid

van die Universitiet van Zululand ingestel is. Die hidrouliese model het bevredigende waardes vir hoë vloedgebeure tydens kalibrasie- en valideringsperiodes gegee. Die model het die Q_{2jr} stadium en snelheidsgebeurtenis in die boonste riviermondkanaal oorskat en die stadium en snelheid in die onderste riviermondkanaal onderskat. Die gesimuleerde snelheid en Hjulström-Sundborg-diagram is gebruik om die fluviale sedimentverspreiding in die riviermondkanaal en vloedvlaktes te ontleed. Die oorstromingskaarte van verskillende stormgroottes het aan die lig gebring dat erosie hoofsaaklik in die aktiewe riviermondingskanaal voorkom en afsetting van alluviale sediment vind op die vloedvlaktes plaas.

Die studie het tot die gevolgtrekking gekom dat 'n fisies-gebaseerde, numeriese vloei model die beste metode is om betroubare skattings vir hidrodinamiese data en inligting in riviermondings met beperkte waargenome data soos die Mlalazi Estuarium te verskaf. Hierdie studie het ook 'n koppeling met die studie van die Mlalazi Mond Model toegelaat wat die statistiese model en Reserwe bepaling studie vir Mlalazi Estuarium gebruik.

Sleutelwoorde: Hidrodinamika, Modelkalibrasie, Modelvalidering, HEC-RAS en Mlalazi-riviermonding

TABLE OF CONTENTS

TABLES

FIGURES

PHOTOGRAPHS

ABBREVIATION AND ACRONYMS

Table I: Abbreviations and acronyms used in the report.

ADP	Acoustic Doppler Profiler
DEM	Digital Elevation Model
DGPS	Differential Global Positioning System
DWS	Department of Water and Sanitation
EPA	Environmental Protection Agency
HEC-DSS	Hydrologic Engineering Center– Data Support System
HEC-HMS	Hydrologic Engineering Center – Hydrologic Modelling System
HEC-RAS	Hydrologic Engineering Center – River Analysis System
HRU	Hydrological Research Unit
GIS	Geographical Information System
MAR	Mean Annual Run-off
m and mm	metres and millimetre
m/s and mm/s	meter per second and millimetre per second
Mm^3	Million cubic metres
Mm^3/a	Million cubic metres per annum
mMSL	metres above Mean Sea Level
POE	Permanently Open Estuary
RMF	Regional Maximum Flood
SLA	Slope Area Method
TOCE	Temporarily Open/Closed Estuary
UNIZULU	University of Zululand
USACE	United State Army Corps of Engineers
USEPA	United State Environmental Protection Agency

Table II: Abbreviations and acronyms used in the report from HEC-RAS model.

E.G. Elev (m)	Energy Gradeline for a given WSEL
Vel Head (m)	Velocity Head
W.S. Elev (m)	Calculated water surface from energy equation
Crit W.S. (m)	Critical water surface elevation. Water surface corresponding to the minimum energy on the energy versus depth curve.
E.G. Slope (m/m)	Slope of the energy grade line at a cross-section.
Q Total (m^3/s)	Total flow in cross-section.
Top Width (m)	Top width of the wetted cross-section.
Vel Total (m/s)	Average velocity of flow in total cross-section.
Max Chl Dpth (m)	Maximum main channel depth.
Conv. Total (m^3/s)	Conveyance of total cross-section.
Length Wtd. (m)	Weighted length based on flow distribution, in left bank, channel, and right bank.
Min Ch El (m)	Minimum channel elevation.
Alpha	Alpha – energy weighting coefficient.
Frctn Loss (m)	Friction loss between two cross-sections.
C or E Loss (m)	Contraction or expansion loss between two cross-sections.

CHAPTER 1. INTRODUCTION

1.1 Background

The Mlalazi Estuary is one of the many estuaries situated along the eastern shoreline of South Africa (Turpie *et al*., 2002). Whitfield (1998) classified this estuary as a Temporarily Open/Closed Estuary (TOCE) since the mouth closes annually about 4% of the time (DWS, 2015). The dynamics of estuary mouths is normally controlled by river flow, wave processes and as well as the tidal processes that function independently but work together to control the mouth of the estuary (McNally and Mehta, 2006; Zhou *et al.*, 2014). The Mlalazi Estuary is fed by the Mlalazi River Catchment which has an average run-off and sediment load of 276 Mm^3/a and 74035 tons per annum respectively (Rasifudi, 2019).

The Mlalazi Estuary is one of the best conserved (80% under natural condition) estuaries in KwaZulu Natal (DWS, 2015). There are signs within the estuary that show that the flow levels are dropping which will affect or reduce the tidal prism (Beck *et al.,* 2004). This could change the dynamics of the estuary mouth which could result in more frequent and longer mouth closures. The macrophyte growth will be altered and without artificial breaching of the estuary, may result in the death of all the mangroves (*Avicennia officinalis*) which are the most important adaptive ecological feature of the system because they require a mouth that is open virtually all the time (Kelbe *et al*., 2019). Flooding is likely to occur in the low-lying area and nutrient loadings will be increased by agricultural run-off, discharged waste from aquaculture and sewerage works from the town of Mtunzini.

Many of the natural and anthropogenic impacts on estuarine systems in this region are generally assessed from subjective expert opinion due to the lack of reliable flow data (Rasifudi, 2019). The purpose of this research project was to develop an understanding of the hydrodynamics of the fluvial system propagating through the Mlalazi Estuary, which is one of the main drivers that controls the mouth dynamics. The DWS (2015) and Zungu (2017) studies emphasised the need for more robust and reliable estimates of the hydrodynamics of the Mlalazi Estuary system. Van Niekerk *et al.*, (2020) highlighted the importance for determining estuary flow requirements and water resource allocations where estuary type serves as an indicator of sensitivity to flow modification and declining quality. The direct flow measurements in the

estuary will require considerable equipment and hydraulics structures that are expensive and time consuming. As an alternative, an understanding of the estuary flow dynamics can be provided by using a detailed and calibrated numerical model (Bate *et al*., 2016).

The knowledge and data gained from such an investigation can be applied to other similar systems such as the Siyaya Estuary. This estuary is near the Mlalazi Estuary and has undergone a prolonged mouth closure due to changes in the fluvial and sediment states of the catchment caused by anthropogenic changes in land use (Kelbe *et al*., 2002). The information gained from these studies is also essential for determining the ecological reserve and support management of anthropogenic activities such as farming, municipal waste, disaster management and flood control activities by mapping the flood zone or high-risk area within the Mlalazi Estuary floodplain.

1.2 Motivation

Many catchments and estuaries are fragile systems that are prone to serious degradation from different anthropogenic impacts (Cooper, 2002). The type, extent and magnitude of these impacts depend on the type of estuary. Many of the impacts and classifications are based on physical, chemical and biological factors. These classifications can take the form of geological features, water and chemical circulation and biological characteristics (EPA, 2000). The basic geological classification, based on the underlying landform, categorises estuaries as drowned river valleys, lagoons, coastal lakes, inlets and river mouths. The chemical circulation approach classifies estuaries as salt wedges, partially mixed, well-mixed and deep Fjord type basins. EPA (2000) has described some estuaries based on their biological communities, such as planktonic, pelagic, benthic and intertidal.

Further classification (Whitfield *et al.,* 2007) has been based on the state of the estuary mouth conditions which regulate the level of tidal interaction between the estuary and marine environments (open, partially open, fully open) and their duration in these states (permanently open [POEs], temporary open [TOCEs]). This later classification includes estuary types that are related to land form and circulation. The main focus of this study is the Mlalazi Estuary that is classified as a TOCE (Whitfield *et al.,* 2007) which is generally restricted to inlet and river mouths with a partially mixed state.

The hydrodynamic processes that operate within an estuary are generally dominated by the interaction between fluvial and marine systems (Pittaluga *et al.,* 2014). These opposing systems are considered to operate independently, creating variable conditions within the estuary. In the TOCE estuaries, the interaction between the fluvial and marine systems creating a mixed circulation system will be fed by run-off from the upstream catchment. The run-off is temporarily stored within the channel and estuary floodplain before interacting with marine tides through a mouth that acts as a bi-directional hydraulic control structure. The regular temporal storage during flood and ebb tides will interact within the random fluvial events, creating the temporary water storage that will further control the water level fluctuations and distribution.

The interaction between the fluvial and marine system in TOCEs will be dependent on the state of the mouth since it acts as a downstream hydraulic control on both the marine tides and river run-off, as illustrated in Figure 1.1. The water storage capacity within the estuary and floodplain, as well as the state of the mouth, are both dependent on the sediment dynamics which are highly variable in time and position. The sediment dynamics at the mouth delta are controlled by the sediment deposition between flood and ebb tides and the opposing scours during large fluvial discharge from the estuary basin, together with the sediment mobility in the mouth basin (Hinwood and McLean, 2001; Kelbe *et al.,* 2019). The sediment dynamics have also been attributed to the sea state, such as storm surges (Taylor *per comm*). These interacting processes lead to a rapidly changing tidal basin at the mouth which continually alters the hydraulic control features of the marine-estuary tidal interactions.

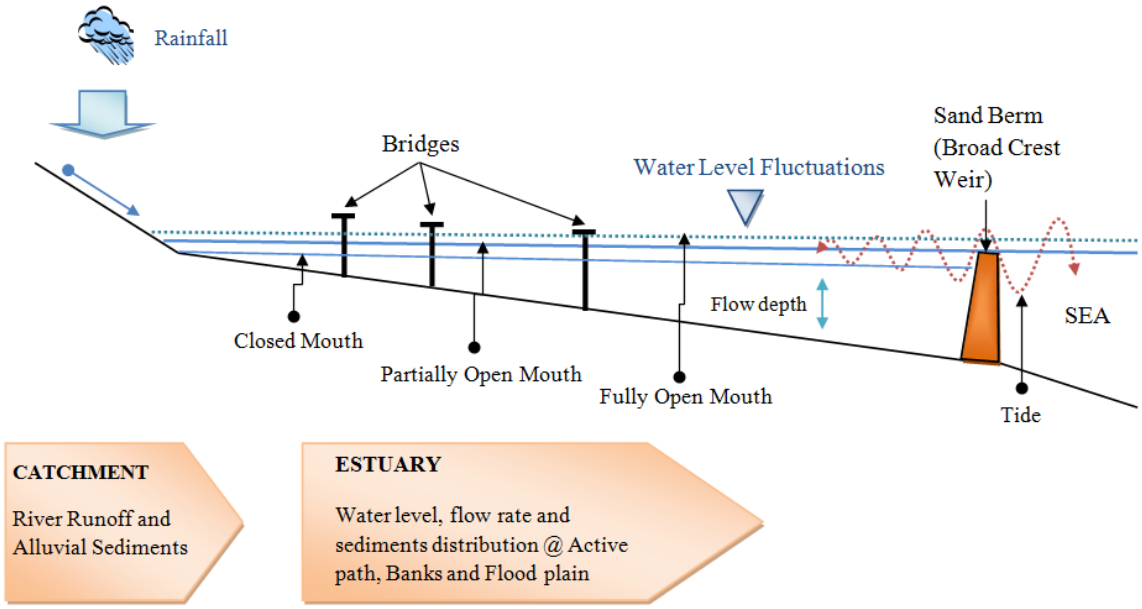

Figure 1.1: Conceptual illustration of the estuary profile of the main fluvial components controlling the hydrodynamic processes through a TOCE.

The marine tides are known or can be predicted with reasonable accuracy and have been provided by the Hydrographic Office of the SA Navy for Richards Bay. The catchment run-off and sediment yield from the Mlalazi Catchment have been simulated by Rasifudi (2019) for a 68-year period which includes drought periods and a range of extreme (1:100) storm events. However, the translation and attenuation of these fluvial events through the estuary are unknown and need to be determined to evaluate their interaction and impact on the estuary and mouth hydrodynamics. Consequently, this study has focussed on deriving the best estimate of the fluvial dynamics in the estuary under specific mouth conditions.

The available data does not provide sufficient information of the long-term fluvial dynamics in the estuary due to tidal interactions, or the extreme fluvial conditions, to determine the estuary response to catchment run-off and sediment yield. Without reliable data, there is a need to employ objective methods for deriving the relevant information. A common and pragmatic approach has been the adoption of suitably-developed numerical models that incorporate all the important flow dynamic features using the available information (Hinwood and McLean, 2001; Bate *et al.*, 2016). Deterministic numerical models have been developed and are available to provide reproducible, comparable and consistent information about the hydrodynamic conditions and to determine impacts of management interventions in the

estuarine system. Hydrodynamic numerical models have been used frequently to provide the best estimate of the data (Moriasi *et al.*, 2007). Models are considered the best pragmatic approach to estimate the required data (Rasifudi, 2019).

1.3 Aim of the Study

To derive estimates of the flow rate, water level (depth/stage) and sediment transport within the Mlalazi Estuary and floodplain that could influence the flow and sediment dynamics at the mouth. To achieve this aim, the following objectives have been set:

1.4 Specific Objectives

a) Identify the processes that control the flow and sediment transport in an estuary and develop a suitable conceptual model of their role and significance in the Mlalazi Estuary.

b) Identify and establish the relevant important features of the Mlalazi Estuary that will significantly affect the hydrodynamic processes.

c) Identify the available numerical hydrodynamic models and determine their suitability to provide the necessary variables on flow and sediment transport through the estuary and floodplain.

d) Identify the data availability and data requirements for the selected model in the study area.

e) Acquire and evaluate the data and setup the selected model code by populating the relevant variable and parameters.

f) Calibrate and validate the selected model.

g) Compute flow, stage and sediment transport time series in the estuary.

1.5 Research Question

How do the flow dynamics and sediment distribution and transport vary along the Mlalazi Estuary over hydrological seasons and during extreme hydrological events?

1.6 Research Hypothesis

A well-calibrated numerical estuarine model, derived from a suitable conceptual model, can accurately simulate the hydrodynamic and sediment transport information of fluvial system in the Mlalazi Estuary.

1.7 Thesis Organisation

This thesis is organised into seven chapters. The first chapter gives an introduction for the research study. The second chapter contains a literature review of estuarine or hydrodynamic models to enable the selection of a suitable model for the study. The third chapter provides an overview of the study area, including the available flow data. The fourth chapter provides the methodologies used in the model configuration. The fifth chapter evaluates the calibration and validation of the model. The model results are presented in the sixth chapter while the seventh chapter focuses on the conclusions and recommendations.

CHAPTER 2. LITERATURE REVIEW

2.1 Introduction

The variations in catchments characteristics, such as climate, land use, topography and underlying geology give rise to a wide variety of estuarine types (Whitefield and Bate , 2007). The estuaries in South Africa can be classified as permanently open estuaries (POEs) or temporarily open/closed estuaries (TOCEs) in terms of the hydrodynamic perspective (Whitefield and Bate , 2007). According to Whitfield and Bate , (2007), "about 25% of SA's two hundred and fifty estuaries are permanently connected to the sea and 75% are temporarily open to the marine environment". The state of the estuary mouth is an indication of the dominance of the competing fluvial and marine processes that tend to scour or deposit sediment.

The estuary mouth is conceived as a downstream hydraulic structure that will control the estuary dynamics. Consequently, the water level fluctuations in the estuary are a surrogate indicator of the mouth state under specific fluvial conditions (Kelbe *et al.,* 2019). To understand the linkages, it is necessary to establish the hydrodynamic response within the estuary to the changing fluvial conditions. The major forces that preserve open mouth conditions are significant run-off from the upstream catchment and the ebb tide, while the major forces that lead to mouth closure are flood tide sediment transport and wave energy (Van Niekerk, 2005).

In some medium to small estuaries (especially in the Western Cape), the mouth can remain steadily open throughout the year. This is due to the degree of mouth protection (e.g., rocky headlands or reefs in the surf-zone) and sub-tidal mouth protection on the continental shelf (rocky shelf running below the surface in the sea). The mouth protection or sub-tidal protection zones tends to dissipate the marine wave energy and turbulence actions. This decreases the ability of waves to transport sediment into the estuary outlet (Whitefield and Bate , 2007). Coastlines with sandy beaches and little or no rocky outcrops tend to have more frequent mouth closures due to the availability and movement of marine sediments.

The outflow velocity from the river or ebb tide flows plays a vital role in sustaining the estuary mouth in an open state by scouring the mouth basin sediments. Man made hydraulic structures (e.g., dams, weir) or natural bedforms (e.g., rapids, sand ripples) often contribute to estuary

mouth closure by inhibiting the river flows. The building of hydraulic structures across water course decreases the fluvial flow rate peaks and thus reduces the ability of the fluvial and ebb tide to transport sediments into the marine environment which were brought into the estuary basin during flood tide (Whitefield and Bate , 2007). The various factors that control or influence the flow and sediment dynamics of the temporarily open/closed estuaries (TOCEs) are described as follow:

a) **Catchment Size** – most permanent open estuaries (POEs) have a large drainage area (Orange River, etc.) with a significantly higher river discharge relative to the cross-sectional area of the mouth throughout the year. Conversely, most temporarily open/closed estuaries (TOCEs) have smaller drainage areas (Mlalazi, Amatikulu, Siyaya, Zinkwazi etc.), with lower river run-off relative to the cross-sectional area of the mouth (Whitfield, 1998). The higher flow rates from relatively large catchments through the mouth are most likely to sustain an open mouth due to greater sediment scouring and transport.

b) **Estuary size and tidal flow** – In large-sized estuaries (greater than 150 hectares (ha)), the ebb tide flow can preserve an open mouth condition once river inflow declines during dry season, with some notable exceptions such as Lake St Lucia. In medium-sized estuaries, which are less than 150 hectares (ha) in size, the tidal flow can retain an open mouth state during spring tides but often closes during neap tides during sustained drought periods. The estuarine lakes, on the other hand, can close due to various factors related to the longer duration of low flow during dry seasons, the high rate of evaporation, a high availability of sediment, and high wave energy (Whitfield and Bate , 2007). The small Mgobezeleni Estuary opens and closes on a semi-regular basis due to the persistent release from the highly buffered fluvial system of the controlling upstream lakes that lead to the regular breaching of the mouth sediment accumulations from marine deposition (Bate *et al.*, 2016).

c) **Sediment** – sediment availability and wave conditions determine the amount of river flows required to maintain the estuary mouth in an open state. Flow rates between 5 to 10 m^3s^{-1} are needed to transport sediment that will maintain a fully open mouth in Kwa-Zulu Natal (KZN) when sufficient sediment is available due to high energy beaches; while along the south-western Cape Coast, 1 to 2 m^3s^{-1} are required to sustain an open

state due to the degree of mouth protection when less sediment is available for the mouth basin (Huizinga *et al.*, 2005).

d) **Tidal variation and amplitude** – The average tidal range (which is the difference between sea levels at high and low tide) in TOCEs varies between 1.0 m during spring high tide and as little as 0.25 m at neap high tide. In POEs the average tidal amplitude varies between 1.0 m (spring tide) and 0.3 m (neap tide) during the high-flow period (Schumann *et al.*, 1999). The marine tidal exchange across the mouth creates a significant lag and attenuation of the estuary tidal range due to the dynamic controls of the mouth sediment characteristics (Kelbe and Taylor, 2016).

e) **Flow channels (ebb and flood tidal)** – the flood tide occurs when large volume of water enters the estuary from the marine state during tidal exchange, which tends to transport large quantity of the marine sediment into the estuary basin (Huizinga *et al.* 2005). The ebb tide has lower-flow velocity from upstream river run-off and the release of temporarily stored flood tide volumes. Tidal interaction between the ebb and flood channels (Figure 2.1) plays a critical role in maintaining the duration of open mouth states (Whitfield and Bate , 2007).

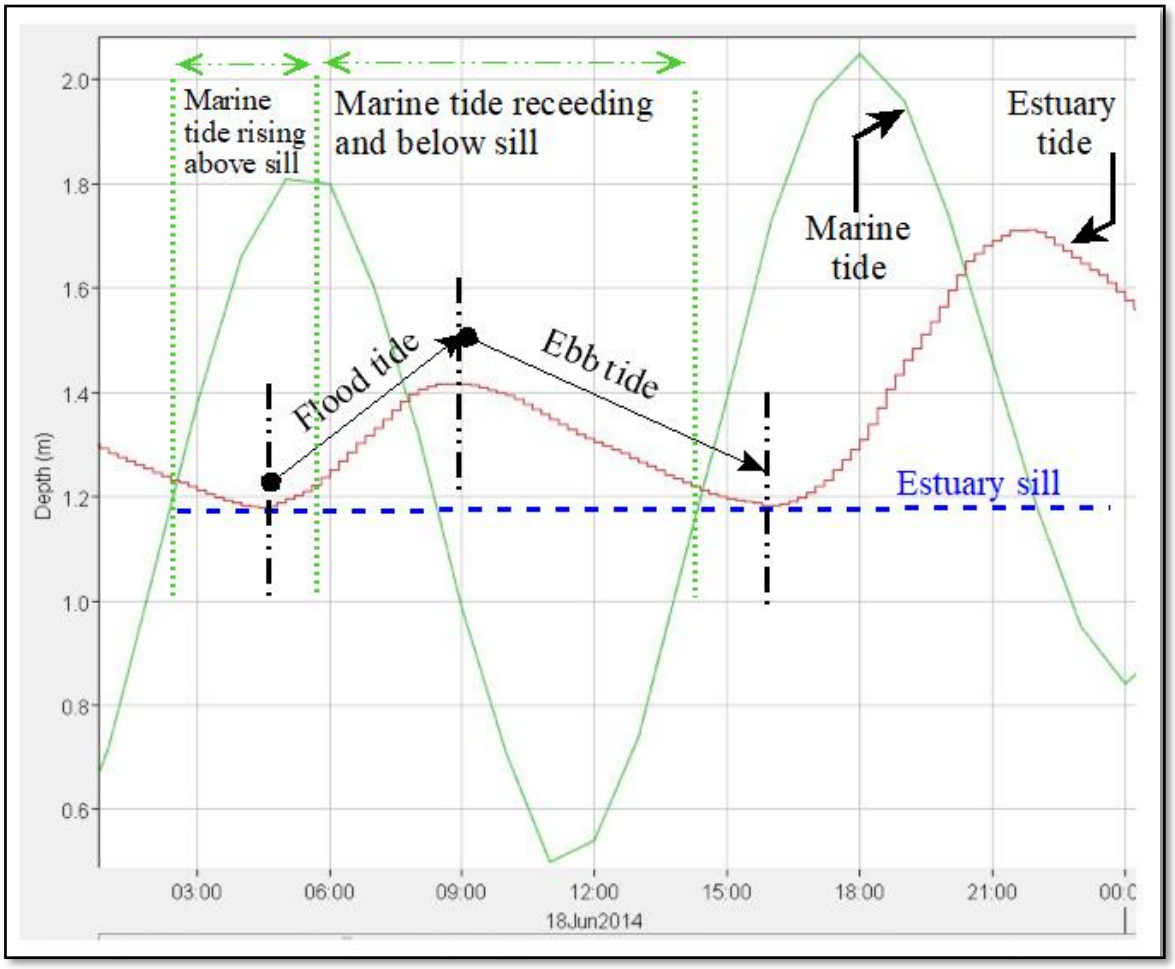

Figure 2.1: The simultaneous exchange of the estuary and marine tidal action for the Mlalazi Estuary (Kelbe *et al.*, 2019).

2.2 Conceptual Model

A conceptual model is a set of conditions that represent a system. Conceptual models will help to describe the main physical drivers and processes that are perceived to control the estuary dynamics needed to be incorporated into the deterministic numerical model to achieve a desirable outcome. In other words, the conceptual model provides the basis of the numerical model. The conceptual models of the flow and sediment dynamics of the Mlalazi Estuary were developed from literature (local & international publications), field measurement data (water level & tidal) and simulated flow/sediment data from the Mlalazi Catchment (Rasifudi *per comm*).

2.2.1 Description of the conceptual model of flow dynamics within Mlalazi Estuary

The water level fluctuations in the Mlalazi Estuary provide an indication of the storage and discharge of fluvial and tidal processes, as shown in the conceptual illustration in Figure 1.1. The sand bar, or berm, at the mouth, is perceived as a broad crest weir, and forms the downstream boundary condition since it is the significant element that controls the hydrodynamics behaviour (storage) of an estuary. The sand berm formed at the estuary mouth as the river inflow is inadequate to scour or transport the marine sediments that are brought in by flood tide and wave processes (Adams *et al.*, 2016). Further increases in the berm height will limit tidal interaction (rise and fall), eventually leading to the mouth closure.

During periods of mouth closure, flooding occurs in low-lying areas due to an increase in water level from river inflow. The only discharge through the mouth is via groundwater flow when there is sufficient fluvial head, and this would be on the marine side during low tides. The flow rate is significantly reduced and there is little deposition of sediment at the mouth basin; and the estuary continues to rise with increased storage of water from the limited run-off (Whitfield and Bate, 2007). The tidal interaction is completely prevented by the formation of the sand berm (broad crest weir) at the mouth inlet. Eventually, the storage of "fluvial" water in the estuary may increase until it is sufficiently high to cause the mouth to breach naturally.

The confluence between the Mlalazi River and its lower tributary, the KwaGugushe (Ntuze) River, form the upstream boundary condition since it is an entry point for bringing freshwater into the estuary. High and intense rainfall generates more run-off from the upstream catchment of the Mlalazi River. More river inflow will produce significantly higher flow rates with high energy to erode and transport fluvial sediments (fine, sand and gravel) into the upper estuary and possibly scour the marine sediment brought in by the flood tide.

The water level fluctuations within the Mlalazi Estuary can vary by as much as 7m above the mean sea level (MSL) during the rainy season (Figure 2.2) when extreme events occur. These fluctuations will vary along the length and across the breadth of the estuary and surrounding floodplain. The storm hydrograph undergoes lag and attenuation due to storage and release in various parts of the estuary and floodplain. Inundation of the floodplain will commence when the water level in the estuary channel overflows the banks with an elevation of between 2 - 2.5 mMSL (Kelbe *et al.*, 2019).

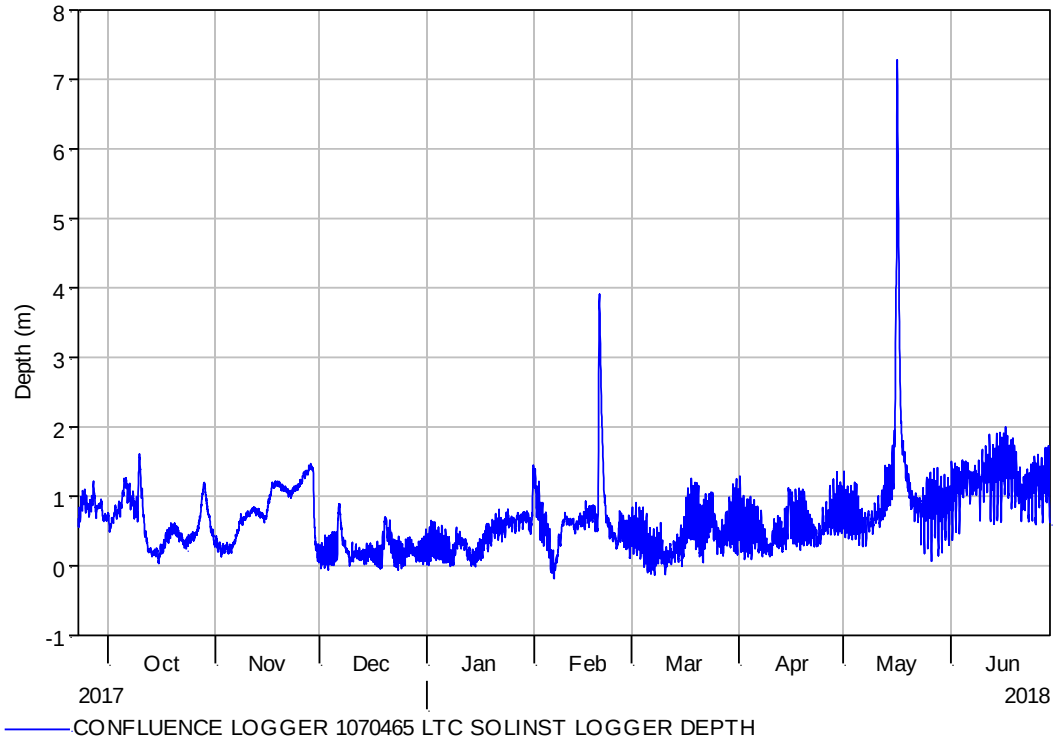

Figure 2.2: The water level fluctuation in the upper reaches of the Mlalazi Estuary showing the fluvial signals in response to a possible changing mouth state.

The estuary mouth becomes partially open when the river inflow is reduced- from high to medium due to a less intense rainfall within the Mlalazi Catchment. The main controlling hydrodynamic factors at this state are the tidal interaction (ebb & flood tides), the inflow river stage, and the height and width of the estuary mouth (Whitfield and Bate , 2007). As the flow rate reduces, the active channel depth becomes shallower. Tidal variation becomes restricted, and the sand berm begins to form. More saline water enters the estuary, especially during spring tides, and the flow velocities are reduced due to higher viscous water.

To derive a long-term assessment of the water level (storage) response within the estuary due to changing fluvial conditions, it was deemed necessary to establish a suitable hydrodynamic model of the estuary. The flood tide will move into the estuary and extend all the way up to the confluence, depending on the height (amplitude), slope and water level variation. The hydraulic structures such as road bridges and culverts play an important role in the estuary as they back flood or confine flow upstream during high flows with less influence on the downstream dynamics. The structures also dissipate the energy of the flood tides as it enters the estuary

causing wave attenuation and lag as it moves down the estuary toward the mouth (Figure 2.3). The sub-tropic dune forest bounded the lower estuary on either sides. Therefore, the fluvial flows and marine tides are forcefully channelled into this narrow section of the Estaury. During extreme storm events (2017 flood event), the water level in the upper estuary can reach a stage of almost 8m MSL, between 4 – 5 mMSL in the middle estuary and that will drop 2 – 3 mMSL at the lower estuary to mouth due to the hydrograph attenuation from flooding in various sections of the floodplain (Figure 2.4). Engelbrecht (2019) projected an increase in temperature (1.5 to 2 °C) for the period 2021 to 2050 over of the central interior and east coast of South Africa. This could lead to frequent tropical storms in the area that will cause significant floods in the Estaury. Despite the destruction of property and loss of life, these extreme flood events will be very benefitial to the Estaury ecologically by brining in fluvial sediment/nutrient and scouring marine sediments at the mouth.

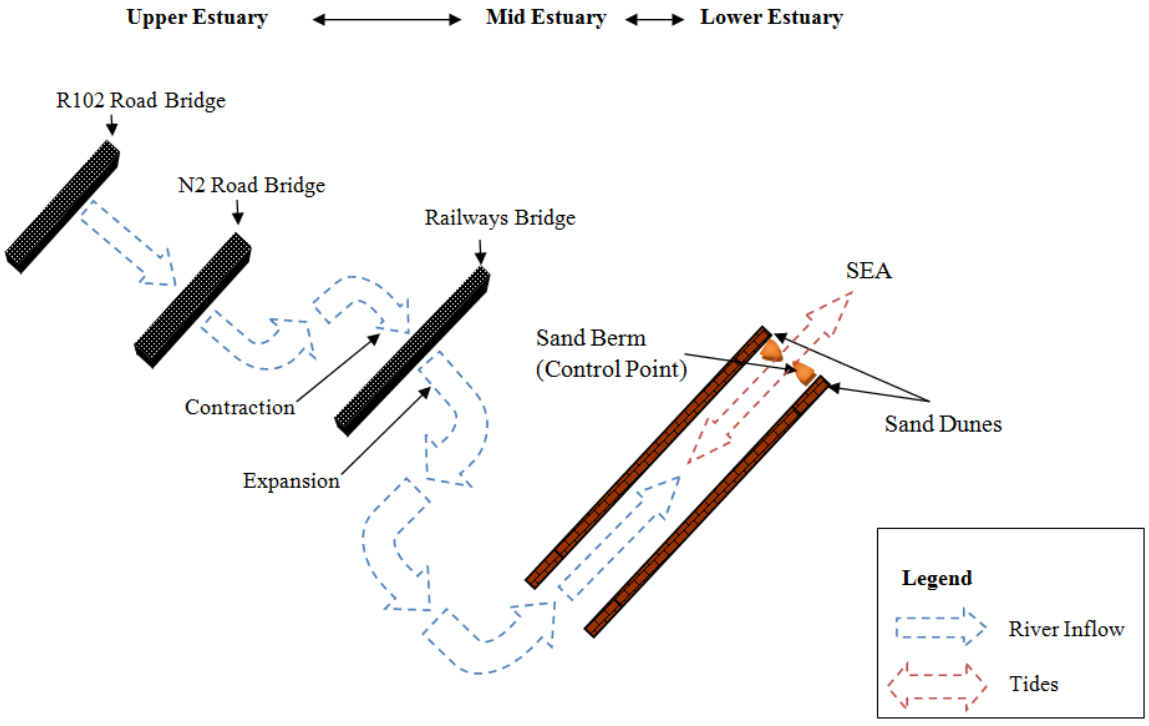

Figure 2.3: The conceptualised storage zones along the Mlalazi Estuary that will exhibit varying water level responses to the fluvial and tidal interactions (Whitfield and Bate, 2007).

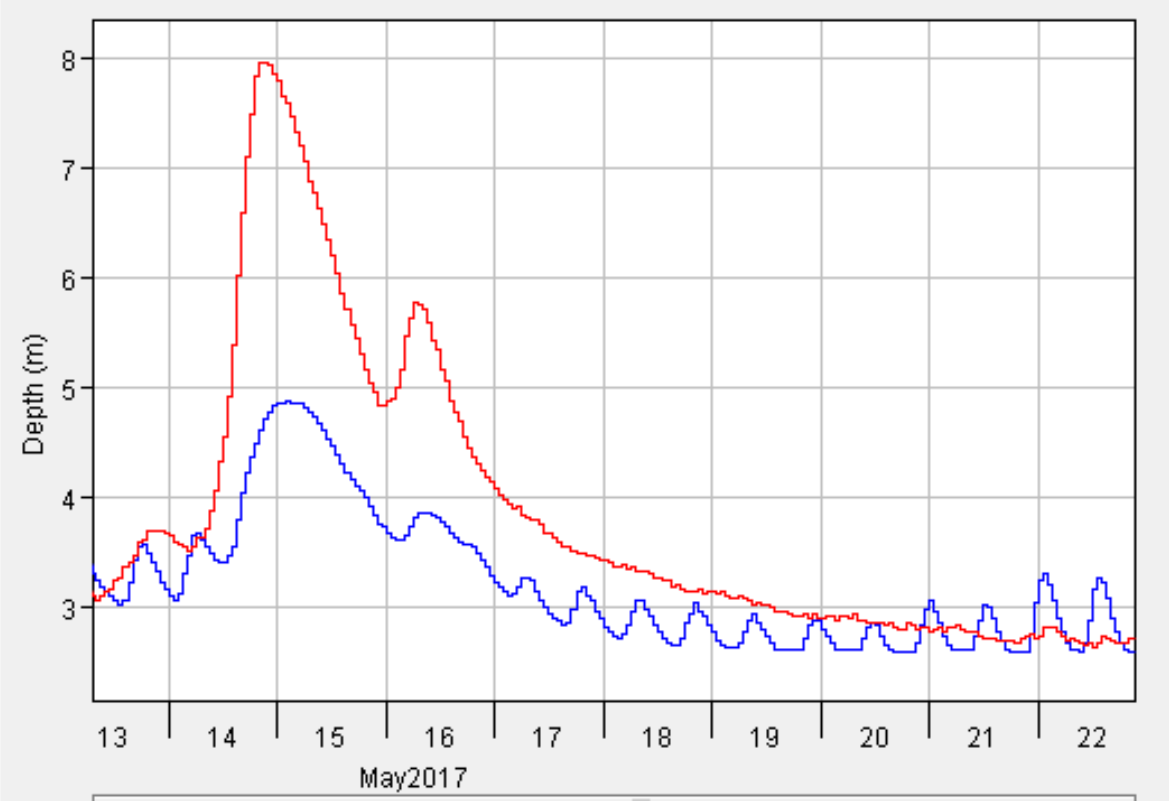

Figure 2.4: The measured flood hydrograph attenuation between the confluence (red line) of the river inflow and approximately 8km downstream (blue line) of the estuary.

2.2.2 Description of the conceptual model for sediment dynamics within the Mlalazi Estuary

The fluvial sediment deposition and transport within the upper estuary is directly proportional to the flow rate from the upstream river run-off and sediment production. The flow rate in open channels is not only influenced by the local terrain (slope or relief) to redistribute sediment downstream, but it is also by controlled water level and the channel geometry (Earle, 2015). The geometry of the stream channel affects the water flow velocity. It was observed by Steÿn (2006) that in straight channels the flow velocity at 60% depth (middle) is much higher than the velocity at the bottom, edges and near the surface. This is due to friction along the riverbed and air resistance forces on the surface. On a bend or curved channel, the stream velocity is higher on the outside of a bend and lower on the inside of a bend. More sediment deposition will take place on the inside of the river bend/curve and high erosion, which occurs outside the curve.

Figure 2.5 shows the conceptual model of the sediment dynamic during average horizontal flow processes within the Mlalazi Estuary. The alluvial silt deposition and erosion take place mostly at the river bends. For example, about 800m downstream of the N2 Road Bridge (B) there is an almost 90^0 bend on the right riverbank. Figure 2.6 illustrates the vertical flow profiles of the straight channel and curved channel (section A & B are shown in Figure 2.4), extracted from geometric data (DEM & bathymetry) of the Mlalazi Estuary. In the straight channel, the silt deposition will equally be distributed on the riverbanks. Whereas at the curved river channel the silt deposition will take place on left bank (-velocity) and erosion will be mostly on the right bank where flow velocity are much higher.

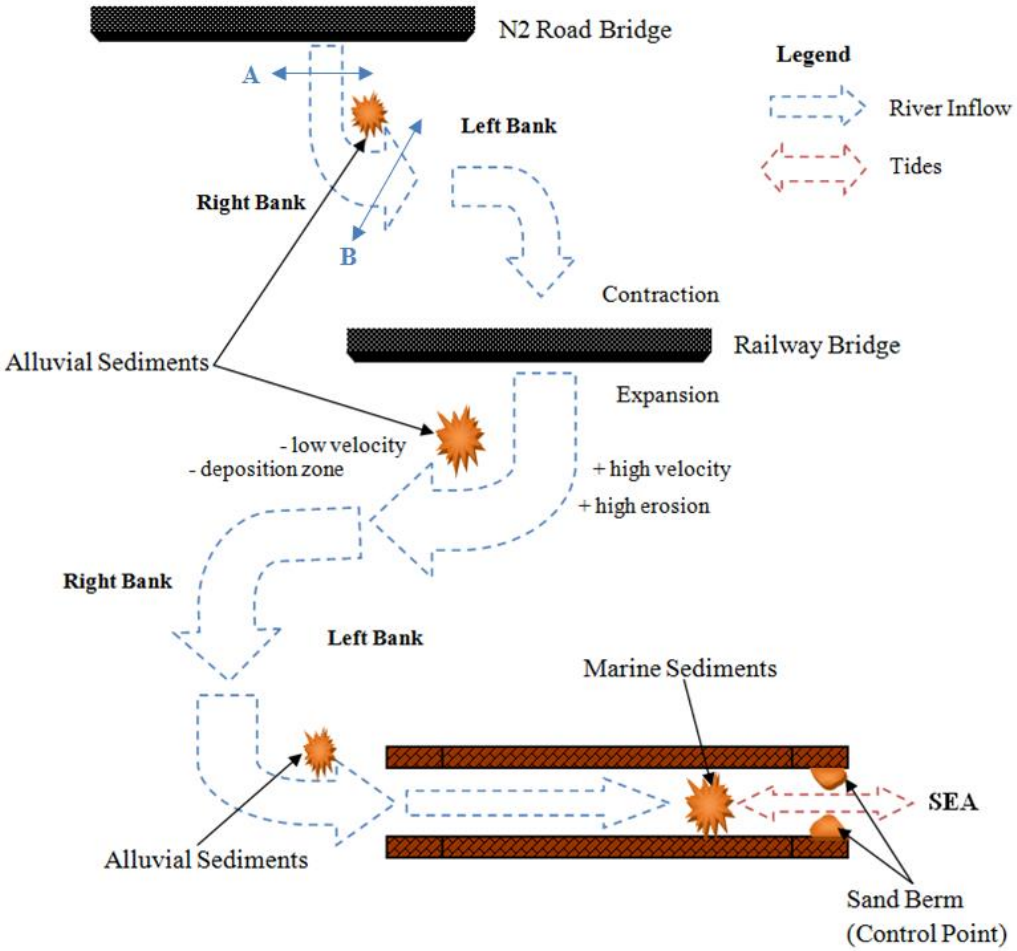

Figure 2.5: The conceptual model for the development of the sediment dynamic model in the Mlalazi Estuary (adapted from Webster *et al.,* 2003).

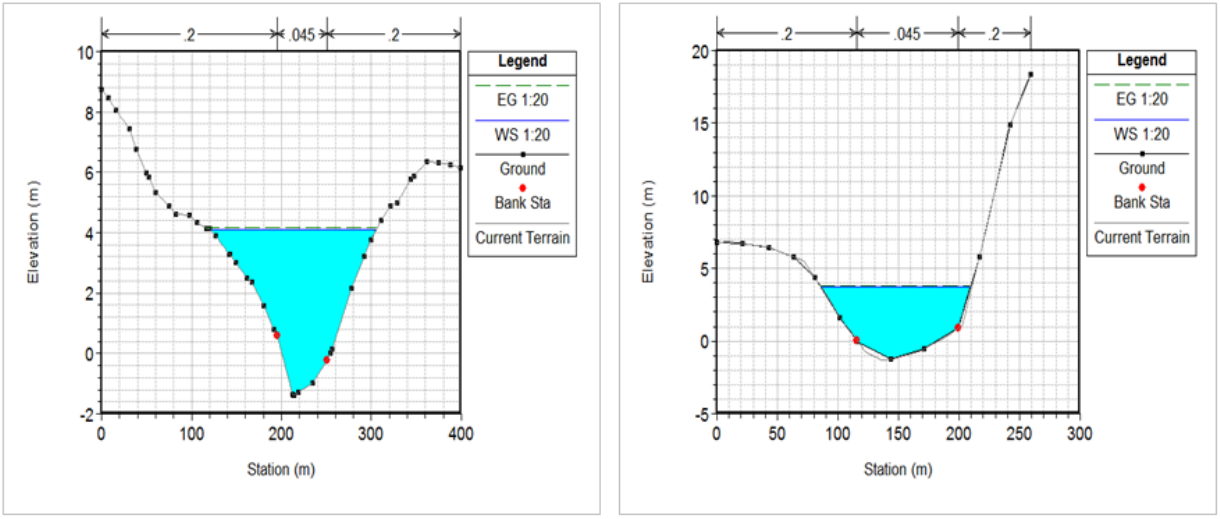

Figure 2.6: The straight stream channel (left) and bend/ curved stream channel (right) downstream of the N2 Road Bridge for flow depth of Q_{20yrs} flood event.

The floodplain is generally narrow upstream of the Railway Bridge, but expands into a very large area of flooding located just downstream of the Railway Bridge embankment.This area covers the low-lying swamps and sugar cane fields with numerous artificial drainage canals. The estuary floodplain creates a temporal storage during high flows. Thus, most of the fluvial sediments from the upstream catchment are transported and deposited on the floodplain where velocities are significantly lower. During low to medium flows within the estuary, the alluvial sediments accumulate around the pillars of the road/railway bridges and culverts (Badenhorst *et al.*, 1989). The non-cohesive (sand and gravel) sediments move on the riverbed of the active channel through the process of saltation and traction (rolling or dragging). The cohesive (silt/clay) sediments will be transported in suspension down to the lower estuary into the mouth and then it may be carried into the sea via suspension and scouring processes. The deposition of these sediments can change the storage properties of the estuary (channel and floodplain) and subsequently the hydrodynamics of the system. Alluvial silt deposition in the upper estuary accumulates over time and extends the banks into the main channel which then enhances the reed growth. As a result, this reduces the channel geometry and increases fluvial flow velocity.

The relationship between the flow velocity and its propensity to erode, transport and deposit sediment particles is best be explained by the Hjulström-Sundborg diagram (Figure 2.7). The

graph shows the flow velocity as the independent variable on the y-axis and particle size distribution as the dependent variable on the x-axis. Pidwirny (2006) described the thick red curve line as the "erosion velocity" - that is the velocity needed to erode and transport the sediment particles along the riverbed and banks. He also highlighted that the thickness of the red line indicates that the erosion particles are not only influenced by velocity but also by various other factors that vary from channel to channel. The blue curve line represents the "settling velocity" which illustrates the velocity for which particular grain sizes will fall out of transport and be deposited (Earle, 2015).

It can be observed from the graph that the clay and silt particles require higher flow velocities for erosion, compared to the larger sand particles. This is due to the strong cohesive bonds between clay and silt particles. Generally, a 0.01 mm silt particle needs a velocity of around 600 mm/s (0.6 m/s) to be eroded, whereas a 1 mm sand particle only requires 100 mm/s (0.1 m/s). But a 1.0 mm/s velocity is needed for 0.01 mm silt grain to remain in suspension. Similarly, a 1.0 mm sand grain will remain in suspension as long the velocity does not drop below 100 mm/s. For a 10 mm gravel particle, a velocity of 1100 mm/s (1.1 m/s) is required to be eroded but only 900 mm/s (0.9 m/s) to be transported along the riverbed. Consequently, the velocity profile along the estuary channel and floodplain are important factors in the identification of erosion and deposition areas.

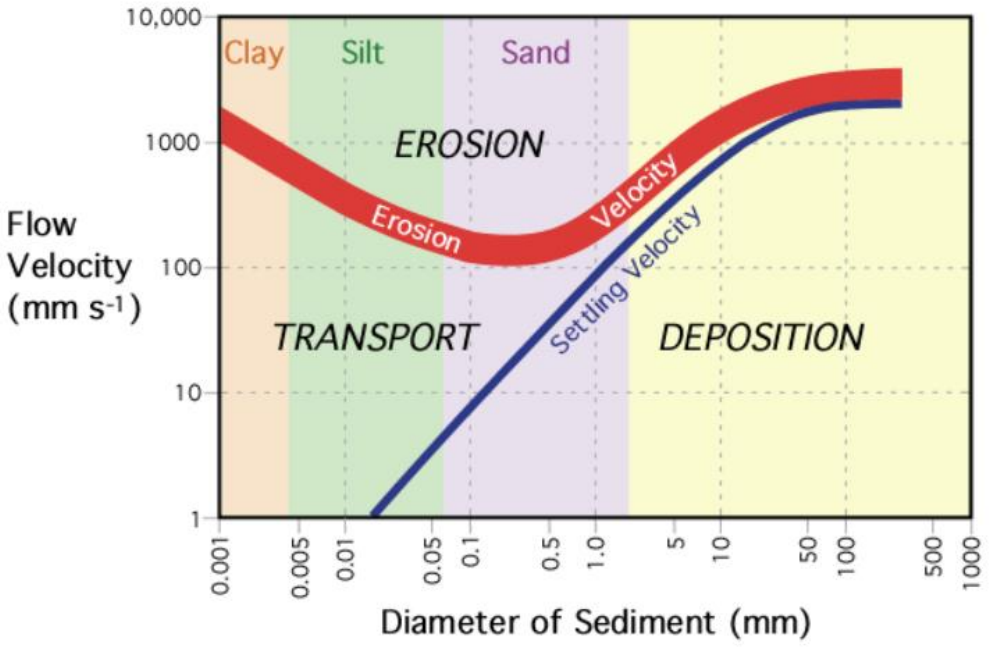

Figure 2.7: The Hjulström-Sundborg graph describes the relationship between flow velocity and grain size erosion, transport and deposition (Earle, 2015 and Pidwirny, 2006).

2.3 Estuarine Models

Mathematical techniques are frequently used to simulate the dynamics of rivers and estuaries for various reasons, ranging from system analysis, conceptual model evaluation and system predictions. There is a large range of models that have been developed, tested and applied throughout the world for the evaluation of estuaries. These models use various techniques to solve the controlling forces using 1, 2 and 3D techniques at varying time scales that require complex mathematical schemes to achieve stability and convergence of the forcing functions. These models involve varying degrees of complexity requiring a range of data and information which is not always available. Consequently, the choice of models involves a process of system review, resource requirements, model configuration, calibration and validation of the model results/predictions.

Most estuarine models use numerical or mathematical methods to predict or route the flow and sediments dynamic of the estuary. The models can implement a structured or unstructured grid. The structured grids (rectilinear or curvilinear) are based on a finite difference solution scheme while the unstructured grids (flexible mesh) are based on a finite volume solution scheme (Symonds *et al.*, 2016). These models can be classified in terms of their availability (open/commercial), degree of causality (complexity), skill/support requirements and data requirements. This study has been restricted to open source or freely available software and has not excluded all commercially available options. Similarly, the choice of model has also been limited to a one-dimensional system due to the scope of the project within the time constraints, available resources and data needs. The available hydrodynamic models are discussed in the next section as a prelude to the choice of model for this project.

2.3.1 Dynamic Estuary Model (DYNHYD5)

The Dynamic Estuary Model (DYNHYD5) is a simple link-node hydrodynamic program capable of simulating variable tidal cycles, wind and unsteady flows in open artificial/natural channels. The DYNHYD5 is the latest version of the modelling program. The United States

Environmental Protection Agency (USEPA) supports, publishes, services and maintains the modelling software through the WASP5 and WASP6 software programs (Soo *et al.,* 2018).

In order for the Dynamic Estuary Model (DYNHYD5) to accomplish suitable simulation studies, the model employs a channel-junction (link-node) network approach (Figure 2.8). The flow velocities and water levels are calculated at each time step, by solving the equation of continuity and momentum using a channel-junction "link-node" model network. This approach solves the "links" the equation of momentum and generates flow velocities, where at the "nodes" the equation of continuity is solved and calculates the flow levels. The assumptions are that the flow is primarily one-dimensional, constant, and that the wavelength is greater than the flow depth, the hydraulic bed slopes are moderate and the Coriolis Effect is negligible (Ambrose *et al*., 1993).

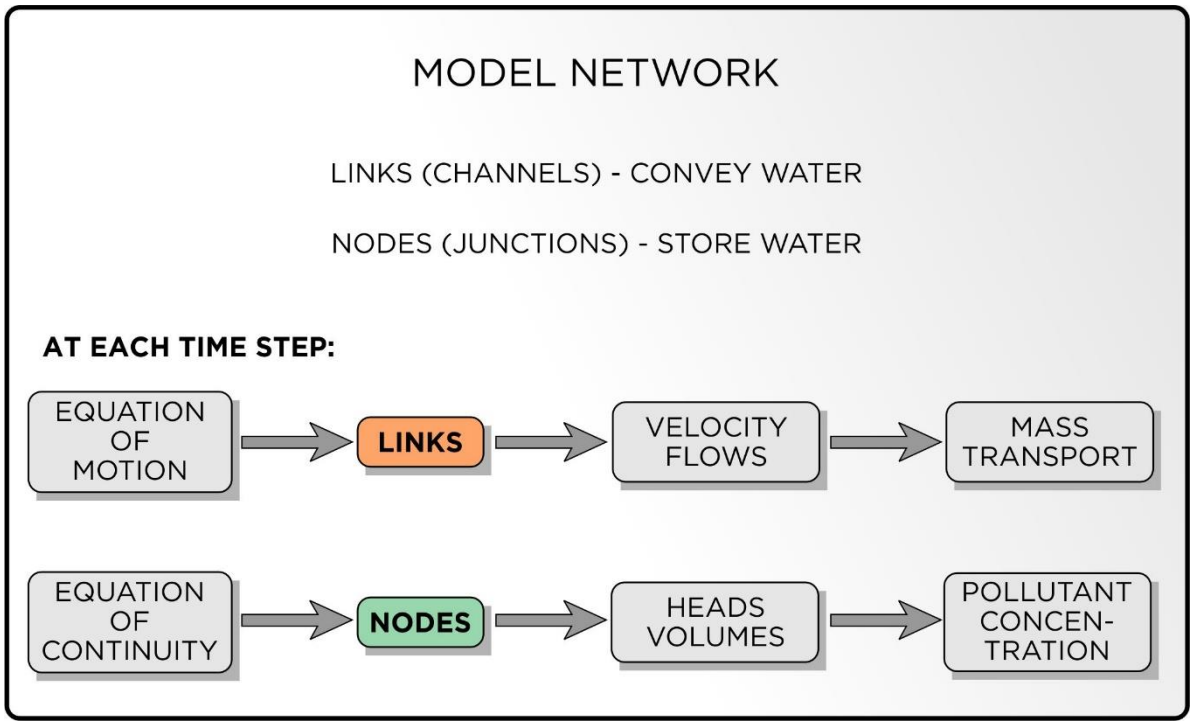

Figure 2.8: Model network processes by the DYNHYD5 model (Ambrose *et al.,* 1993).

2.3.2 ANUGA Hydrodynamic Model

ANUGA is a two-dimensional hydrodynamic model developed by the Australian National University and Geoscience Australia (ANUGA) to simulate natural hazards (e.g., stream flooding, storm surges and tsunamis). The computation procedure in ANUGA utilises the

finite-volume method to solve the Shallow Water Wave Equation. The modelled area is built by applying a mesh of triangular cells. The water level/depth and horizontal momentum (in x-y direction) values are obtained at each of the triangular elements by solving the main equations (Putra *et al*., 2016). A key advantage of the ANUGA model is that it can simulate the process of wetting and drying as flow enters and leaves the modelled area. The ANUGA model can accurately model the hydraulic jumps and waves due to the capability of the finite-volume method to accommodate discontinuities in the solution (Robert *et al.,* 2015). ANUGA also has the advantage of utilising rainfall data as a direct input or as a combination with the hydrographical data without inputs from a hydrologic model (Putra *et al*., 2016).

The ANUGA model is used by Wollongong City Council in Australia to validate the small development and major flood studies submitted by consultants. Van Drie *et al.,* (2016) study showed a comparison between the well-calibrated hydrologic model (Mike 11) and the ANUGA model applied in the Towradgi Creek Catchment. The ANUGA model was set up using local rainfall directly on the 2-Dimensional grid. The simulation showed an exceptional good fit with the observed water levels. In contrast with the same data, the Mike 11 model results showed a poor fit (overestimate) with the flow levels but correctly estimated the high peak. Van Drie *et al.,* (2016) concluded that the ANUGA model can be applied without the input from a hydrologic model. However, they strongly recommended the use of the hydrologic model to validate the ANUGA model setup.

2.3.3 Adaptive Hydraulics (AdH) Model

The Adaptive Hydraulics (AdH) Model is a program that can define both saturated and unsaturated groundwater, overland flow, 3-D Navier-Stokes, and 3-D Shallow Water problems, in addition to 2-D shallow water problems (Scott *et al*., 2012). The model was developed at the Coastal and Hydraulics Laboratory (CHL), prepared for the U.S. Army Corps of Engineers. The Adaptive Hydraulics (AdH) has the unique ability to dynamically refine the domain mesh in areas where more resolution is needed at certain times due to changes in the flow conditions (Berger *et al.,* 2010). The model can simulate sediment transport that is coupled to changes in flow dynamics and riverbed morphology.

The ability of the Adaptive Hydraulics (AdH) model to simulate wet and dry conditions under varying flow conditions or tidal change is suitable for shallow marsh environments, beach

slopes and floodplains. The AdH model is designed in such a manner that supercritical and subcritical flows can be represented at the model boundaries as well as internal to the system. It has the ability to simulate vessel transport as well as bridge decks and culvert entrances as pressure field applications. The model was planned to work in conjunction with the Surface Water Modeling System (SAM) and the Groundwater Modeling System (GMS). These systems are modelling packages for building models, running simulations and visualising results (Berger *et al.*, 2010).

2.3.4 MOHID Water Model

The MOHID Water model is an integrated numerical modelling software that can be used to simulate flows in surface water bodies (rivers, lakes, wetland, etc.), subsurface porous media flow and infiltration in catchments. The model is known as a "hydrodynamic model". Initially it was used to study estuaries and coastal areas employing the finite-differences method. The model was developed further to include a three-dimensional (3D) setup, baroclinic effects and full discretisation to a finite volume method (Leitão *et al*., 2008). These additional packages allow the MOHID model to simulate the flow in surface water bodies where the flow rate is lower than the speed of the pressure wave (Brito *et al*., 2016).

The MOHID hydrodynamic model was developed at the Marine and Environmental Technology Research Centre (MARETEC) at Instituto Superior Técnico (IST), which belongs to the Technical University of Lisbon in Portugal. The modelling system is built in such a way that the transport processes of momentum, mass and heat are simulated in the water column. Figure 2.9 shows a schematic of the model where the mass can be conveyed in the dissolved and particulate phases of both water and sediment columns. The transport processes of momentum, mass and heat processes in the water column are simulated using the Eulerian (fixed grid) and Lagrangian referential. The non-turbulent flow is modelled using the Navier-Stokes equations (Leitão *et al*., 2008).

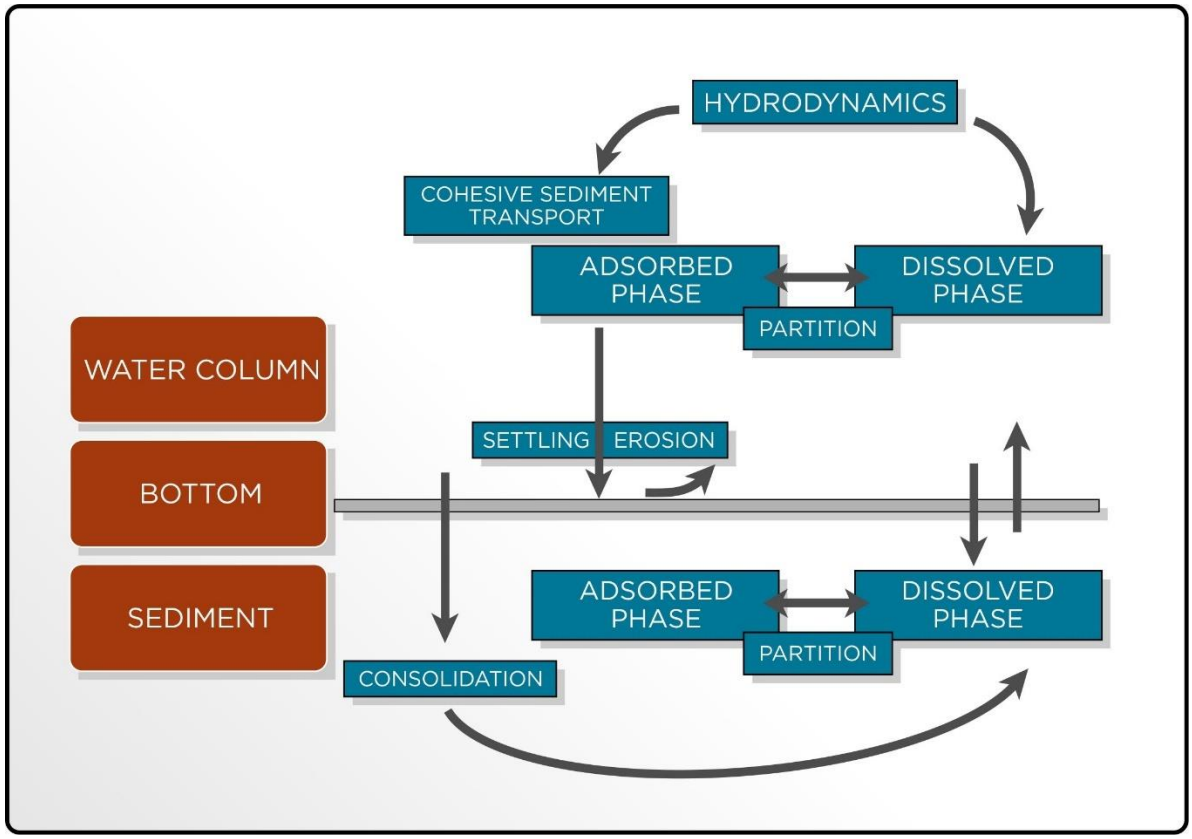

Figure 2.9: Transport processes simulated by the MOHID water model (Leitão *et al.,* 2008).

2.3.5 Environmental Fluid Dynamics Code (EFDC) Model

The EFDC (Environmental Fluid Dynamics Code) model is a general-purpose modelling package for simulating multi-dimensional flow, transport and biogeochemical processes in surface water systems including rivers, lakes, estuaries, reservoirs, wetlands, and near-shore to shelf-scale coastal regions (Torres *et al*., 2015).The EFDC Model was originally developed at the Virginia Institute of Marine Science and the School of Marine Science of the College of William and Mary, and later sponsored by the US Environmental Protection Agency (USEPA).

The EFDC model utilises the sigma coordinate system (Meller *et al*., 2002) on the vertical direction (aligned with the gravitational vector) and the Cartesian or curvilinear orthogonal coordinates in the horizontal plane (Torres *et al*., 2015). The coordinate system allows the model to build the structure with cells of finite elements. The model computational scheme solves the horizontal momentum and continuity equations on a staggered grid using an external-internal, mode-splitting scheme. The external mode is linked with a barotropic long wave motion, and it is solved using a semi-implicit scheme. The internal mode is linked with

the vertical shear of the horizontal velocity components and is solved using a fractional step scheme. The transport equations are also solved using a fractional step scheme with implicit and explicit diffusion (Tetratech, 2007). The structure that utilises the EFDC model for flow dynamics process in surface water mass is shown in Figure 2.10.

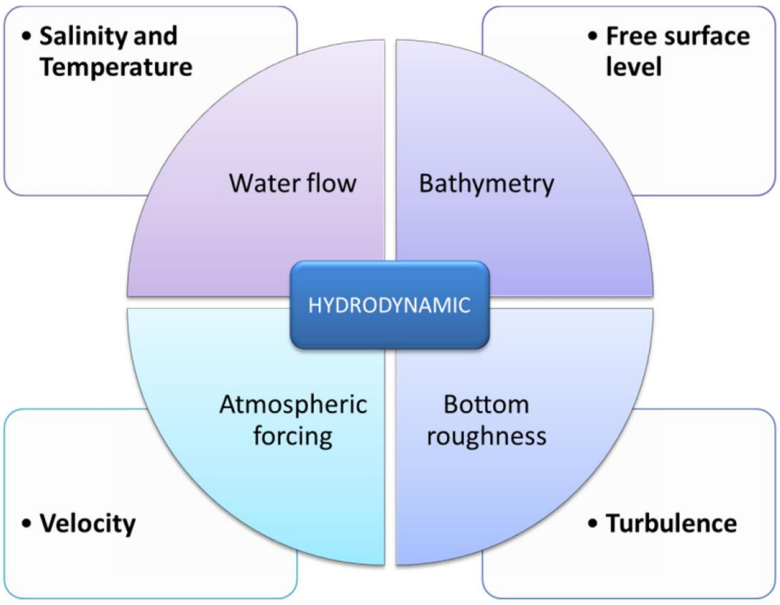

Figure 2.10: Structure of the EFDC hydrodynamics model (Torres *et al.,* 2015).

2.3.6 TELEMAC Model

TELEMAC model is a 2D and 3D modelling system designed to simulate transient free surface flow of water or fluid dynamics. The models were developed by the National Hydraulics and Environment Laboratory of the Research and Development Directorate of the French Electricity Board (EDF-DRD), in collaboration with other research institutes (Mensencal, undated). It was mainly adapted and improved to simulate flow dynamics, water quality, water waves and sedimentology in coastal areas, estuaries, rivers and lakes.

The computation engine of the TELEMAC model system is based on the finite-element and finite-volume methods to solve the shallow water flow and sediment transport equations (TELEMAC, 2000). The spatial discretisation of the 2D domains is based on grids composed of triangular elements of various sizes and shapes. The 3D spheres are discretised by grids of prismatic elements. The main results at each node of the computational mesh are the depth of water and the depth-averaged velocity components (TELEMAC, 2014).

2.3.7 Delft3D Model

The Delft 3D model is a world-leading 3D integrated modelling system suite to investigate hydrodynamics, sediment transport and morphology and water quality for fluvial, estuarine and coastal environments. The model was developed by Deltares, which is an independent institute for applied research in the field of water resources. The Delft 3D model solves the unsteady shallow-water equations (Navier-Stokes equations) in two (depth-averaged) or three dimensions. The mathematical system of equations consists of horizontal momentum, continuity (mass) equation, transport equation and turbulences/waves (Deltares, 2014).

The vertical momentum equation does not take into account the hydrostatic pressure and vertical acceleration, which are assumed to be small in comparison to gravitational acceleration (van Rijn and Walstra , 2003). The Delft3D model adopts a structured grid (Cartesian rectangular, orthogonal curvilinear or spherical) to solve hydrodynamics and sediment transport equations using a cell-centred finite difference method. Delft3D can also adopt the unstructured mesh (triangular, quadrilateral, and polygonal cells with at most six sides) grid to simulate spatial discretisation of the equations using a cell-centred finite volume method (Symonds *et al.,* 2016).

2.3.8 MIKE11 AND MIKE21 Models

The MIKE11 model is a 1D (cross section integrated) modelling system for rivers, open channels, reservoirs and hydraulics structures. MIKE21 is a 2D (depth-averaged) modelling system for free surface water flows in rivers, lakes or reservoirs, and coastal and estuarine environments. Both models are the products of Danish Hydraulic Institute (DHI) and they are applied worldwide to solve water resource problems.

The MIKE 11 model solves the mass and momentum equations which are based on an implicit finite difference method established by Abbott and Ionescu (1967). The method is built to solve any form of the Saint Venant Equations (kinematic, diffusive, or dynamic). The water level and flow are calculated at each time step, by calculating a six-point Abbot method with the mass equation positioned on h-points and the momentum equation positioned on Q-points. The hydraulic resistance is based on the friction slope from the empirical Manning's or Chezy

equations where the channel roughness is modified in several ways to account for variation on the cross-sectional area (Fleenor and Jensen , 2003).

The MIKE21 2D model is based on an unstructured grid (orthogonal curvilinear or spherical) to solve horizontal hydrodynamics equations and sediment transport equations using a cell-centred finite volume method (Beck and Basson , 2008, Symonds *et al.*, 2016). An unstructured grid provides a degree of flexibility and enables smooth representation of the geometric data (DHI, 2013).

2.3.9 HEC-RAS Model

The Hydrological Engineering Centre – River Analysis System (HEC-RAS) is a modelling system for simulating surface water profiles for 1D flows (cross section integrated), steady flow, unsteady flow and sediment transport in natural or artificial channels (May *et al.,* 2000, Timbadiya *et al*., 2011). The computation engine for the HEC-RAS program was developed by the U.S. Army Corp of Engineers (USACE). The program solves the continuity and momentum equations with an implicit linearised system of equations using Preissman's second order box scheme (Kane *et al.*, 2017). In a cross-section, the overbank (floodplain) and channel are assumed to have the same water surface elevation, though the overbank volume and conveyance are separate from the channel volume and conveyance in the implementation of the conservation of mass and momentum equations (HEC, 2016).

The simultaneous system of equations generated for each time-step (and iterations within a time-step) are stored within a skyline matrix scheme (Bathe and Wilson , 1976) and solved with a direct solver developed specifically for unsteady river hydraulics (Haghiabi and Zaredehdasht , 2012). The state variables for the numerical method are flow discharge and river stage/level, which are computed and stored at each river sections or transects. The hydraulic resistance is based on the friction slope/gradient from the empirical Manning's equation. The channel roughness can be symbolised with Manning's (n) or roughness height's (k) (Fleenor and Jensen , 2003).

2.4 Model Selection

The main attributes of these models described above are listed in Table 2-1. Four of the models are available on a commercial basis and the remaining five are freely available.

Table 2.1: The comparative analysis of the reviewed estuarine models.

Estuarine Models	Data Requirement for Flow and Sediment routing			Calibration Parameters	Hydrodynamics and Sediment Transport Method	Availability and Support
	Geometric set-up	*Boundary conditions*	*Calibration/validation*			
DYNHYD5	Grid raster and bathymetric data interpolated	River discharge, wind data and tidal data	Water level data or flood survey marks, direct flow velocity measurement (ADP or current meter), and sediment samples.	Channel Resistance (Manning friction coefficient)	Network "link-node" approach	Commercial product
ANUGA (2D)	Grid raster or TIN and bathymetric data interpolated	Rainfall data, rivers flow data and wind data	River stage data and current flow velocity measurement.	Channel Roughness (Manning friction coefficient)	Finite-volume method	Commercial product
ADH (2D)	Grid raster and bathymetric data interpolated	Fluvial data, sediment data and tidal data	Water level data or flood survey marks, direct flow velocity measurement (ADP), and sediment samples.	Channel Roughness (Manning)	Backwater Analysis and Ackers-White	Open source
MOHID (3D)	Grid raster and bathymetric data interpolated	River discharge, wind data, sediment data and tidal data	Water level data or flood survey marks, direct flow velocity measurement (ADP), and sediment measurements.	Channel Roughness (Manning) and Wind coefficients	Finite-differences method and Eulerian/Lagrangian particle transport scheme	Commercial product
TELEMAC (2D)	Grid raster and bathymetric data interpolated	Rivers' discharge, tidal data and wind data	Water level data or flood survey marks, direct flow velocity measurement (ADP or trace method), and sediment measurements.	Channel Roughness (Chezy, Manning or Strickler)	Finite-element or finite-volume method (2D) and three fractional steps (3D)	Open source
EFDC (3D)	Grid raster and bathymetric data interpolated	Rivers' run-off, tidal data and wind data	Water level data or flood survey marks, direct flow velocity measurement	Roughness height and Wind drag coefficient	Finite different scheme on a staggered grid, three	Open source

Estuarine Models	Data Requirement for Flow and Sediment routing			Calibration Parameters	Hydrodynamics and Sediment Transport Method	Availability and Support
	Geometric set-up	*Boundary conditions*	*Calibration/validation*			
			(ADP or trace method), and sediment measurements.		time level Scheme and Eulerian/Lagrangian particle transport scheme	
Delft3D	Grid raster and bathymetric data interpolated	Rivers' discharge, tidal data and wind data	Water level data or flood survey marks, direct flow velocity measurement (ADP or trace method), and sediment measurements.	Bed roughness coefficient (Manning)	Cell-centred finite difference method and finite volume method	Open source
MIKE11 (1D) and MIKE21C (2D)	Aerial and satellite imagery, Bathymetry/DEM, or Lidar data	Rainfall data, fluvial (flow and sediment) data and tidal data	Continuous water level data or flood survey marks, direct flow velocity measurement (ADP), and sediment samples.	Channel Roughness (Chezy or Manning) and contraction/expansion losses	Six-point Abbot method, cell-centred finite volume method and Ackers-White	Commercial product
HEC-RAS (1D)	Aerial and satellite imagery, Bathymetry/DEM, or Lidar data	Continuous fluvial (flow and sediment) data	Continuous water level data or high-water marks, direct flow velocity measurement (ADP), and sediment samples.	Channel Roughness (Manning) and contraction/expansion losses	Standard step method (Steady), four-point implicit scheme (Unsteady) and Ackers-White	Open source

The HEC-RAS hydrodynamic model was selected due to its availability, compatibility, general application and GIS support packages (HEC-geoRAS and HEC-DSS). HEC-geoRAS is used to extract the geometric data (pre and post processing data) from a terrain surface and delineate a floodplain from the computed water surfaces (Fleenor and Jensen , 2003). The model is relatively easy to set up and calibrate. The major advantages of HEC-RAS are its processing capacity, high-performance computing, numerical robustness and complete outputs with detailed technical reports/tables. The model is a hydrodynamic/sediment transport model created by the US Army Corp of Engineers (USACE) and it is freely available (does not require a licence) for use by all users, although there is very limited support for the general user. The USACE and NOAA's National Weather Services (NWS) utilise the HEC-RAS model to accurately predict the 1D coastal river flows and stages at over 4,000 locations in the United States of America (USA), in order to provide critical water information to coastal end-users (Mashriqui, 2010).

There are seven sediment transport potential functions available in HEC-RAS to route fluvial sediment of the Mlalazi River through the mouth of the Mlalazi Estuary. Azarang and Bajestan, (2015) used the HEC-RAS (version 4.1) sediment model to simulate the morphological change (erosion & deposition) of the Karun River using the four sediment transport functions, namely Enguland-Hansen, Ackers-White, Larsen and Toffaleti. The Enguland-Hansen and Ackers-White methods gave results of higher accuracy compared to other methods based on the model performance indicators, Nash-Sutcliffe Coefficients (NE), which achieved values of 0.74 and 0.61 respectively. This study prefers the Ackers-White sediment transport function for its flexibility, wide sediment class range and ability to compute a total combined sediment load brought in by the Mlalazi River (Rasifudi, 2019).

The major disadvantage of the HEC-RAS model is that it takes time to run the simulation of sediment transport, especially when long-time records are available; for example, it took 12 hours to perform simulations in the Karun River (Iran) due to the daily flow records of five years (Haghiabi and Zaredehdasht , 2012). It was discovered by Haghiabi and Zaredehdasht, (2012) that the presentation of sediment analysis within HEC-RAS (Version 4.1) is based on the imperial system (*fps*) while the switch to the SI mode is inactive. The drawback is that the Manning's roughness coefficient (n) is the only parameter used to calibrate the HEC-RAS flow model and it works best for high rivers flows not necessarily low flows (Ochiere *et al.*, 2015).

The numerical instability problem during the simulation of unsteady analyses is often experienced in HEC-RAS model and this is due to poor geometric data (DEM and bathymetry) and/or poor model configuration. The instability can be overcome by adjusting the computation time interval in the program. Mkhwanazi (2003) used the HEC-RAS (version 2.0) model to successfully route the one-dimensional steady and unsteady flow analysis for the natural (upper and middle) and canal (lower) sections of the Mlazi River, respectively. The levels of inundation under uncertainty (Q_{20yr}, Q_{50yr} & Q_{100yr}) were determined for the Mlazi canal to identify problematic areas of the adjacent low-lying areas, in order to mitigate floods for the eThekwini Metro Disaster Management. The major setback with this study was a lack of historical data to calibrate and validate the model but the aerial satellite imagery and field photographs were used to validate the HEC-RAS delineated flood lines.

CHAPTER 3. STUDY AREA

The Mlalazi Estuary for the purpose of this project is defined as the active channel and floodplain segment from the confluence of the main Mlalazi River and its northern tributary KwaGugushe (Ntuze) River to the estuary mouth (Figure 3.1). The development of a conceptual model(s) of the main controlling features of the estuary dynamics to support the numerical model configuration of the hydrodynamic of this system needs hydrological and geomorphologic data for this area. Therefore, this chapter outlines the available data, monitoring and some of the methods used to acquire the data within the study area.

3.1 Location

The Mlalazi Estuary is situated near the small town of Mtunzini on the north coast of Kwa-Zulu Natal Province. This estuary is fed by the Mlalazi River, which has a catchment area of about 954 km^2 (Rasifudi, 2019). The Mlalazi River flows in a north easterly direction towards the Indian Ocean. The river has two main tributaries, namely the Mkukuze River and the KwaGugushe (Ntuze) River (Rasifudi, 2019). The estuary forming the main area of interest for this project extends from the confluence of the Mlalazi River and the KwaGugushe (Ntuze) River to the mouth situated along the Indian Ocean shoreline in the east (Figure 3.1). It is formed by a drowned river valley that has been modified over geological times by changing sea level and sedimentation processes (Taylor, 2017). The upper estuary is confined within the predominantly consolidated shales from the Ecca Formation. The lower estuary is emerging onto a broad coastal plain comprising unconsolidated coastal sandy soils and high frontal dunes that have a significant impact on the development and evolution of the estuary (Kelbe *et al.*, 2019).

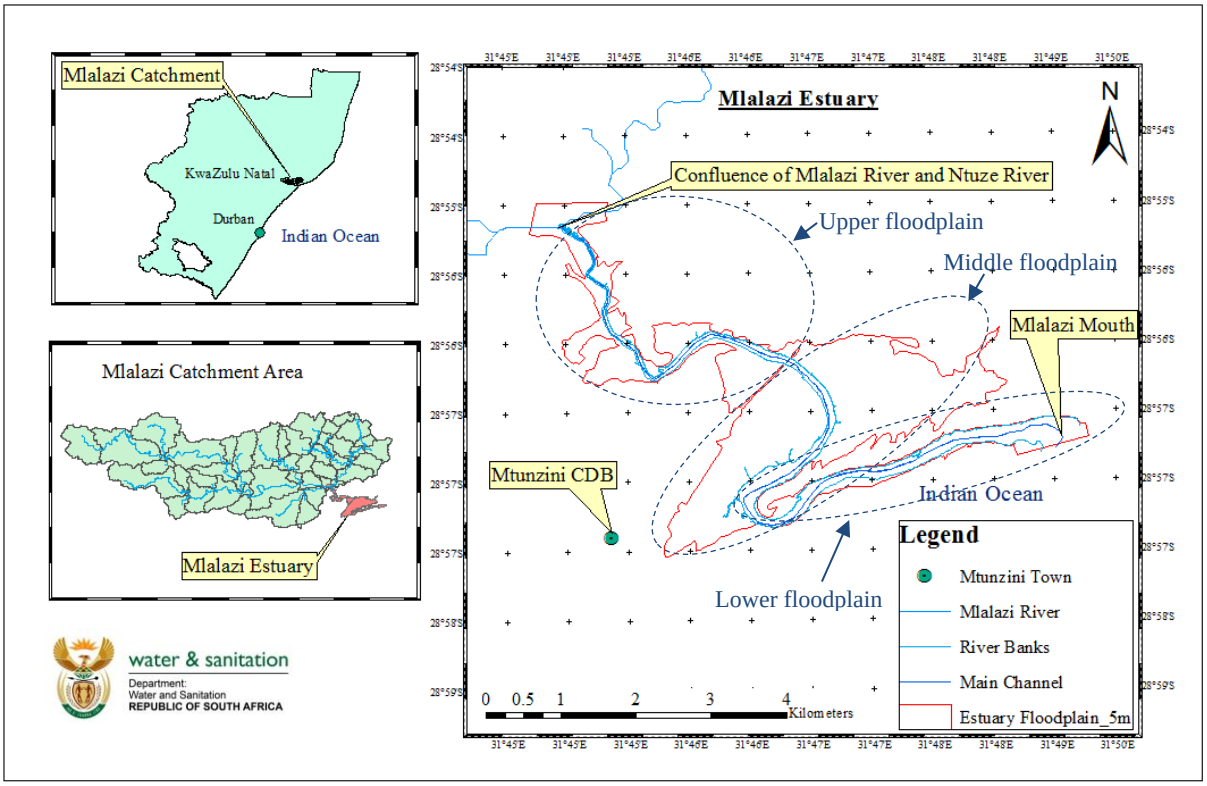

Figure 3.1: The stream network of the Mlalazi Catchment, the location and adjacent floodplain of the Mlalazi Estuary.

3.2 Geomorphology

The development of the flow and sediment dynamic model(s) require a good channel bathymetry and floodplain topography (DEM) to reliably simulate the flow routing of fluvial events from the catchment through the estuary channel and floodplains. No historical geometric data was available for the Mlalazi Estuary channel apart from a few river transects surveyed by Badenhorst *et al.*, (1989) after the 1987 flood event, as described later in the section. However, a huge effort was made by Kelbe and Taylor (2019) to create a 1m Digital Elevation Model (DEM) of the Mlalazi Estuary and floodplain below the 10mMSL contour using various sources of information (Figure 3.2). The bathymetry of the main channel from confluence to mouth was measured (Figure 3.3) by Taylor (HRU) and Bachoo (Ezemvelo Wildlife) using a Differential Global Positioning System (DGPS), coupled to a water level logger dragged along the channel bed. Subsequently, the Department of Water and Sanitation (DWS) also conducted a 6km bathymetric survey from the mouth to the Railway Bridge using an Acoustic Doppler Profiler (ADP) instrument, coupled to a Differential GPS (le Roux, 2018).

Figure 3.2: Available geometric data (1m DEM and bathymetry) for the Mlalazi Estuary.

The derived DEM was used to obtain the elevation profile within the Mlalazi Estuary, which ranges from 105m (above MSL) in the upper reaches to -1.5m (below MSL) in the lower reach. ArcGIS was used to incorporate the estuary elevation contours and river bathymetry into a 10 x 10m raster DEM. However, the DWS bathymetry was not available when the model development commenced but it can be utilised at a later stage should further model accuracy be required. In this study, satellite imagery from Google Earth in 2017 was used to digitise the centreline of the main river channel and riverbanks from the confluence of the estuary to the downstream end (mouth) of the estuary. This data was used to generate geometric data (river cross sections) for the estuary for the numerical model and will be explained in detailed in the next chapter.

3.3 Hydraulic Controls

Land use and geomorphic features have a strong influence on the hydrodynamics of the floodplain. The main hydraulic controls are described in the next sections. However, it is noted that there is a gauging weir just upstream of the confluence at the upstream end of the estuary on the Ntuze tributary that must have a large impact on the sediment transport into the estuary.

3.3.1 Estuary floodplain

The confluence (upstream) and mouth (downstream) are the main external boundary conditions that control the water level variations in the estuary. The Mlalazi River transports fresh water derived from precipitation and groundwater in the upper catchment areas into the estuary. The mouth influences the way in which an estuary responds to the outflow from fluvial events and the tidal influence (Schumann, 2013) forming control boundaries functioning much like a compound broad-crested weir (as indicated in the previous chapter). The flow and sediment dynamic features are controlled by the active channel of the Mlalazi Estuary and the surrounding floodplain when the water level in the main channel exceeds approximately 2m MSL (Kelbe *et al.*, 2019).

The upper floodplain from the confluence to the Railway Bridge (Figure 3.3) on the estuary is bordered by hills and covered mainly by commercial sugar cane and forestry plantations. The presence of vegetation on the floodplain will reduce the flow rate of surface run-off due to increased surface roughness. However, the sugar cane landscapes in the low-lying areas are designed with networks of well-defined drainage canals (Photographs 3.1, 3.2 & 3.3). The network of drains quickly channel flow into the floodplain on a rising hydrograph and drain the same area during the receding hydrograph and thus prevent waterlogging and reducing flood storage in this area.

Photograph 3.1: Sugar cane drainage canal in the upper channel above the R102 Highway Bridge

Photograph 3.2: Swamped sugar cane fields along drainage canals between the R102 and N2 Road Bridges during extreme fluvial event (Feb 2018).

Photograph 3.3: Flooded sugar cane fields below the N2 Road Bridge (Feb 2018)

During low or average flows of the Mlalazi River, these drainage systems are fed mostly by groundwater. The quick flows generated from 1:10 year (Q_{10yrs}) flood return does not inundate the floodplain but can fill up the very low-lying canals as illustrated in Photograph 3.3. Therefore, hydraulic drag at this stage is not controlled by the sugar cane plantation patterns but by their drainage channel system. The extreme floods tend to overflow the canals (see Photograph 3.2) and the sugar cane fields create a considerable drag on the flood propagation. The drag is determined by the vegetation type and management practice on the floodplains.

The **middle** estuary floodplain is the expansive flooding area beginning just downstream of the Railway Bridge embankment and extending all the way down to the estuary car park. This area is over 5km wide in some sections. The floodplain on the left (north) bank is a highly transformed landscape of mainly commercial sugar cane farms with a well-drained system. Floodplain on the right (south) bank is mostly part the Mlalazi Nature Reserve with some drainage canals and expansive areas of mudflats and salt marshes. The southern plain is sub-divided into different vegetation units that were identified by Kelbe *et al.*, (2019) as follows:

a) Delta fan is an area just below the Railway Bridge, where the fluvial sediments were channelled and deposited overtime by the high river flows. The site is colonised by the woody plants.

b) Old sugar cane fields which still have drain channels that seep groundwater from the dunes.

c) Supratidal area is usually flooded by high tides from the marine environment and gave rise to a salt marsh (Photograph 3.4) as evaporation concentrates on the saline water on the soil.

d) Intertidal area gave rise to the Mangrove forests (Photograph 3.5) since there are channels which bring in seawater from high marine tides and carry the outflows of groundwater and surface flows.

e) Reed growth (Photograph 3.6) is concentrated on the area adjacent to the main river channel, where fine alluvial sediments are deposited over time. The site has an old levee constructed in the 1960s during a dredging program, used to channel high flows to form a pathway parallel to the main channel.

Photograph 3.4: Salt marsh and sedges below the Railway Bridge on the right bank

Photograph 3.5: Mangrove forests below the Railway Bridge on the right bank

Photograph 3.6: Swamp forest and reed beds below the Railway Bridge on the right bank

All these hydrogeomorphic features and vegetation types have different degrees of drag (roughness coefficient) on the flood wave propagation. The hydrodynamic model requires these drag coefficients for each cross-sectional profile running perpendicular to the main channel flow path. It is very difficult to determine the hydraulic roughness on the floodplain transects below the railway embankment due to these large variations in vegetation dynamics. The high flow generated from the 1:10 year (Q_{10yrs}) flood return does inundate these areas since the soil is highly saturated. Therefore, hydraulic drag at this stage is not controlled only by the domain vegetation pattern.

The **lower or mouth** floodplain extends from the estuary car park to the mouth. The floodplain channel is relatively narrow and is about 4km long. The lower Estuary floodplain is bounded by relatively high vegetated (sub-tropic forest) coastal dunes (Photograph 3.7). High flows do not overflow a large floodplain in the lower and narrow channel. However, the relatively narrow cross sections along this section of the estuary are prone to increased velocities relative to upstream section that may lead to an increased sediment-carrying capacity that could contribute to scouring the accumulated marine sediments brought in by the flood tide (Photograph 3.8). Therefore, the hydraulic drag is mainly controlled by the roughness of the riverbed. The sand berm formed by an accumulation of the marine sediment over time also plays an important role in reducing the flow rate by increasing the surface roughness and increased wetted perimeter.

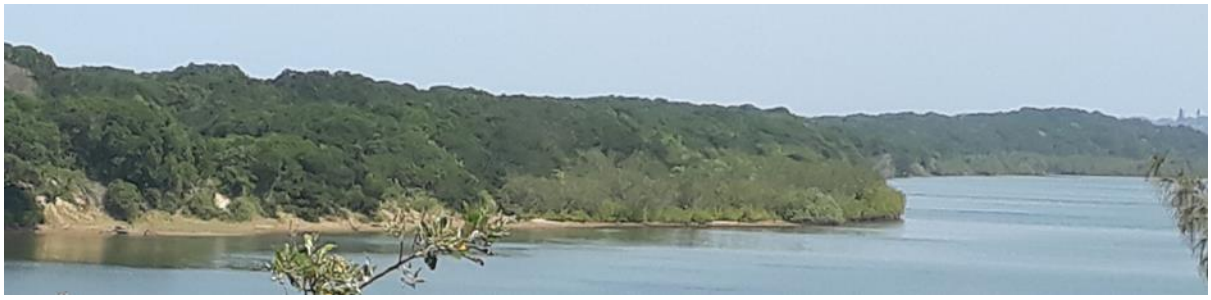

Photograph 3.7: The lower Estuary floodplain is bounded by relatively high vegetated (sub-tropic forest) coastal dunes

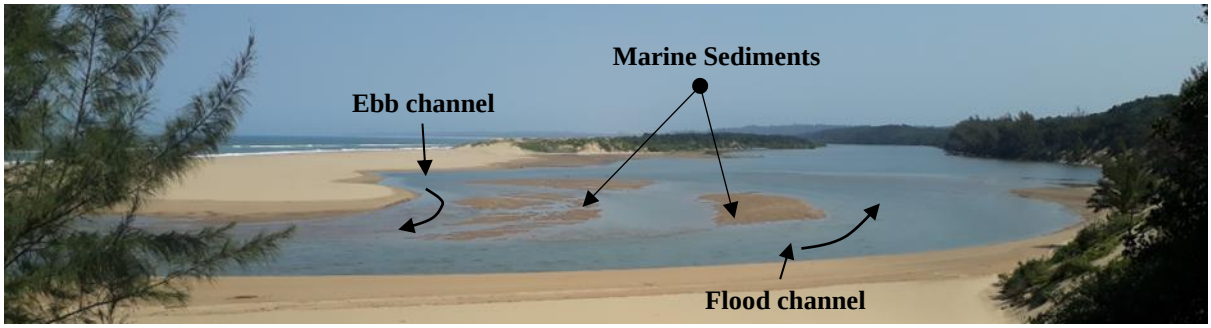

Photograph 3.8: The Mlalazi Estuary mouth basin during the flood tide

3.3.2 Estuary Channel

The actual path length of the estuary is about 12km long from the confluence of the main Mlalazi River and its KwaGugushe (Ntuze) tributary down to the estuary mouth. The width of the main channel ranges from 30m in the upper reaches to 200m towards the mouth (Photograph 3.8). The depth of the active pathway of the estuary is from 0.3m to nearly 5m. There is a sharp almost 90^0 bend to the left (north) about 800m downstream of the N2 Road Bridge (Figure 3.3). A further 600m downstream of the bend there is another sharp bend to the right before the Railway Bridge. There is a 90^o bend before entering the lower 4km section near the mouth.

As a norm, river bends tend to force the main flow to be directed toward the outside of the bend and as a result more erosion can occur on the outside banks due to higher stream velocities. More sediment deposition may take place on the inside of the bend, where the flow velocity is lower. The U-shaped bend on the lower estuary tends to constrict and increases the flow rate leading into the mouth channel.

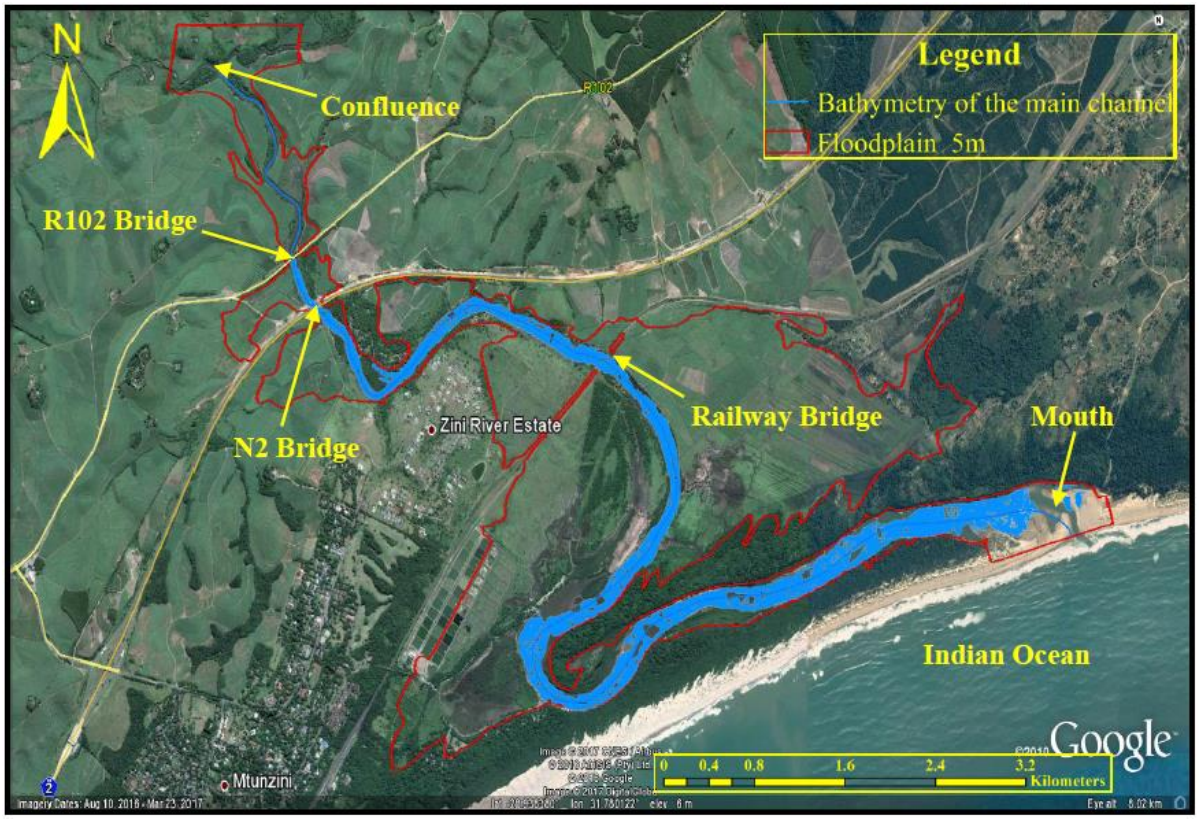

Figure 3.2: Location of hydraulic structures (Bridges), bathymetric survey (blue) of the active channel and floodplain basin (red) in the Mlalazi Estuary (kelbe *et al.*, 2019)

There are four bridge structures built across the Mlalazi Estuary (Figure 3.2) that also affect the flow rate and sediment transport, especially during floods.

a) The R102 Road Bridge is situated about 1km downstream of the confluence. This is roughly 120m long and 10m wide, with three bridge pillars (2m wide each) constructed inside the estuary channel (Photograph 3.9).

b) The old Steel Arch Bridge (Photograph 3.10) is positioned about 20m upstream of the R102 Road Bridge. The old bridge is about 115m long and 5m wide with three bridge pillars inside the channel.

c) The N2 Road Bridge is positioned approximately 400m downstream of the R102 Bridge and was recently constructed due to the extension of the N2 road. The length of the N2 Road Bridge is roughly 120m; the width is 20m and the three pillars which are 2m wide each.

d) The Steel Railway Bridge in the mid-estuary is about 140m long and 7m wide, with three pillars in the active channel (Photograph 3.11). Just downstream of the Railway Bridge the pillars are relic pillars from previous structures.

The bridge structures play an important role in the estuary hydrodynamics since they constricted flow upstream during high flows with less influence on the downstream dynamics. The structures also dissipate the energy of the flood hydrographs as they enter the estuary, causing wave attenuation and lag as it moves down the estuary toward the mouth.

Photograph 3.9: The R102 Road Bridge (old N2 Bridge) in the upper estuary

Photograph 3.10: The old arch bridge and R102 Road Bridge in the upper estuary

Photograph 3.11: The Railway Bridge in the upper estuary

3.4 Climate

The study area lies on the eastern shoreline of South Africa in the sub-tropics where the weather is controlled by the anticyclonic circulation from the Indian Ocean and low-pressure systems (Kelbe, 1988, Bate *et al.*, 2016). The area is vulnerable to extreme high rainfall events due to tropical cyclones that produced over 500mm of rainfall in two to three days during Cyclone Domonia and Imboa in 1984 (Kovac *et al.*, 1985 and Chikoore, 2005). This area receives rainfall during the drier months (June/July), where a monthly average of 30mm/month on the upper reach and 42mm/month on the lower reach were recorded (Rasifudi, 2019). This is due to the cold fronts travelling up the east coast of South Africa under the influence of the mid-Atlantic cyclonic activity in the southern oceans (Bate *et al.*, 2016). The weather patterns normally produce more rainfall in summer months (October to March) than the winter months (April to September). The daily rainfall distribution within the Mlalazi Catchment from 1950 to 2018 is shown in Figure 3.3. This period showed numerous storm events exceeding 200mm/day.

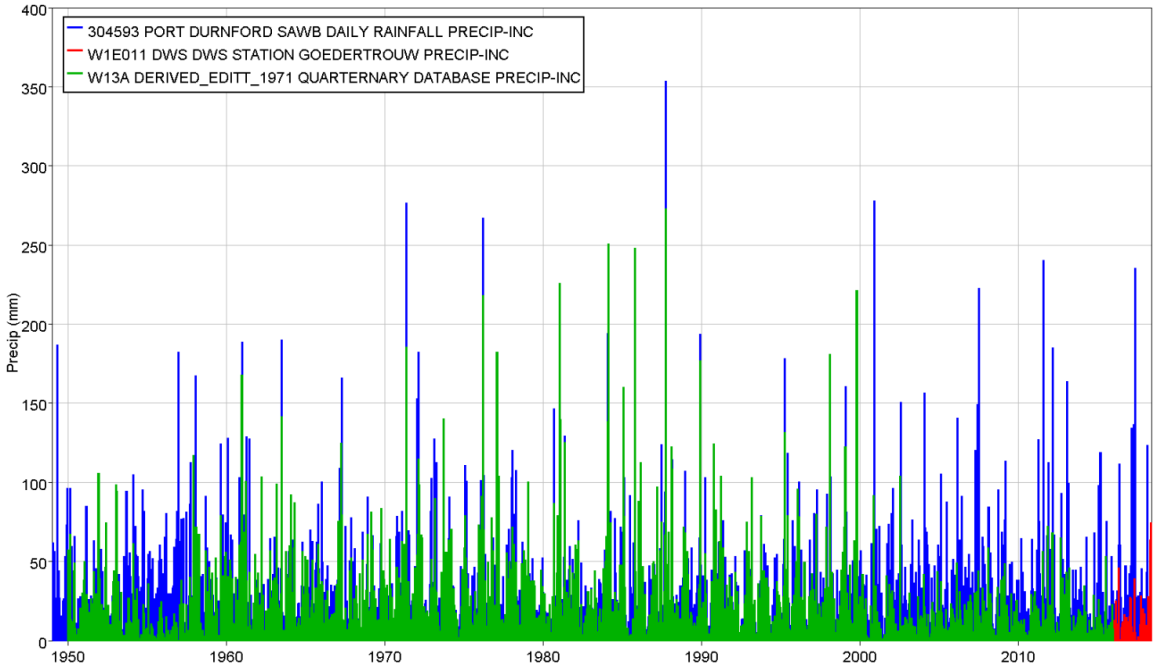

Figure 3.3: The daily rainfall data for the Inland (green/red) and coastal (blue) weather stations within the Mlalazi Catchment. The patched (red) rainfall data is the adjacent Mhlathuze Catchment (Rasifudi, 2019).

There is a considerable difference in the rainfall values between the two regions due primarily to orographic effects. However, there is also some disparity between sites for some of the extreme rainfall events that may influence the classification of their return periods. Two cyclones (Domonia & Imboa) in 1984 caused catastrophic flooding in the region and were not well recorded in the available historical rainfall series record shown in Figure 3.4 (Rasifudi, 2019). A cut-off low caused a greater flood event in 1987, which has been described as a possible 1:150-year event by Kovacs (1988). However, it is worth noting that Kovacs (1988) suggested that the rainfall in the Mlalazi region exceeded the proposed 1:200-year rainfall event derived by Adamson (1981).

It should be noted that such flood events will differ in some manner, even though they have the same magnitude (HEC, 2018). The variations are mainly due to factors such as:

a) The differences in the rainfall patterns (intensity, duration and direction, etc.);

b) how wet the drainage area or catchment was before the storm event; and

c) whether the centre of the storm event was over the upper, central or lower reaches (trophic or sub-trophic) of the catchment.

Tropical cyclones Domoina and Imboa in 1984, which both landed within two weeks apart on the Zululand coast, were perfect examples. Figure 3.4 illustrates the pathway of the cyclones Domoina and Imboa along the Indian Ocean. Cyclone Domoina crossed the Zululand coast on 01/02/1984 after following a zig-zag route from Mauritius, Madagascar and the Mozambican coast. Two weeks later, Cyclone Imboa developed in the northern Mozambican channel on 10/02/1984 and took a southwards direction. It reached the Zululand coast on 18/02/1984 but immediately turned back towards the ocean (Kovacs *et al.*, 1985). The actual rainfall recorded along the Mlalazi coast for Domoina and Imboa, was 194mm and 178mm respectively, therefore it was expected that the magnitude of these events would be similar (Rasifudi, 2019).

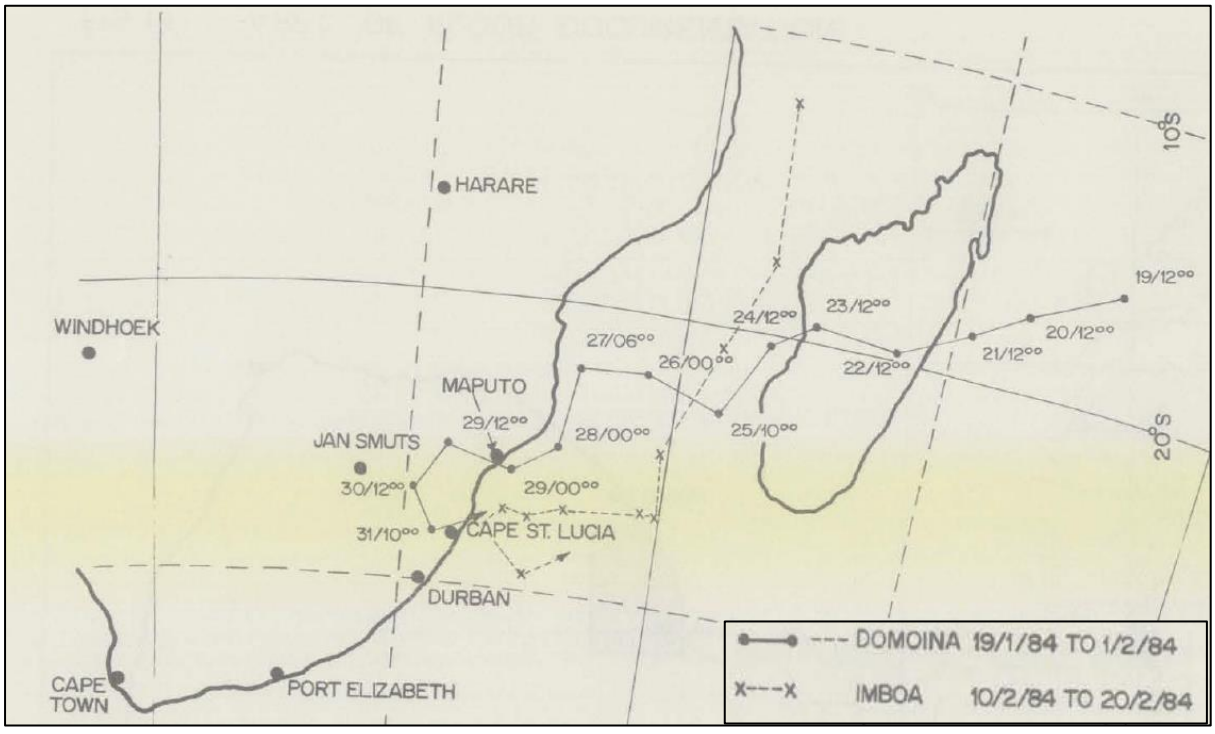

Figure 3.4: The routes of the Domoina and Imboa Cyclones in the Indian Ocean (Kovacs *et al.*, 1985)

The rainfall (Figure 3.3) and evapotranspiration (Figure 3.5) data were used by Rasifudi (2019) as the main input parameters to simulate the river run-off (m^3/s) of the Mlalazi River feeding into the estuary, using the HEC-HMS numerical catchment model. The Mean Annual Precipitation (MAP) ranged from 1119mm/year in the upper reaches (inland) of the catchment

to 1104mm/year in the lower reaches (toward the coast). The mean annual temperature in Eshowe is 19.0°C and in Mtunzini 21.2°C. Throughout the year, variation in the temperatures between the driest and wettest months is 6.4°C at Eshowe (inland) and 7.6°C at Mtunzini (coastal).

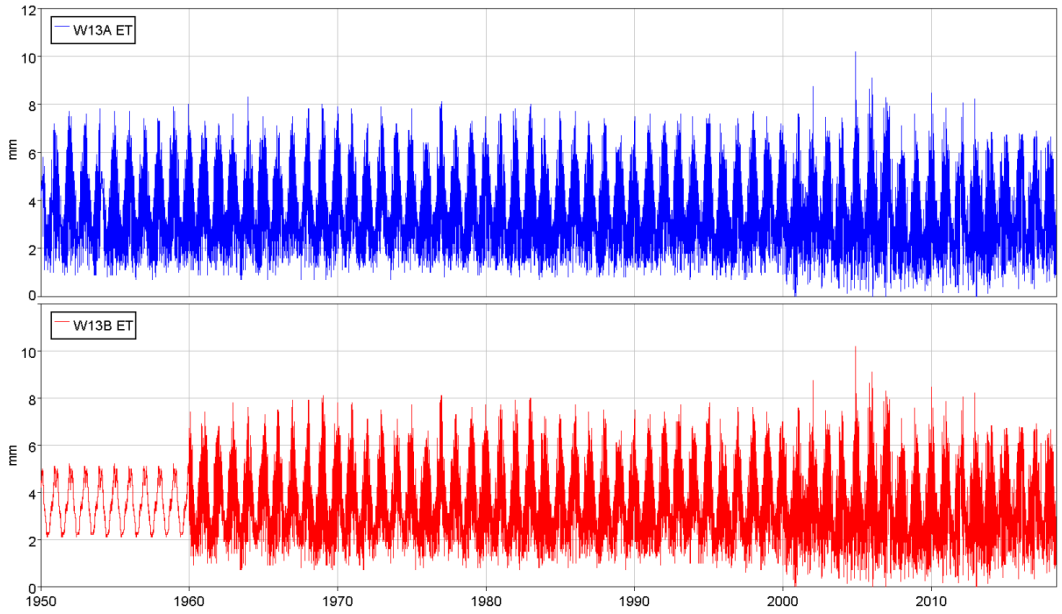

Figure 3.5: The daily evapotranspiration data for the inland (W13A) and coastal (W13B) weather stations within the Mlalazi Catchment from 1950 to 2018 (Rasifudi, 2019)

According to *www/windfinder.com* at the station base at Richards Bay, the monthly average wind speed (Figure 3.6) varied from 7m/s to 16m/s over the past 16 years (11/2001 to 01/2017). The average air temperatures which influence the evaporation rate varied from 28°C to 21°C. The prevailing (monthly average) wind directions were generally SSW to NNE (13.0%) or SW to NE (13.7%) or ENE to WSW (9.1%). The high wind speed (depending on the direction) has a large influence on estuary marine interaction with the hydrodynamics and sediment transport in the estuary since it enhanced wave action

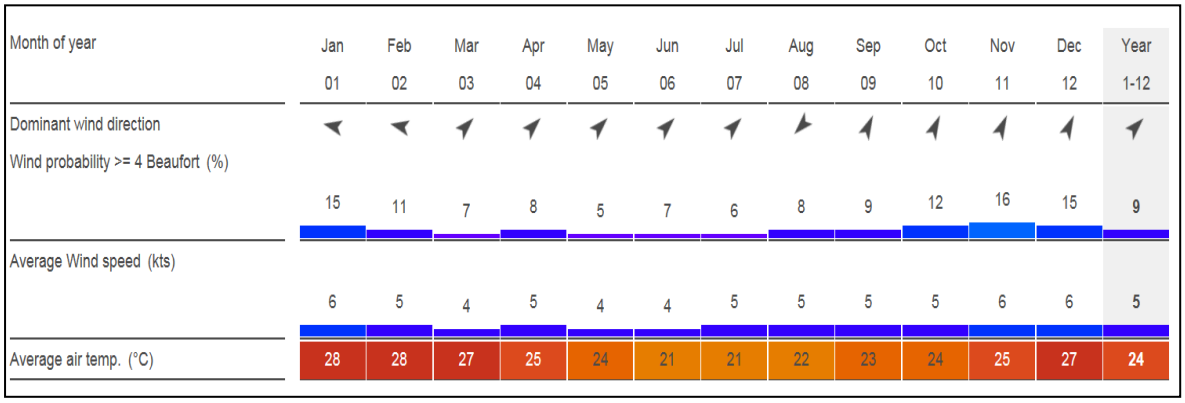

Figure 3.6: The average monthly air temperature, wind direction distribution and wind speed 2001 to 2017 at Richards Bay (source: *www/windfinder.com in 2017*)

3.5 Water Level Measurements

For the parameterised numerical estuarine model to accurately simulate the water level and energy slope, it requires observed water level measurements along the active pathway in order to calibrate the model parameters. Monitoring sites were established at various locations along the estuary (Figure 3.7) to assist in understanding the hydro dynamics of the study area and to support the development and calibration/validation of the flow model. These monitoring sites were installed by DWS, the Hydrological Research Unit and Ezemvelo Wildlife between 2014 and 2017. These sites were equipped with various automatic water level loggers and several were installed in perforated steel pipes. However, not all the loggers were installed in pipes but secured to the bank on the channel bed. These loggers were intended to capture the relative change in water level, salinity and temperature on a continuous basis. Consequently, the water level series were all adjusted to an approximate common datum using the surveyed logger series where the series overlapped (Kelbe *pers comm*).

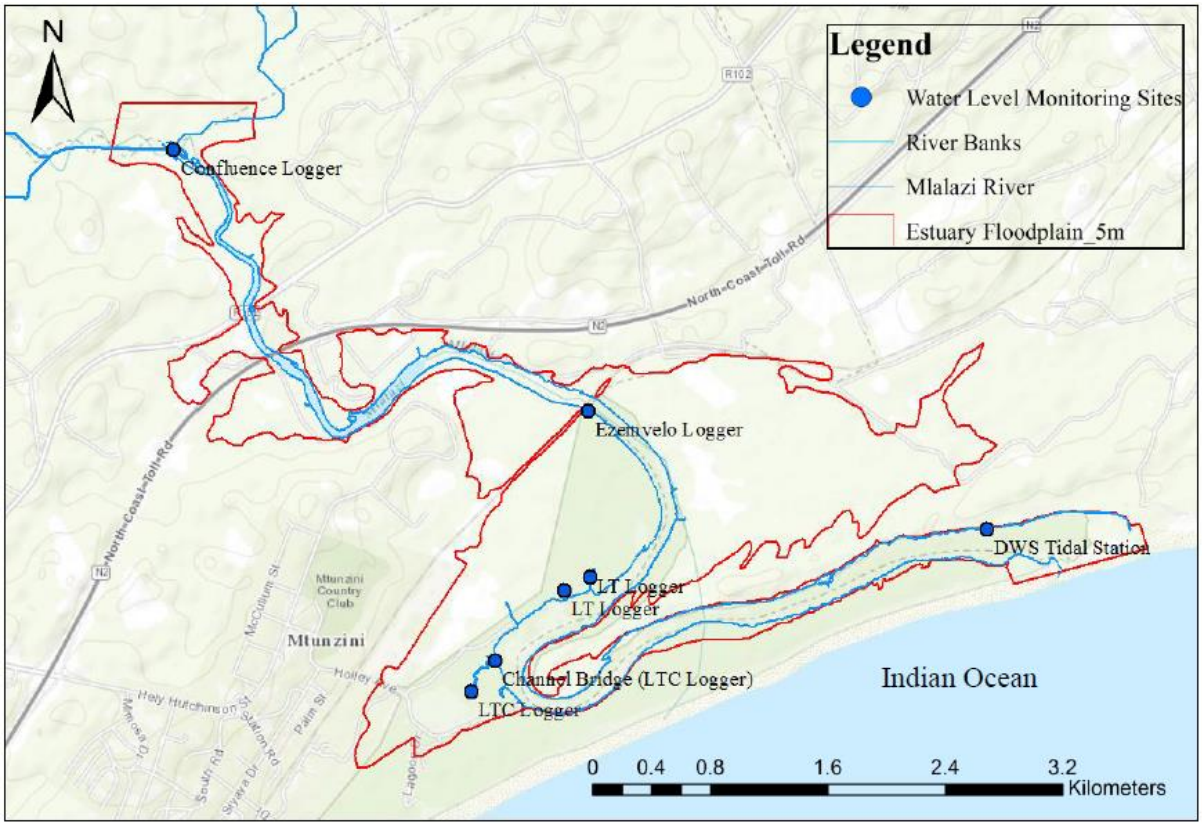

Figure 3.7: Water level monitoring sites at various locations along the active channel of the Mlalazi Estuary

The data loggers measure the water level fluctuations of the estuary in response to tidal and fluvial processes. The 1:10 (Q_{10yrs}) and 1:50 (Q_{50yrs}) flood events were captured by the water level logger positioned at the confluence during the period of observation (Figure 3.8). The average water level at the Railway Bridge for the period 2015 to 2016 (Figure 3.9) was recorded by Bathos (per comm) to be 1.15mMSL. A LTC data logger located about 5km upstream of the mouth was able to record a 1:20 year fluvial flood event on the May 2017 (Figure 3.10). The Department of Water and Sanitation (DWS) installed a tidal station (W1T001) near the Mlalazi Estuary mouth on the 01 April 2014. The tidal station consists of an automatic data logger installed in the steel inlet pipe and gauge plate for manual water level reading (Photograph 3.12).

The vented data logger from this tidal station experienced technical problems in 2015 however when it was flooded during the mouth closure. The logger was replaced by the DWS- KZN regional office in 2018 and the data was not available for this project. The average flow value

(1:2 flood event) within the estuary was recorded from the time series of the Ezemvelo logger (Oct 2015 – Sep 2016) at the Railway Bridge (Figure 3.10), the HRU LTC data logger (Sep 2016 – Feb 2018) at the lower estuary (Figure 3.10) and the DWS (W1T001) tidal station (Sep 2016 – Feb 2018) shown in Figure 3.11. The average water levels do not agree, due primarily to the different monitoring periods.

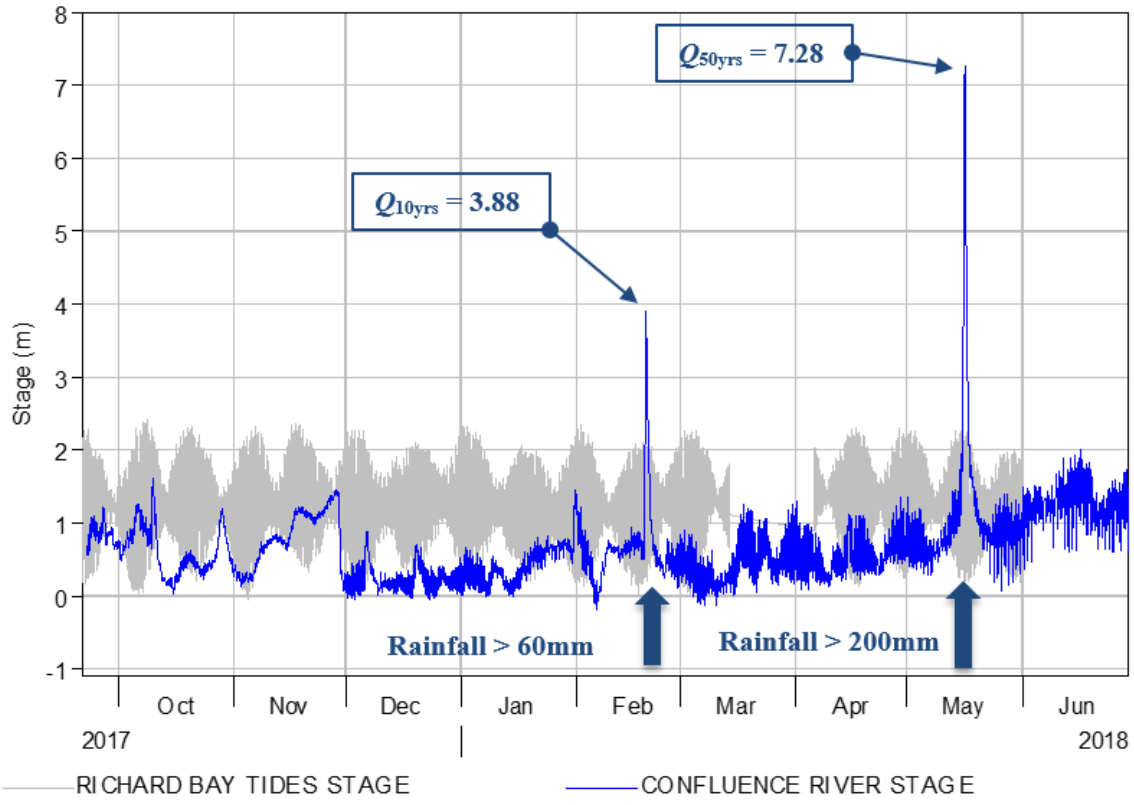

Figure 3.8: The observed water level data (hourly) at the confluence (blue) superimpose on the marine tide (grey). This logger was not surveyed so the stage was adjusted to correspond to selected tidal records from the surveyed records at the Railway Bridge (Figure 3.10).

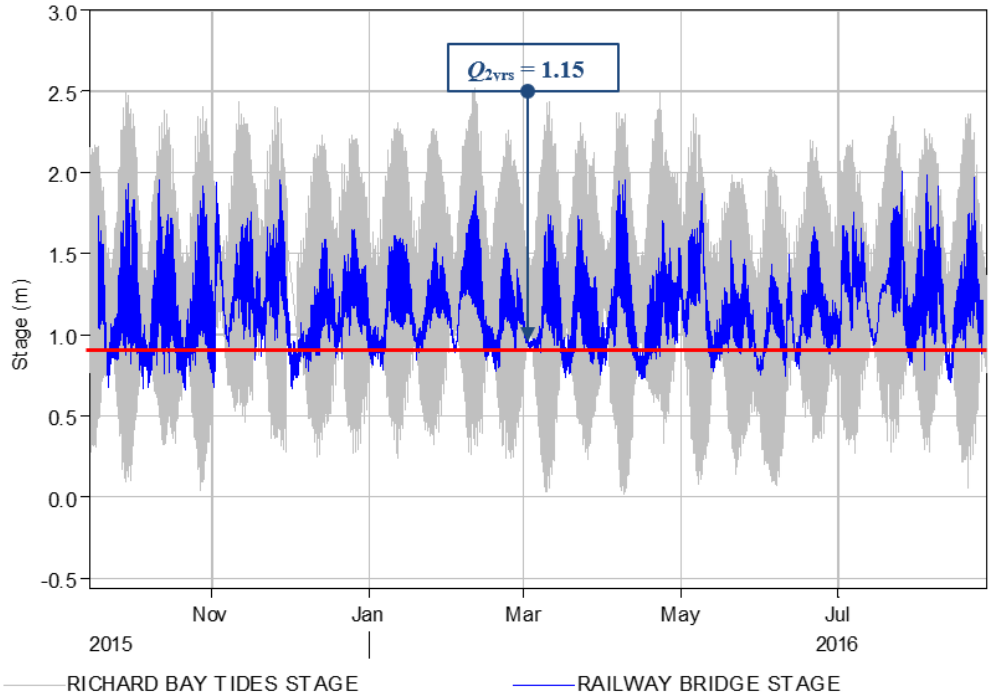

Figure 3.9: The observed water level data (blue) at the Railway Bridge (Santos *per comm*). The grey time series is the Richards Bay tide (mMSL).

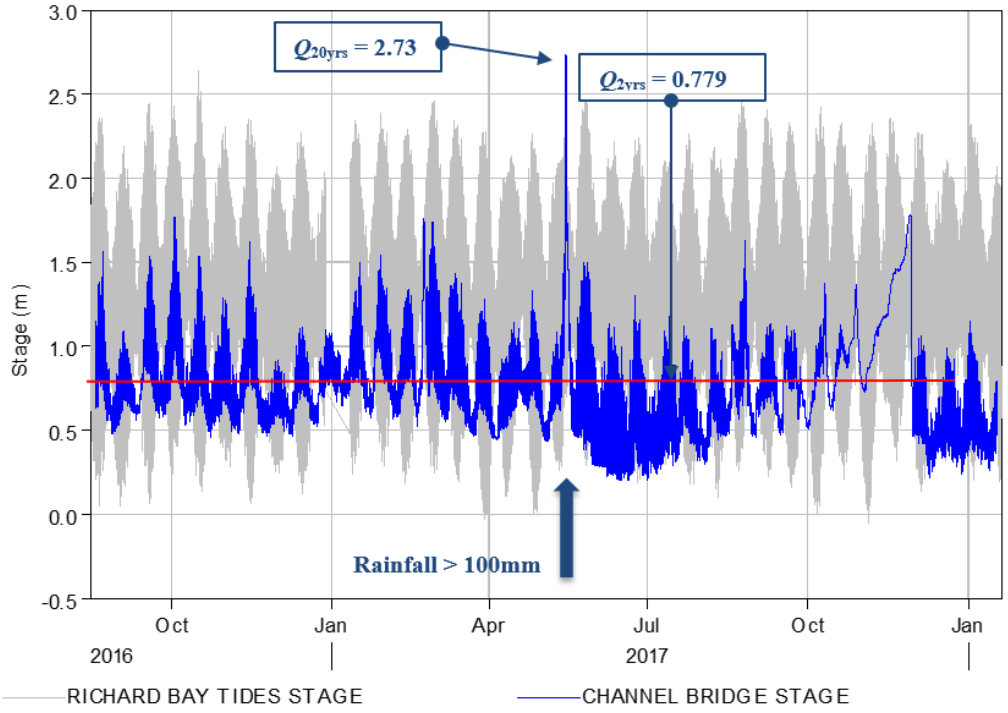

Figure 3.10: The hourly observed water level data (blue) near U-shape bend (Channel Bridge), about 5km upstream of the mouth

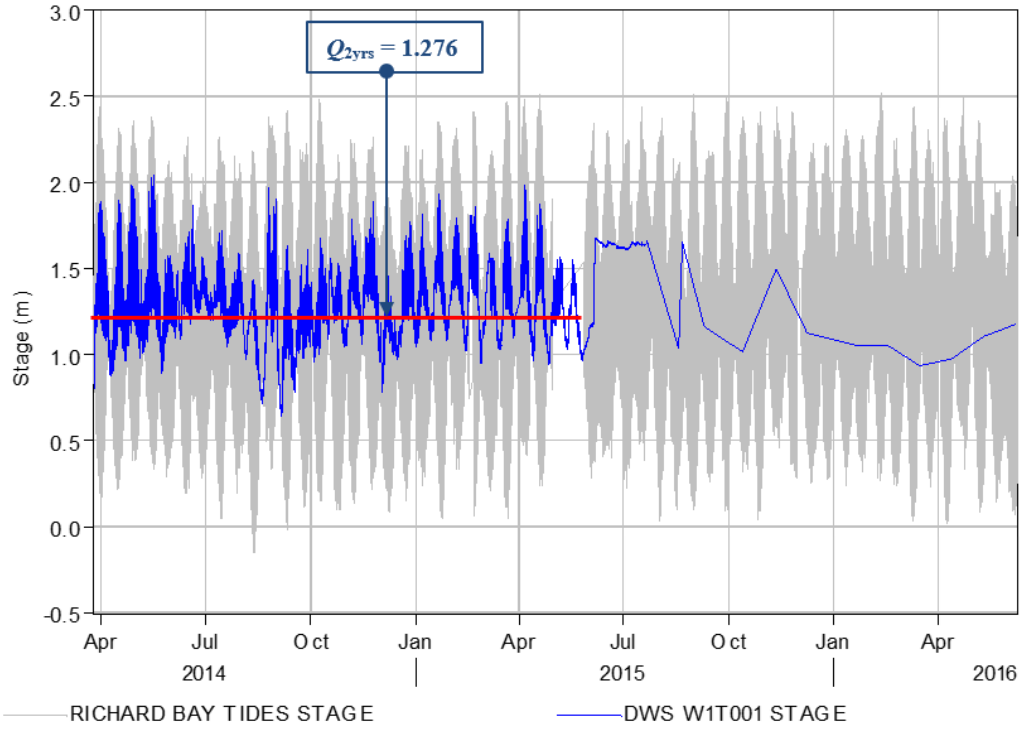

Figure 3.11: The observed water level elevation data from DWS tidal data (W1T001), about 500m upstream of the mouth. The logger failed in May 2015 when it was flooded, and all subsequent readings were manual observations at random periods of the tidal cycle.

Photograph 3.12: DWS officials preparing ADP measurement at W1T001 tidal station (photo by le Roux).

3.6 Marine Tidal interaction

The marine tidal data could not be measured for the Mlalazi Estuary, so it was necessary to acquire the sea level data from a Richards Bay site. The Hydrographic Office for the South African Navy based in Richards Bay supplied the marine tidal data plotted in Figure 3.12 for the period from 2013 to 2018. The marine tides (ebb and flood) have a large influence on the hydrodynamics of the estuary. Tidal data will be incorporated into the estuary numerical model as a downstream boundary condition.

The marine tidal wave has been observed to propagate upstream to the confluence with the catchment river 12km upstream (Figure 3.13) under drought conditions but there was no indication that the salt water wedge reached the confluence. From the salinity observations, Kelbe *et al.*, (2019) indicated that the tidal prism could extend approximately 6km upstream from the mouth, suggesting the tidal wave at the confluence was due to backup storage.

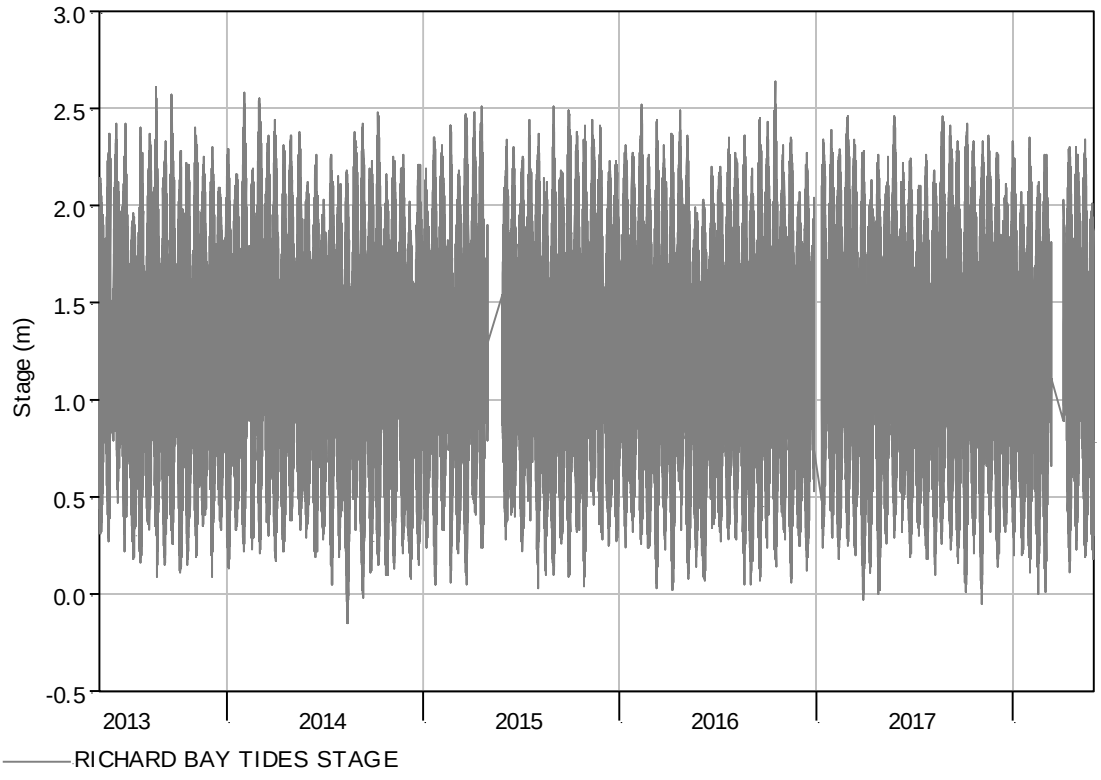

Figure 3.12: The tidal data (hourly) for Richards Bay, sourced from SA Navy, Hydrographic Office

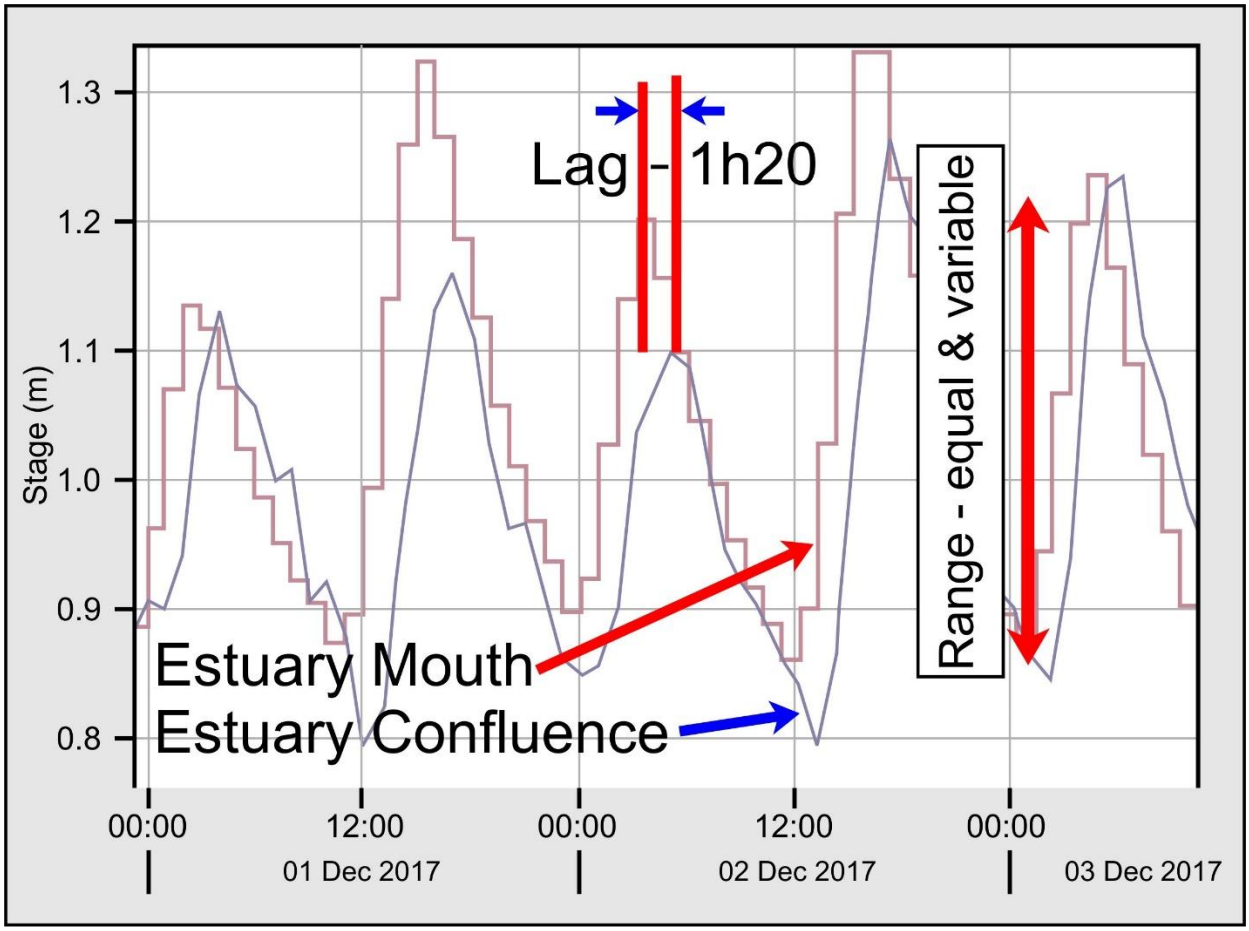

Figure 3.13: The simultaneous water level measurements at the mouth and confluence illustrating the magnitude, lag and attenuation of the tidal wave under conditions of no fluvial inflow (Kelbe *et al.*, 2019)

3.7 Flood Events

The 1987 flood was the largest measured event since records began and caused considerable flooding in the estuary (Photograph 3.13). The regional rainfall for the Mlalazi Catchment was analysed by various organisations. Kovacs (1988) indicated that this event may have been greater than a 1:100-year event (more like a 1:150-year event) but other analyses indicated the rainfall may have been greater than the 1:200-year values (Adamson, 1981). Kovacs used a Slope Area Method (SLA) to determine the regional maximum flood (RMF) of 930m^3/s for the Mlalazi Estuary on the 29/09/1987. The method has a model error of <30%. The slope area method (SLA) is entirely based on a numeric calculation of the Manning's equation for determining discharge, written as:

$Q = \frac{1.486}{n} AR^{2/3} S^{1/2}$	*(3-1)*

Where: Q = is the discharge, n = Manning's roughness coefficient, A = cross-sectional flow area, R = hydraulic radius of the flow (area/wetted perimeter), and S = is the slope [drop in elevation/length (dimensionless)].

The slope-area method is a function of slope, channel dimensions and channel roughness, and therefore field data are required for an estimation of peak discharge. These hydraulic data include determining the elevation and location of high-water marks along the stream indicated by debris, measurement of channel cross-section and wetted perimeter by surveying, and selection of a roughness coefficient for the section of stream in question. Using these observations after the 1987 flood, Kovacs (1988) calculated a maximum discharge rate of over 900m^3/s.

Photograph 3.13: The 1987 flood event at the R102 road bridge (old N2) within the Mlalazi Estuary (photo by Anon)

A number of river transects were surveyed at strategic locations along the Mlalazi Estuary (Figure 3.14) by Badenhorst *et al.*, (1989). The river transects or cross sections (Figure 3.15 – 3.19) were surveyed using a dumpy level surveying instrument and flow levels were determine using high water marks or debris on trees and bridge pillars. The survey also indicated major flood levels in 1932 and 1969 at the N2 Bridge (Figure 3.15) and Railway Bridge (Figure 3.17). The most important thing about this historical data is that the river cross sections or transects were surveyed before and after the 1987 flood event, to determine the amount of sediments that had been scoured and/or deposited. The surveyed data by Badenhorst *et al.*, 1989 shows little erosion or scouring of sediments along main channel even after the major flood event of 1987.

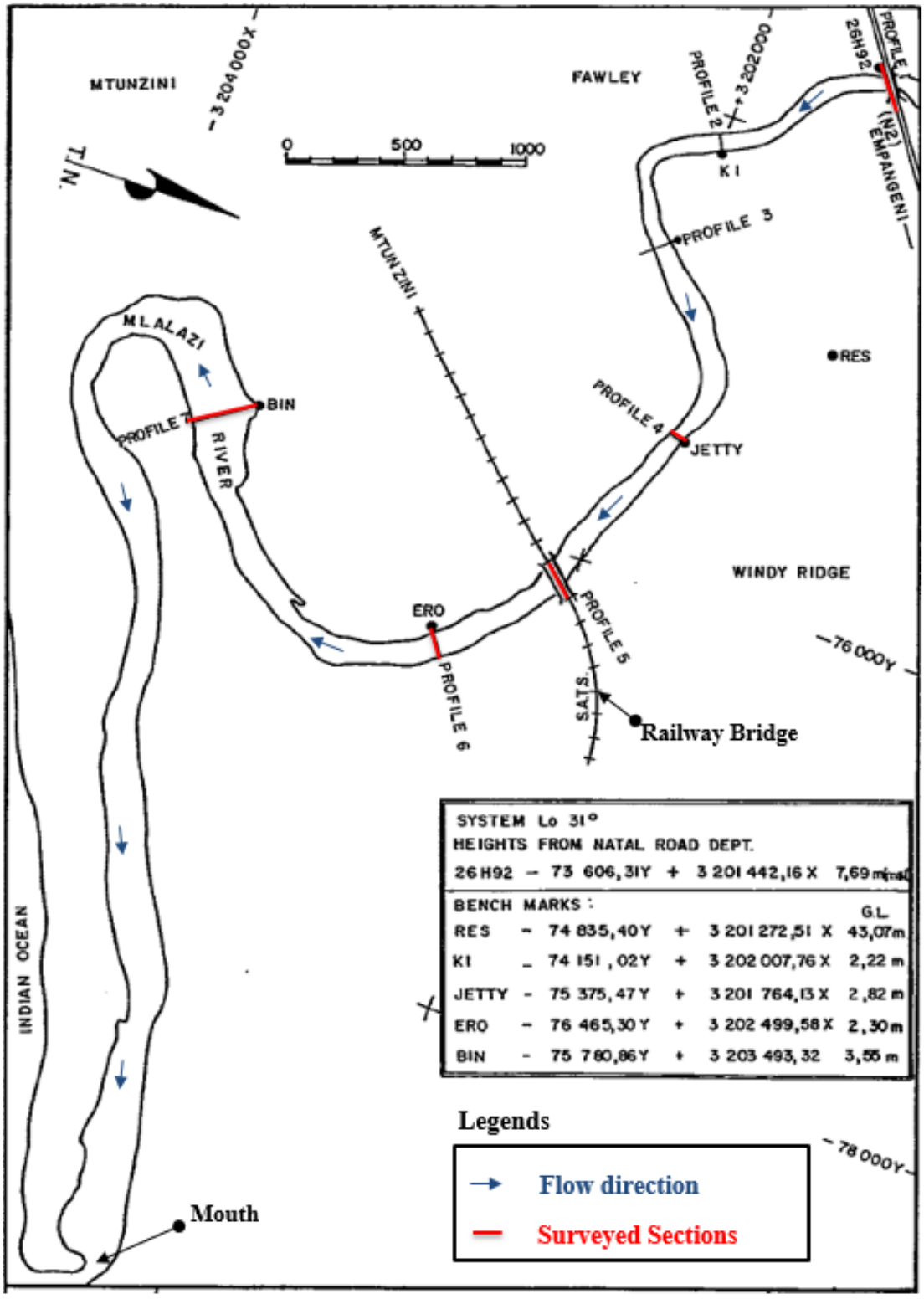

Figure 3.14: The historical 1987 flood survey of the river cross sections within Mlalazi Estuary (Badenhorst *et al.,* 1989).

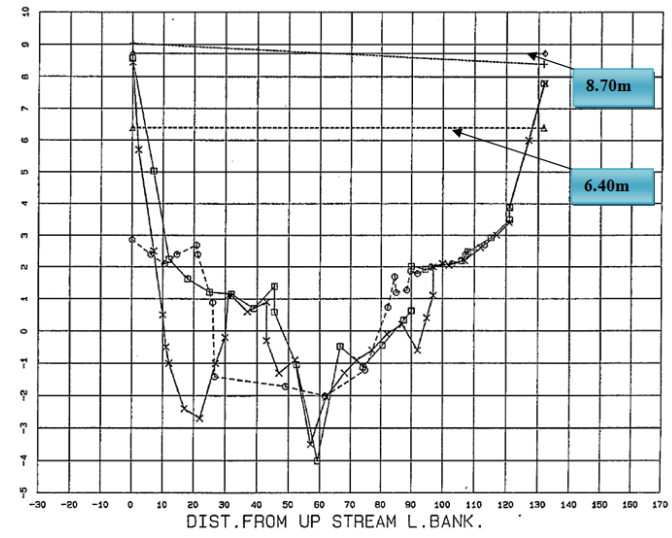

Figure 3.15: The measured water levels at N2 Road Bridge for 1969 and 1987 flood events. Pre and post cross-sectional data surveyed on the 24/02/1987 and 11/10/1987 (Badenhorst *et al.*, 1989).

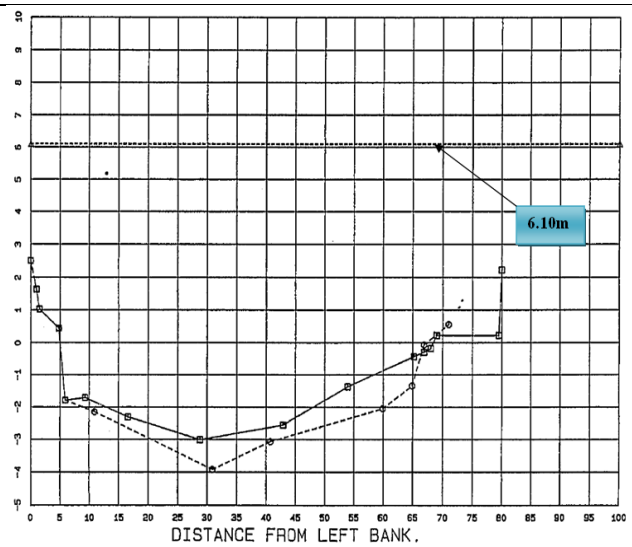

Figure 3.16: The measured water level downstream of the N2 Road Bridge for 1987 flood event. Pre and post cross-sectional data surveyed on the 24/02/1987 and 11/10/1987 (Badenhorst *et al.*, 1989).

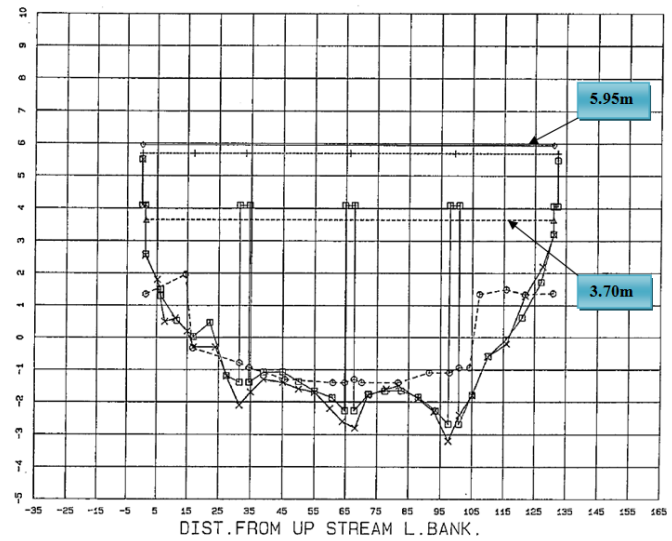

Figure 3.17: The measured water levels at the Railway Bridge for 1969 and 1987 flood events. Pre and post cross-sectional data surveyed on the 24/02/1987 and 11/10/1987 (Badenhorst *et al.*, 1989).

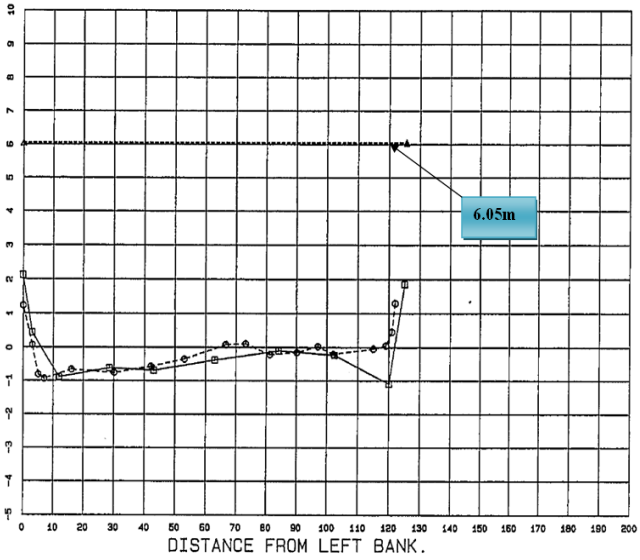

Figure 3.18: The measured water level 600m downstream of the Railway Bridge for 1987 flood event. Pre and post cross-sectional data surveyed on the 24/01/1987 and 11/10/1987 (Badenhorst *et al.*, 1989).

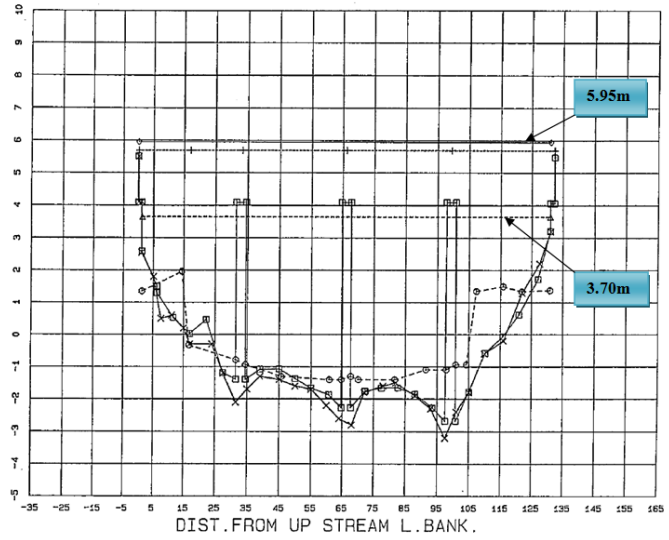

Figure 3.19: The measured water level for 1987 flood event approximately 4km upstream of the mouth. Pre and post cross-sectional data surveyed on the 24/02/1987 and 11/10/1987 (Badenhorst *et al.*, 1989).

It is important to note that the flood survey method depends on high-water marks, reliable equipment and experienced surveyors to successfully carry it out. High-water marks are determined from the upper limit of stains and debris deposited on the trees, hydraulic structures (bridge) and buildings. Brunner (2008) highlighted the following challenges encountered when estimating flood marks:

- The debris lines can be caused by wind and wave actions to be higher than the actual water level.
- Capillary action (adhesion and cohesive forces) causes high-water markings on buildings and bridge piers to be elevated upward.
- Flood marks on bridge piers are often equal to the energy gradeline, not the average water level.
- High-water marks on the floodplain or riverbank are often higher than the water level in the main channel particularly if the channel flow is supercritical. Water is moving slower on the overbank and may be closer to the energy gradeline.

The flow velocity from the 1987 flood events at strategic locations within the Mlalazi Estuary was estimated by flood survey data (cross-sectional area) for a RMF of 930 m^3/s derived by Kovacs (1988). For any given flow in a natural channel, the discharge (Q) at a cross section is expressed by:

$Q = VA$	*(3-2)*

Where: A = is the flow cross-sectional area normal to the direction of the flow and V = is the average flow velocity.

The depth-averaged flow velocity is defined as the discharge divided by the cross-sectional area. The 1987 bathymetric data was used to determine the channel slope, hydraulic radius and cross-sectional areas. This was done in order to calculate discharge (Q) using equation 3-1. Then depth-average velocities were estimated at N2 Bridge and Railway Bridge for 1969 flood event at various sites along the estuary. The 1969 event had the same magnitude as the 2018 event (Photograph 3.14 & 3.15). A summary of the estimated depth-averaged flow velocities at the Mlalazi Estuary (Badenhorst *et al.,* 1989and Kovacs, 1988) is indicated on Table 3.1 and used for model calibration. The following factors influence the flow velocity distribution:

- Presence of river bends/curves
- Shape of the cross-sectional area
- Channel slope and roughness of the boundaries
- Flow obstructions across the main channel due to the presence of hydraulic structures (bridge piers) and rock outcrops.

Table 3.1: Estimated flow dynamics data from 1969 and 1987 flood surveyed in the Mlalazi Estuary (from Badenhorst *et al.* 1987).

Date	Location	*Flow (m^3/s)	Cross-sectional Area (m^2)	Flood Level (m)	Velocity (m/s)
1969	N2 Road Bridge	522	804.11	6.40	0.65
11/10/1987		930	1064.58	8.70	0.87
11/10/1987	D/S of N2 Bridge	930	616.375	6.10	1.51
1969	Railway Bridge	522	583.39	3.70	0.90
11/10/1987		930	828.286	5.95	1.12
11/10/1987	D/S of Railway Bridge	930	786.154	6.05	1.18
11/10/1987	Middle estuary (bend)	930	1508.145	4.95	0.62

*RMF: slope area method D/S: downstream flood level: Badenhorst *et al.* 1987

The 1984 Cyclone Domonia caused catastrophic flooding along the east coastline of South Africa. The isohyetal map of the rainfall storm on the 28/01/1984 – 02/02/1984 by Kovacs *et al.*, (1985) indicated a rainfall of 500mm (coastal) and 400mm (inland). The flood peak of this cyclone was never measured within the Mlalazi Estuary. However, the peak stage above the confluence (at W1H012 gauging weir) reached an elevation of over 9m above the weir datum (DWS, 2018). In 2018, a significant flood was experienced in the catchment where the flood peak reached a stage of 7.28 mMSL and 3.20 mMSL, which were measured at the upper estuary (confluence) and lower estuary (bend/channel bridge) respectively (Figure 3.20). It can be seen from Photographs 3.14 & 3.15 that the old arch and R102 road bridges back flood or confined flow upstream during the 2018 storm event with less influence on the downstream dynamics (turbulent or super-critical flow). The exact amount of rainfall for this event is unknown but the magnitude of flooding is slightly lower than the floods caused by the 1984 Domonia Cyclone event. Therefore, this event would show a return period of approximately 1:50-year flood.

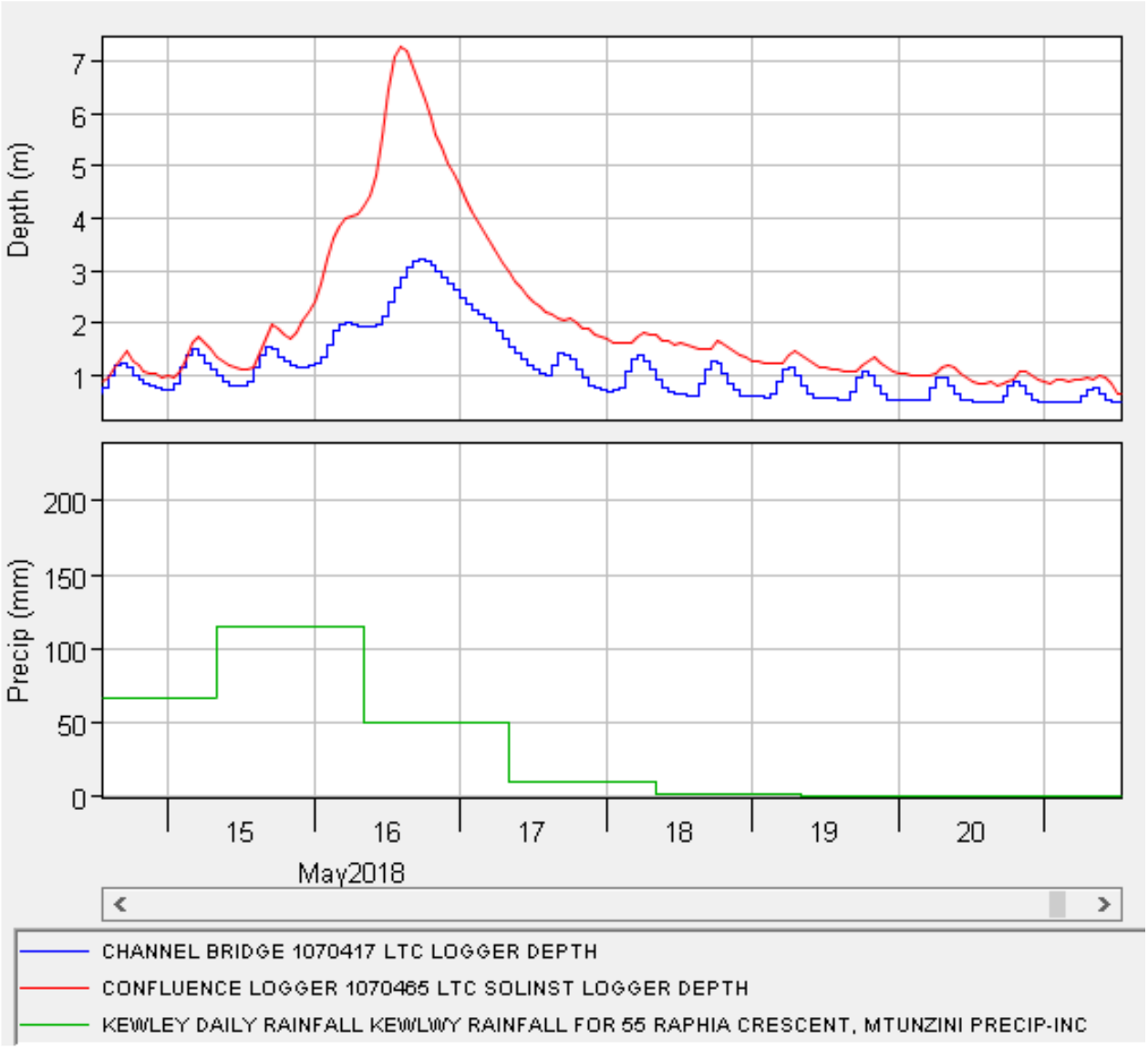

Figure 3.20: The simultaneous measurements of the river stage (upper graph) at the confluence (red line) and lower estuary (blue line) approximately 4 km from the mouth. The lower graph shows rainfall recorded along the coastal region (Kelbe *et al.*, 2019).

Photograph 3.14: Old Arch Bridge and R102 Concrete Bridge in the upper estuary during the May 2018 flood event several hours after the peak flood (Photo by Kelbe)

Photograph 3.15: Turbulent (super-critical) flow under R102 Road Bridge during the rising flood event in May 2018 (Photo by Kelbe)

Another major rainfall event of 100 mm was recorded in May 2017 along the inland area that caused considerable flooding in the Mlalazi Estuary. The flood peak for this rainfall event was 2.73 mMSL near the U-shape bend (bridge channel) in the lower estuary (Figure 3.21). The old canals in the sugar cane fields between the prawn farm and the estuary in the nature reserve were flooded (Photograph 3.16). This event would show a return period of approximately 1:20-year flood return**.**

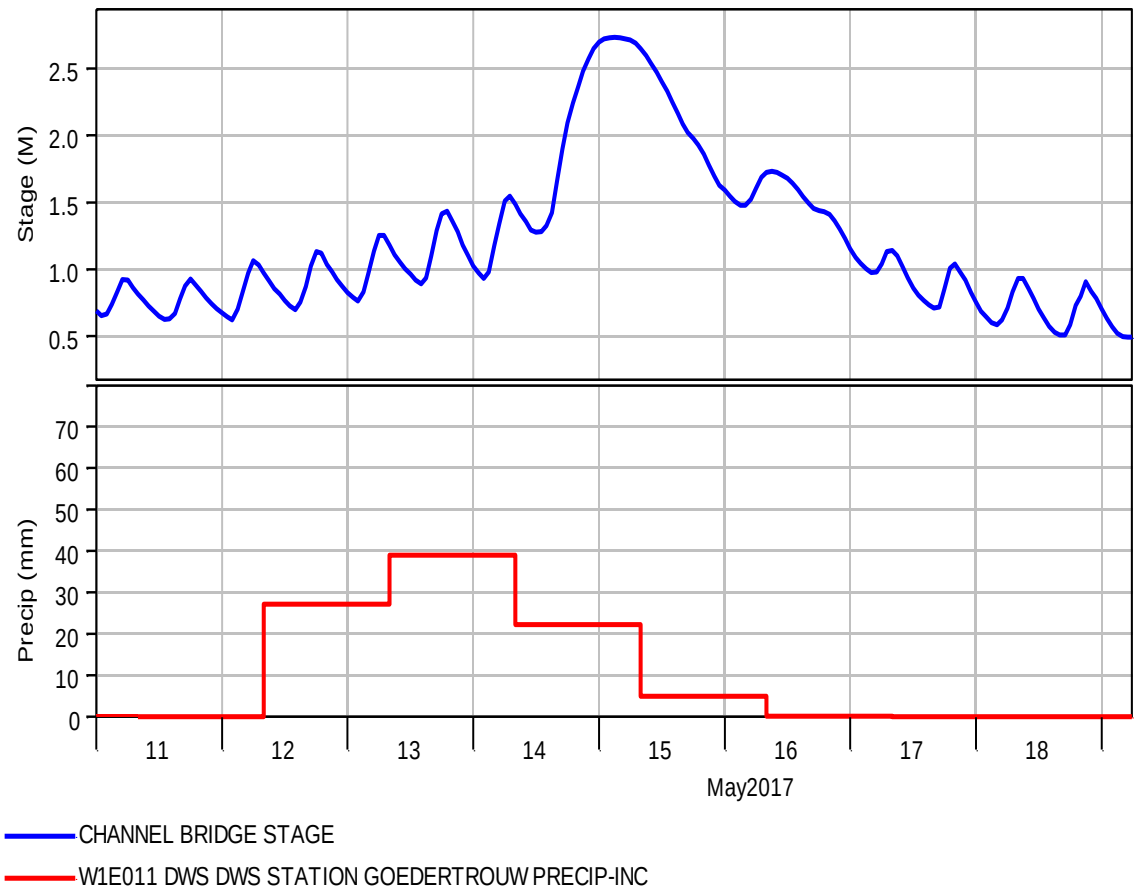

Figure 3.21: The upper graph shows the recorded river stage at the lower estuary (blue line) and the lower graph is the rainfall data (red line) recorded along the inland region.

Photograph 3.16: Extent of the inundation of the old, canalised sugar cane fields between the prawn farm and the estuary in the Mlalazi Nature Reserve.

The probable magnitude of the flood from the identified events is summarised by the measured water level data in the Mlalazi Estuary in Table 3.2. These observations have been used for hydrodynamic model calibration and validation in a subsequent section.

Table 3.2: Observed water level data in the Mlalazi Estuary.

Measured Sites	Distance from the confluence (km)	Probable Flood Event	Sourced	Date	Peak Level (mMSL)
Confluence	0.00	1:10	LTC logger	19/02/2018	3.88
		1:50	LTC logger	16/05/2018	7.28
		1:100	Rasifudi, 2019	2019	9.00
N2 Road Bridge	2.00	1:50	1969 Survey	1969	6.40
		1:100	1987 Survey	27/09/1987	8.70
D/S of N2 Road Bridge	4.00	1:100	1987 Survey	27/09/1987	6.10
Railway Bridge	5.30	1:2	Ezemvelo logger	2015 - 2016	1.15
		1:50	1969 Survey	1969	3.70
		1:100	1987 Survey	27/09/1987	5.95
D/S of Railway Bridge	6.05	1:100	1987 Survey	27/09/1987	6.05
Middle Estuary	7.92			27/09/1987	4.95
Lower Estuary (Bend/Channel Bridge)	9.29	1:2	LTC logger	2016 - 2017	0.779
		1:20	LTC logger	15/05/2017	2.73
		1:50	LTC logger	16/05/2018	3.20
Mouth (Tidal Station)	12.0	1:2	DWS Station	2014 - 2015	1.276

D/S: downstream

CHAPTER 4. MODEL CONFIGURATION

As stated previously, model configuration requires considerable equipment and hydraulic structures, which are expensive and time consuming, to directly measure water level, flow rate and discharge continuously within the Mlalazi Estuary. While the Department of Water and Sanitation (DWS) and other organisations (Ezemvelo Wildlife) have conducted limited water level measurements, there are insufficient flow measurements to provide a full understanding of the flow dynamics of the estuary.

The most practical method of determining the hydrodynamics of the estuary over the full range of fluvial events is through the development and application of a suitable numerical model of the controlling system that is well calibrated and validated. However, all numerical models must be developed based on a well-grounded conceptual model derived from available information and field measurements of physical drivers of physical systems. This chapter describes the approach and methods used to set up and calibrate the HEC-RAS flow dynamic models.

4.1 Model Setup

The configuration of the HEC-RAS estuarine model(s) required reliable simulation of the flow and sediment dynamics, which required the following accurate and reliable geometric, hydraulic and hydrologic data:

a) geometric data consisting of cross-sectional geometry transects (width, depth, etc.) of the estuary channel and adjacent surrounding floodplain perpendicular to the flow path;

b) hydraulic data comprising the channel gradient (slope) friction characteristics and energy gradient; and

c) hydrologic data describing the flow discharge and sediment from the upstream catchment.

The upstream end of the Mlalazi Estuary begins just before the confluence of the Mlalazi River and its tributary the Ntuze River. The active flow path in the estuary channel is about 12 km

long from the upstream end to the mouth. For this channel length, a total of 174 cross sections at different interval spaces, ranging from 60m to 200m, were constructed within the Mlalazi Estuary (Figure 4.1). These geometric transects (cross sections) were derived from a 1 m digital elevation model (DEM) sourced from Kelbe per comm and the 12km river bathymetric data described in the previous section. The interval spacing depended on the rate of change in the transect profile.

The river cross sections were digitised in ArcGIS across the channel and floodplain DEM using the support program, HEC-geoRAS, which is also made available by USACE. The order of digitisation was from the left side to the right side facing the downstream direction. Normally, the HEC-RAS estuarine flow model simulates the river flow rate and water level in a downstream direction (backwater calculations). For this reason, all cross sections needed to be digitised in the same downstream direction and perpendicular to the main river channel and flow path in the floodplain. The river sections were extended across the floodplain to an elevation of 10 m (above MSL), the height of the maximum recorded flood event. The distances between each cross section was derived based on flow uniformity and close enough to each other to avoid model instability, especially when running a continuous (unsteady) flow simulation.

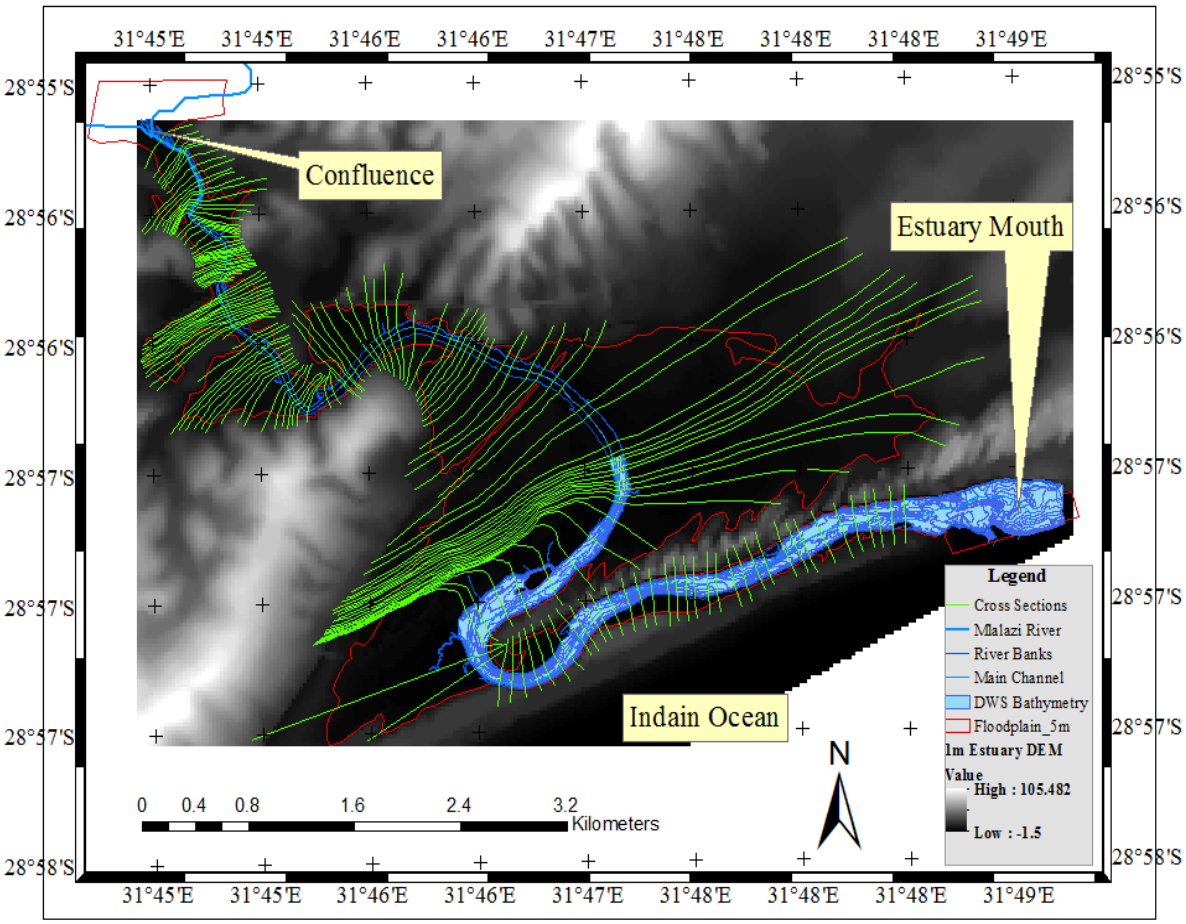

Figure 4.1: Geometric data of the Mlalazi Estuary derived from HEC-geoRAS

Normally, when the cross sections are spaced too far apart, the computational algorithm may become unstable and have difficulty balancing the energy between subsequent sections (HEC, 2016). The HEC-RAS program allows one to interpolate or insert additional sections between the immediate upstream and downstream sections where instabilities occur. This alleviates the need to go back to HEC-geoRAS for generating the additional cross sections. There are various river sections that were inserted (Figure 4.2) to avoid the instability issues especially around the sharp river bends within the estuary.

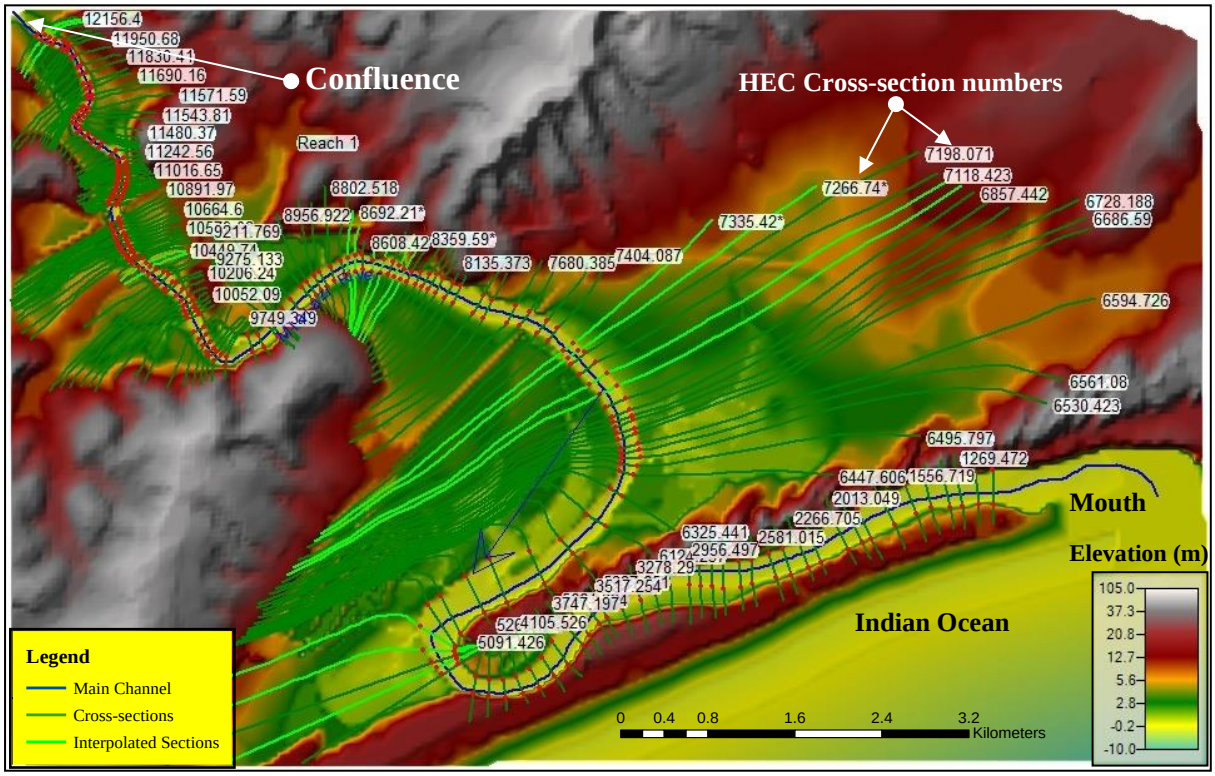

Figure 4.2: Imported geometric data for the Mlalazi Estuary on HEC-RAS. The imported river cross sections (green) and the "interpolated" river sections (lime), where each transect is labelled on the left with a station number that represents the distance upstream from the mouth boundary transect

4.2 Upstream Boundary Conditions

The river inflow and sediment transported from the upstream Mlalazi Catchment are the main drivers that control the estuary dynamics. Therefore the river discharge series and extreme events form the upstream boundary condition for the estuary model. The catchment model (HEC-HMS numeric model) was used by Rasifudi (2019) to simulate the continuous run-off/discharge and sediment load (Figure 4.3) of the Mlalazi River. The simulated record is for a 68-year period, from 1949 to 2018, which incorporated a full range of extreme storm events. The catchment model used rainfall as the main input parameter to simulate the Mlalazi River run-offs. The 15-year observed flow data from the Ntuze River Nested Catchment was used to calibrate and validate the model (Rasifudi, 2019).

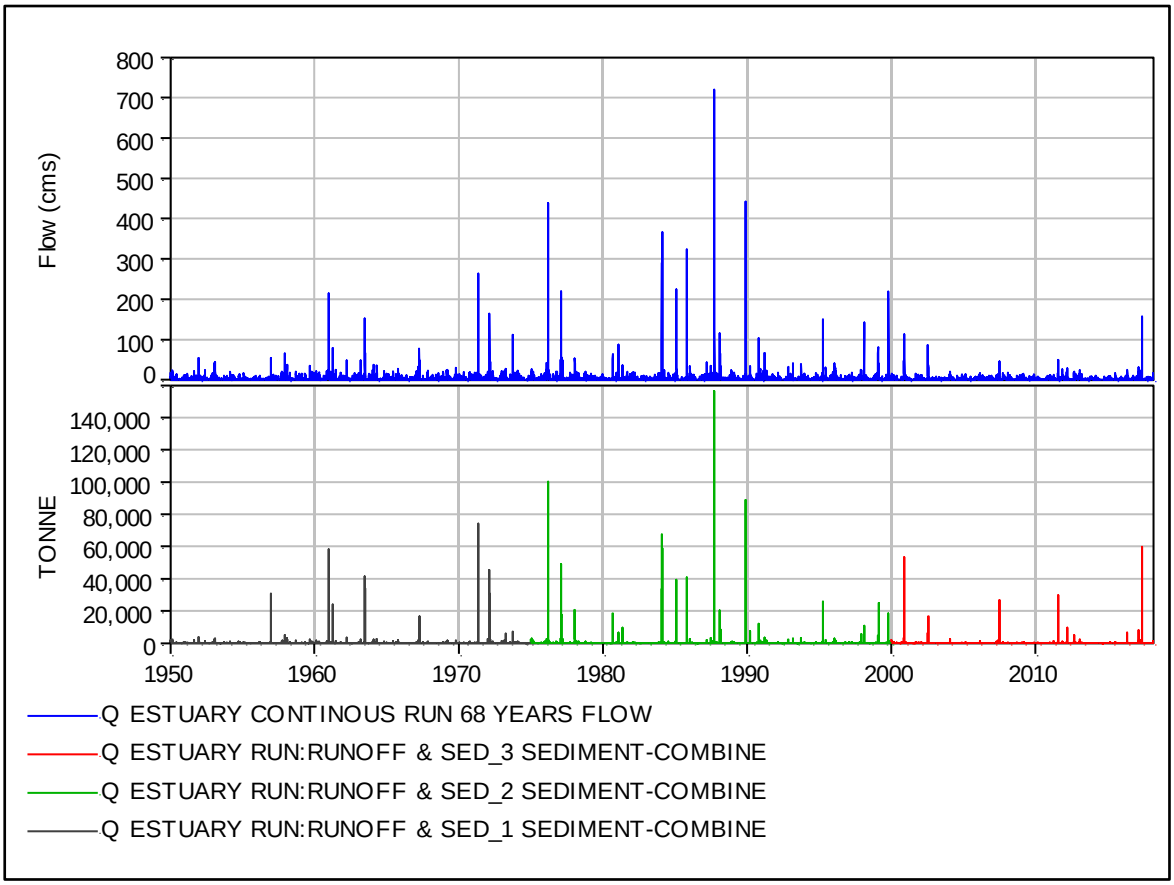

Figure 4.3: Daily simulated flow (m^3/s) and sediment load (tonnes/day) from the Mlalazi River from 1950 to 2018 derived using the catchment model (HEC-HMS) (Rasifudi, 2019)

The flow and sediment data was saved in HEC-DSS program and supplied by Rasifudi (2018). The Hydrologic Engineering Center – Data Support System (HEC-DSS) is a database system designed by US Army Corps of Engineers (USACE) to efficiently store, analyse, display and retrieve hydrologic data. The HEC-DSS program has an HEC-DSSVue (HEC-DSS Visual Utility Engine), which is a graphical user interface (GUI) program for viewing, editing and manipulating the database files. The HEC-DSS database in this study was used to calculate a frequency distribution plot (Figure 4.4) of the Mlalazi River inflow, derived from the catchment model run-off for the 68-year predictions. The probability of events of various flow rates (Q_{2yr}, Q_{10yr}, Q_{20yr}, Q_{50yr} and Q_{100yr} return period), was obtained from the fitted exponential curve.

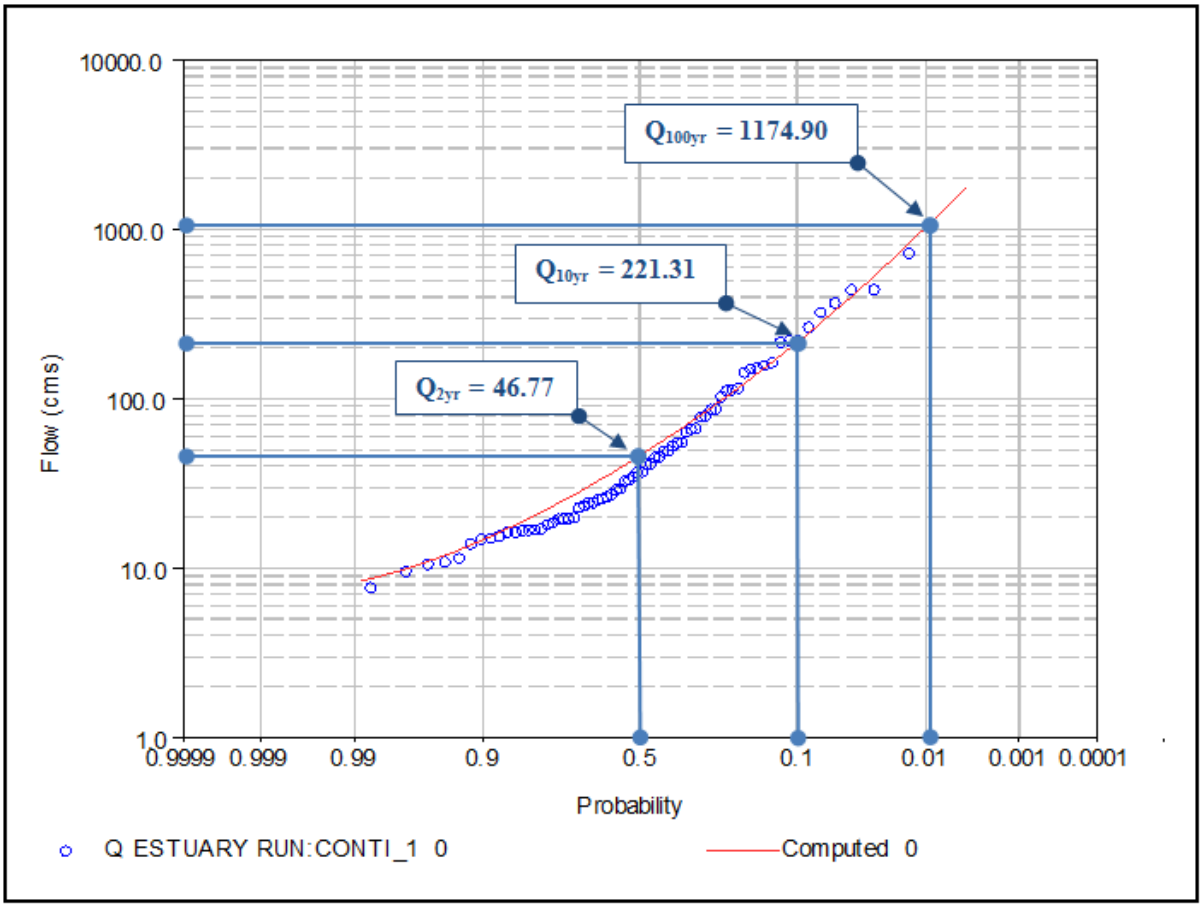

Figure 4.4: Frequency distribution curve for simulated flow data of the Mlalazi River derived from the Catchment Model (HEC-HMS) (Rasifudi, 2019)

The flood events for various return periods shown in Table 4.1 were entered as the upstream boundary conditions for steady flow routing at the HEC River Station (RS) number: 12156.4 on the upper estuary (confluence). The friction slope ($\bar{S}_f = 0.001$) was obtained from the river bathymetry and entered as the downstream boundary condition. The Q_{2yr} return flood represents the average flow (the value is equalled or exceeded one in every two years) within the Mlalazi Estuary. The Q_{10yr}, Q_{20yr}, Q_{50yr} and Q_{100yr} return periods are represented by flood events that were observed on the Feb 2018, May 2017, Domonia/Imboa Cyclones and 1987 extreme flood respectively.

Table 4.1: Upstream boundary condition data derived from frequency distribution plot (Figure 4.4)

Source	Peak Discharge (m^3/s) for Various Return Periods					Upstream Boundary Location
	Q_{2yr}	Q_{10yr}	Q_{20yr}	Q_{50yr}	Q_{100yr}	
Catchment Model (HEC-HMS)	46.77	221.31	371.54	767.36	1174.90	Confluence

4.3 Flow Routing Model

- The HEC-RAS flow model is a widely used numeric model that simulates the hydraulics of water flow through open channels (e.g., river, canal, dams, estuary, etc.) and floodplains. The assumptions applicable to the HEC-RAS flow model were obtained from publications (Chow, 1959) and HEC (2016). The assumptions are as follow:

- Steady flow is applicable for the Mlalazi Estuary due to steep, well-defined channels and extensive inundation of the adjacent low-lying areas.

- Unsteady flow conditions are applicable during flood events, whereby the flow velocity varies due to the presence of hydraulic structure and river bends.

- Flow is non-uniform in which the depth, discharge and average velocity along the length of the channel gradually vary along the length of the channel.

- Flow is strictly one-dimensional, and velocity is in the direction of flow only.

4.3.1 Steady Flow Routing

Steady flow routing in an open channel is based on the solution of the one-dimensional conservation of energy equation (Bernoulli's Equation), given in Equation (4-1). The model calculates the flow velocity (V_i) and water level (Y_i) from one river cross section to the next by solving the energy equation (4 -1) with a given flow rate, through the process called the standard step method (STM). The STM is a computational technique installed within the HEC-RAS program, used to simulate one-dimensional (1D) surface water elevation in open channels with constant mixed flow under steady state conditions. Figure 4.5 shows the conceptualisation

of terms in the energy equation between two cross sections. The assumption for steady flow simulation is that no energy is lost or gained between river sections.

$$Z_2 + Y_2 + \frac{a_2 V_2^2}{2g} = Z_1 + Y_1 + \frac{a_1 V_1^1}{2g} + h_e \qquad (4\text{-}1)$$

The potential energy in Equation 4-1 is represented by elevation of the main channel (Z_2, Z_1), kinetic energy is characterised by the velocity head ($\frac{a_2 V_2^2}{2g}$,$\frac{a_1 V_1^1}{2g}$), the pressure head (water surface elevation in mMSL) at river sections (Y_2, Y_1) and the energy head loss (h_e). Energy head losses (h_e) are defined by the friction losses and contraction or expansion losses between two cross sections (Equation 4-2). The equation for the energy head loss is as follows (HEC, 2016):

$$h_e = L\bar{S}_f + \mathrm{C}\left|\frac{a_2 V_2^2}{2g} - \frac{a_1 V_1^1}{2g}\right| \qquad (4\text{-}2)$$

The friction loss for steady flow routing in HEC-RAS is a function of the friction slope ($\bar{S}_f$) over a specified distance derived from a weighted reach length (L) between two cross sections. The friction slope at each river transect is calculated from the Manning's equation (4-3) as an average conveyance. The expansion or contraction loss coefficient (C) is applicable when the flow jumps from the sub-critical to critical or super-critical, as suggested for a specific event shown at the R102 Road Bridge (Photograph 3.11 & 3.12) during the May 2018 extreme flood event.

Table 4.2: Typical 'C' values for sub-critical flow contraction and expansion coefficient (HEC, 2016)

	Contraction	Expansion
No transition loss computed	0.0	0.0
Gradual transition	0.1	0.3
Typical bridge sections	0.3	0.5
Abrupt transition	0.6	0.8

Where there is small change in a river channel, the flow tends to be subcritical, and thus the coefficients of contraction and expansion values are changed to 0.1 and 0.3, respectively. The maximum value for the contration and expansion coefficient is 1.0.

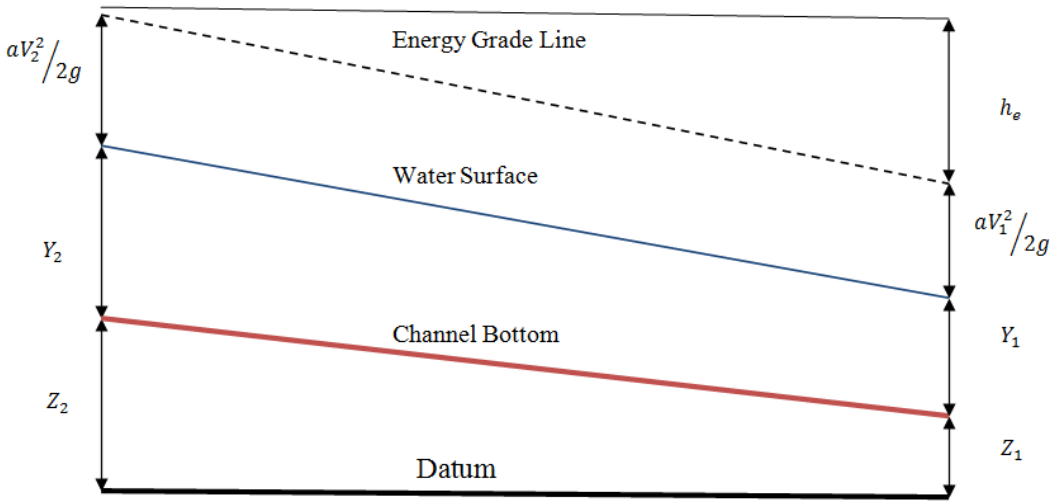

Figure 4.5: Systematic diagram representing the energy equation (HEC, 2016.

Figure 4.6 shows the total conveyance for the cross section which is obtained by adding the three subdivision conveyances (left bank, main channel and right bank). Conveyance is determined within each subdivision from the Manning's equation:

$Q = KS_f^{1/2}$	*(4-3)*

$K = \frac{1.486}{n} AR^{1/2}$	*(4-4)*

Where: K = conveyance for subdivision, n = Manning's roughness coefficient for subdivision, A = flow area for subdivision, R = hydraulic radius (area/wetted perimeter) for subdivision.

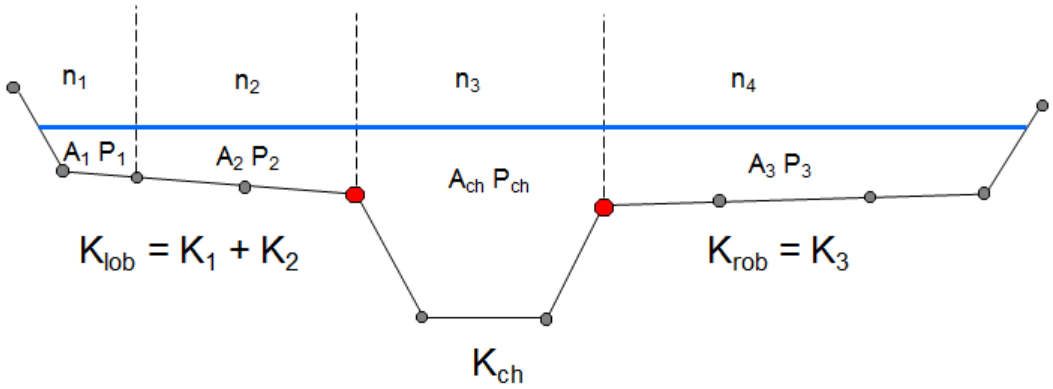

Figure 4.6: Illustration of the Conveyance Subdivision Method (HEC, 2016)

Figure 4.7 shows a cross-sectional profile across the extensive floodplain below the Railway Bridge where there are different vegetation types (sugarcane, canals, mud flats, mangroves, reeds etc.). On the left floodplain, mainly sugar plantations are found, making it easy to determine the Manning's 'n' roughness for high flows. However it should be noted that the n-value for low-medium flows will be different due to drainage canals that quickly channel flow into the main river system. The floodplain on the right has different vegetation types and therefore a weighted average n-value was determined. This process will be explained further in the calibration section (Chapter 5).

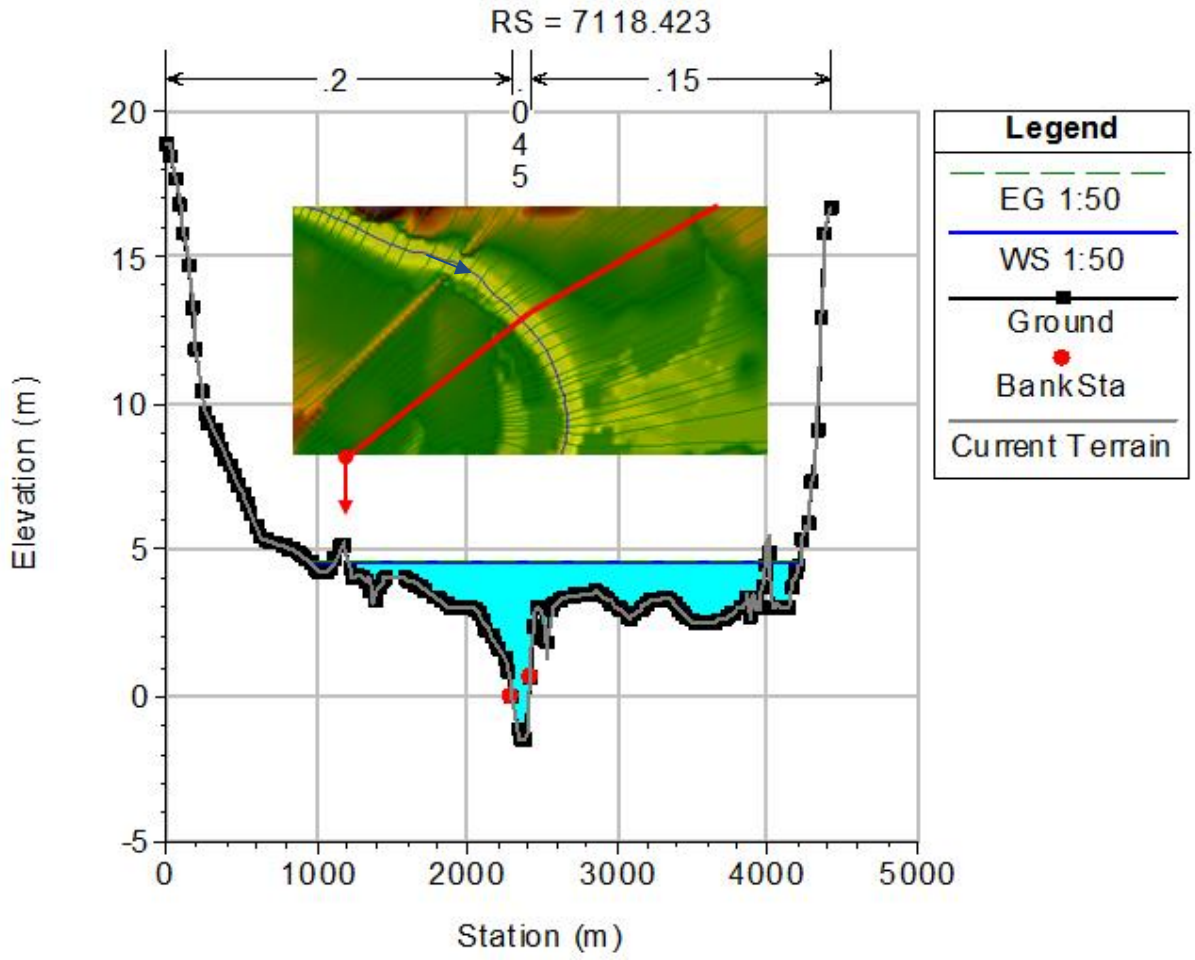

Figure 4.7: The cross-sectional profile below the Railway Bridge showing the different vegetation types. The R.S. represents the river cross section number (7118.423) generated from the HEC-geoRAS model.

Equations 4-1 and 4-2 were used to determine the unknown surface water elevation at the downstream cross section. The computation procedure of the standard step method (STM) uses the following iterative steps:

a) The program assumes a water surface elevation (WS) at the river cross section for a subcritical profile or upstream cross section if a supercritical profile is being calculated.

b) Based on the assumed water surface elevation (WS), the corresponding total flow conveyance and velocity head are determined.

c) Using values from the second step to calculate friction slope ($\bar{S}_f$) to then solve Equation 4-2 for determining the energy head loss(h_e).

d) The energy equation 4-1 is solved for $WS_2 = Z_2 + Y_2$ using values from the second and third step.

e) The program then compares the calculated value WS_2 with the value assumed in the previous step; repeat the first step through to the last until the values agree to within specified limits (0.003m).

4.3.2 Unsteady Flow Routing

The flow in an open channel is unsteady if the depth of flow changes with time (Chow, 1959). The unsteady flow routing in the HEC-RAS program solves the mass conservation and momentum conservation equations (1-D Saint Venant Equations) using an implicit finite different method. For unsteady flow, only friction loss is used. The unsteady flow dynamic equation solver in HEC-RAS was adapted from Dr. Robert L. Barkau's Unsteady Network Model (UNET) in 1992. In the implementation of the conservation of mass and momentum equations (4-5 & 4-6), the overbank and the main channel are assumed to have the same water surface, even though the overbank flow volume and conveyance are separated from the main channel flow volume.

The conservation of mass (continuity) equation (4-5) is developed by adding up the rate of flow at which mass is flowing in and out of a control volume and setting the net in-flow equal to rate of change of storage. The momentum equation (4-6) represents the rate of change of velocity with respect to time for a control volume. The conservation of momentum is measured by the rate of change in momentum which is equal to the external forces (hydrostatic pressure, gravity and friction) acting on the system (HEC, 2016).

$\frac{\partial A}{\partial t} + \frac{\partial Q}{\partial x} - q_1 = 0$	*(4-5)*

$\frac{\partial Q}{\partial t} + \frac{\partial (VQ)}{\partial x} + gA(\frac{\partial z}{\partial x} + S_f) = 0$	*(4-6)*

Where: x = distance along the channel, g = acceleration of gravity, t = time, z = elevation of the water surface above a specified datum, q_1 = lateral inflow per unit distance, Q = flow, A =

cross-sectional area, S = storage from non conveying portion of cross section, S_f = friction slope and V = velocity

The equations (4-5) and (4-6) are solved using a four-point implicit box finite difference scheme. They are stored with a skyline matrix scheme and reduced with a direct solver developed specifically for unsteady river hydraulics (HEC, 2016). The river flow (Q) and stage (z) are simulated and stored at each cross section. The implicit finite different method is restricted in its ability to handle the transitions from subcritical to supercritical flow, since a different solution algorithm is required for different flow conditions. However, HEC-RAS overcomes this limitation by employing a mixed-flow routine to patch solutions in these reaches (Timbadiya *et al.*, 2011).

CHAPTER 5. MODEL CALIBRATION AND VALIDATION

Model calibration is the process of obtaining the best estimate of the model parameters by comparing the predicted and observed data for specific condition, with the specified parameters. Both manual and automated calibration methods were used in this project. The model parameters that were estimated for the hydrodynamic model to be evaluated and adjusted within acceptable limits are described in this section.

Parameters should indicate that the geomorphology (DEM) of the estuary has a direct influence on the flow dynamics. The relevant parameters (elevation profiles and cross sections) have been derived from physical measurements and it was assumed they are reliable, intransient and would not be adjusted during the calibration. The catchment run-off data by Rasifudi, (2019) was the best estimate available and was only evaluated during the model validation. The main unknown parameter was the roughness coefficient considered in the calibration process. However, it was also necessary to evaluate the accuracy and reliability of the available observation data used to calibrate the model in this section. This chapter also looked at the continuous flow simulation as an independent data set derived from the HEC-RAS (version 5.0) flow model. The simulation was used to test the calibration parameters from specific storm events in the Mlalazi Estuary.

Model validation is the process of showing that the calibrated model parameters continue to provide a reasonable estimate for some independent set observations. In addition, it gives an evaluation of the model's capability to accurately replicate known data (Uzair and Koran, 2017). Application of the model to an independent set of run-off events would describe the anticipated estuarine dynamics.

5.1 Calibration of the model

The calibration of models using standardised techniques requires a primary (historical) database of critical variables and statistical expertise. Knowledge and experience are used in categorising variables as dependent or independent. An equation-fitting method is subjectively chosen for the regression of dependent variables onto independent variables. Conventionally,

data-based regression is emphasised in this setting as "forward" regression. The principle is straight forward:

With adequate primary data, regression coefficients can be found that make the equation more adaptable to the data.

When primary data exist (thus providing a standard), regression equation errors can be computed. Supposedly, preliminary data are available for all system variables (subsystem). In that case, a composite error term should be included in the system equilibrium equation (subsystem) to account for the unavoidable algebraic imbalances. The observed stage data within the Mlalazi Estuary was obtained from a flood survey of several extreme storm events and additional water level measurements over the past four years, including that of 27/09/1987 (Badenhorst *et al.*, 1989) between the confluence and lower portion of the estuary (Table 3.2).

High watermarks, indicated by debris on trees and road bridges/piers, were used to measure water levels at various sites in the estuary for the 1987 flood survey. Photographs 5.1 and 5.2 give examples of such conditions for the 1987 and 2018 floods, respectively. The peak flow during the 1987 event was approximately 1-2m higher than the stage in these photographs, as shown by the accumulation of cane debris on the arch bridge (Kelbe, *per comm*).

Photograph 5.1: The old N2 Road Bridge several hours later the main flood peak had receded following an approximate 1:100-year rainfall event in September 1987 (photo by Kelbe).

Photograph 5.2: Storm debris along the river banks of the channel illustrating the elevation to which flood waters reached during the 2018 flood in the upper reaches of the estuary (photo by Kelbe)

The criteria for the estuarine flow model evaluation adopted for this study (HEC-RAS) involved the following:

- Net difference (predicted error) between observed and simulated water levels
- Per cent bias (*PBIAS*) for the steady flow event, which is defined as:

$$PBIAS = \left[\frac{\sum_{i=1}^{n}\left(Y_i^{obs} - Y_i^{sim}\right) * 100}{\sum_{i=1}^{n} Y_i^{obs}}\right] \qquad (5\text{-}1)$$

Where, Y_i^{obs} = observed water level (m); Y_i^{sim} = simulated water level (m) and n is the total number of observations. The ideal value of PBIAS = 0, which shows an accurate model simulation compared to the observed data. Positive PBIAS values indicate an understatement of the flow model and negative values an overstatement of the model (Gupta *et al.*, 1999). Based on the evaluation model guidance described by Moriasi *et al.*, (2007), the PBIAS of 25% is satisfactory, and >25% is unsatisfactory.

- Root Mean Squared Error (RMSE) for unsteady flow, which is defined as follows,

$$RMSE = \sqrt{\frac{\sum_i^N (W_o - W_s)^2}{N}} \qquad (5\text{-}2)$$

Where, W_o = observed water level (m), W_s = simulated water level (m) and N = total number of data points.

- The regression analysis where the regression curve is used to estimate a variable Y with its relationship to a variable X. The regression line indicates whether there is a strong relationship between X and Y. The closeness of the two variables is known as the correlation coefficient, r, given by:

$$r^2 = \frac{\sum_{i=1}^{n}(x_i - \bar{x})(y_i - \bar{y})}{(n-1)S_x S_y} \qquad (5\text{-}3)$$

Where, i has values of 1, 2, 3,..., n; x_i is the direct measurement value; y_i is the corresponding simulated value; n the sample size; S_x the variance of the measured values (x); S_y . The variance of the corresponding simulated values(y) is indicated as follows: x the mean value of x; and y the mean value of y.

The correlation coefficient (r^2) ranges from −1 to 1. The coefficient was used to determine the relationship between the observed and simulated data. The value of r = 0 shows that no linear relationship exists between observed and predicted data, but for $r^2 = 1$ or are = −1, a perfect positive or negative linear relationship exists, respectively. Higher values of r^2 indicate comparatively less error, and values higher than 0.5 are considered acceptable (Moriasi *et al.* 2007). The correlation coefficient (r^2) method was used to rate the model performance of different storm sizes (Q_{2yr}, Q_{10yr}, Q_{20yr}, $Q_{50yr,}$ and Q_{100yr}) during the calibration period where the relevant information was available.

5.1.1 Event-based approach (steady flow)

The HEC-RAS steady flow model uses an energy equation to route river run-off down a sloping river channel of specified width and riverbed roughness. The channel width was digitised from

Google Earth imagery (2017) and used in creating the DEM and in the specifications of the model channel and floodplain cross sections (Figures 5.1 & 5.2). The slope/gradient of the riverbed was obtained from the bathymetric data incorporated in the DEM using the HEC-geoRAS to specify the channel elevation profile. The calibration procedure assumed these physical parameters were invariant and were not adjusted in the model calibration. An example of the cross-sectional profiles at selected locations in the estuary's upper and middle reaches showed the channel and floodplain specifications. The estimated Manning coefficients are shown in Figure 5.1 & 5.2, respectively. The red dots represent the edge (banks) of the channel. The 1987 flood reached an elevation of approximately 9m above mean sea level (MSL) at this section. This was illustrated by using the height of debris shown in Photograph 5.1, which would also have been observed along the banks and bridges.

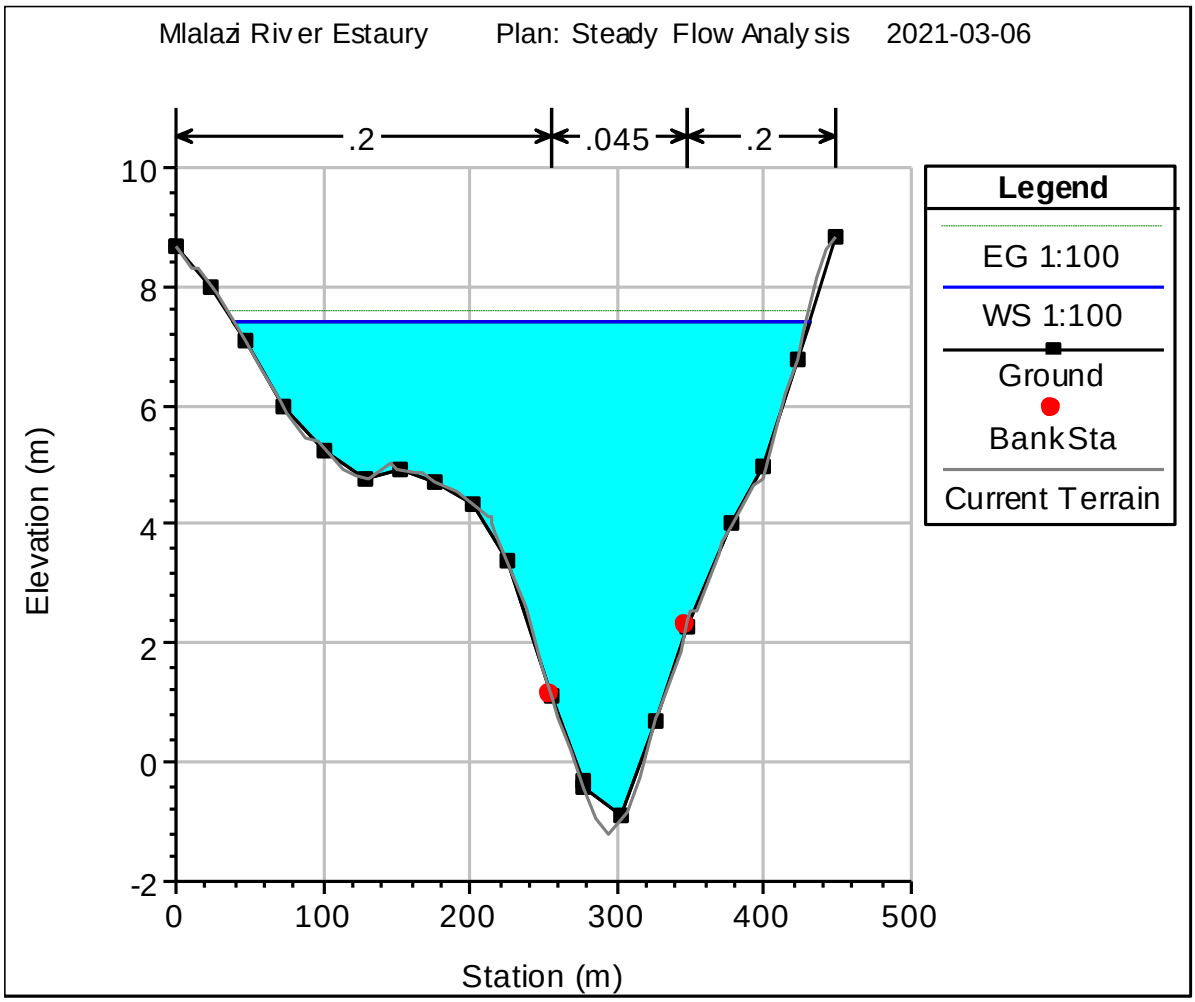

Figure 5.1: The 1987 flood (Q_{100yr}) simulation at the upper estuary channel and floodplain, where approximately 9mMSL's surface water elevation was recorded.

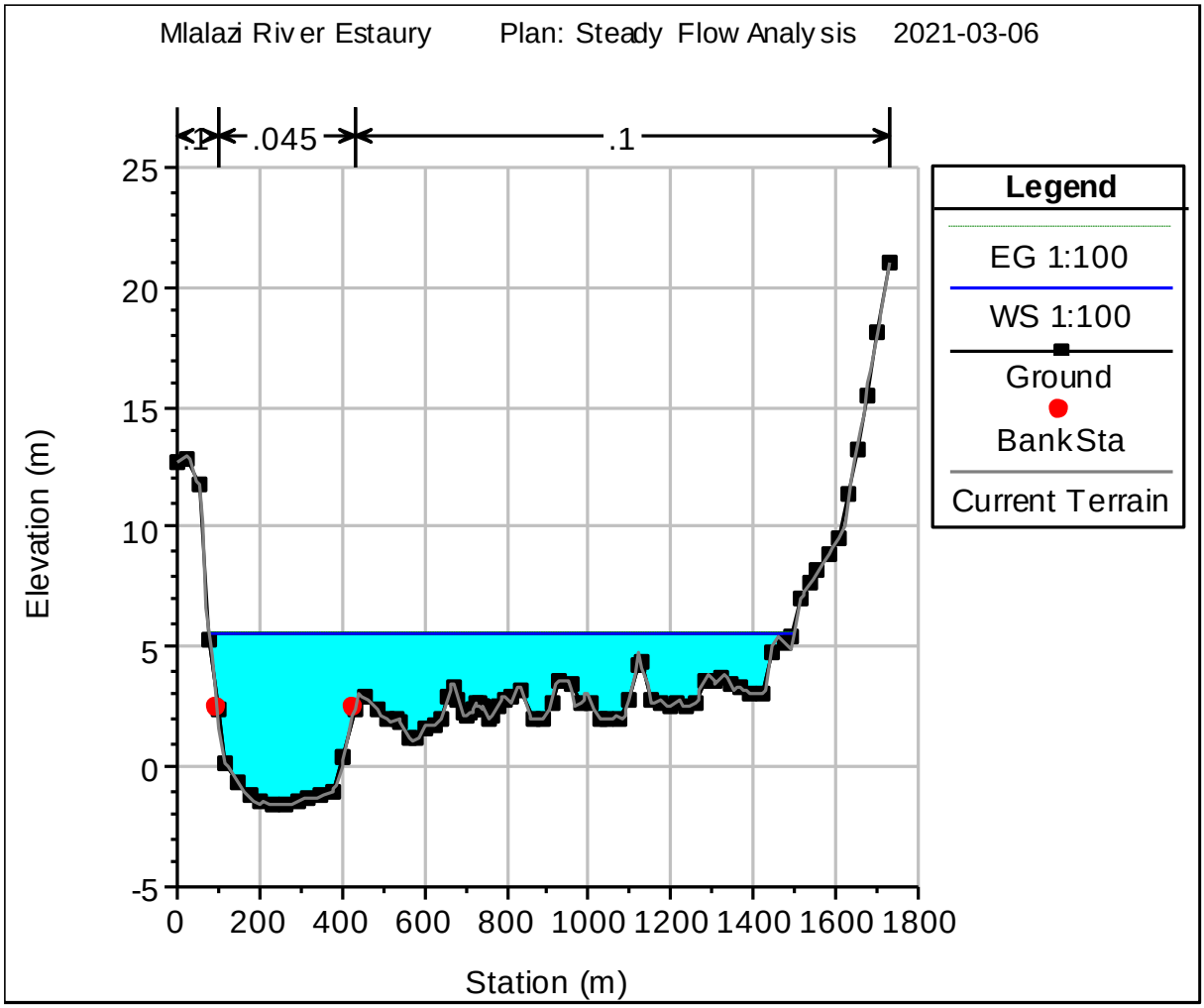

Figure 5.2: The 1987 flood (Q_{100yrs}) simulation at the middle estuary channel and floodplain, where approximately 5mMSL's surface water elevation was recorded.

The channel and flood banks roughness- numbers were estimated from land cover. Manning's roughness coefficient (n) was derived from published information related to various natural channels (*https://www.engineeringtoolbox.com/mannings-roughness-d_799.html*). This was based on a field survey of the estuary channel and floodplain as described in Section 3.3 (Chapter 3). This was identified as the primary parameter for calibration of the estuarine model predictions of flow. The n-value, which is highly variable, depended on riverbed roughness, vegetation characteristics, channel irregularities in river sections, obstructions, and flow depth (Ambrose *et al.*, 1993). The range of Manning's n-values in the literature for a natural stream on the main channel varied by more than an order of magnitude (minimum & maximum), ranging from 0.025 to 0.150, and for floodplain channels 0.025 to 0.200, depending on the land use type.

During the steady-state model calibration, the HEC-RAS flow model was run repetitively for each specific storm. The Manning roughness coefficient (n) was systematically adjusted at each river cross section to improve the predicted with the available (actual) measured water levels. During high flow, the active water body over-topped the river banks and flooded the surrounding plain in successive increments of the active water body. Unfortunately, the model's roughness coefficient represents an area average that could change with increasing storm magnitudes as the wetting perimeter changes. For the average flow contained within the channel banks, the floodplain parameters were not applicable in the model calibration because the flow was contained within the channel but became increasingly important with increasing storm size. Table 5.1 shows the selected roughness n-values along the river banks/floodplain used for calibrating the different flood events.

Table 5.1: The Manning's n-value for the calibration of different flood events for the various land use types identified on the floodplain of the Mlalazi Estuary

Flood Events	**Manning's n roughness**			**Main features on the floodplain**
	Left Bank	*Channel*	*Right Bank*	
1:2	0.025	0.030	0.025	Land use on the **upper floodplain** is mainly commercial sugar cane farming with drainage canals. The mangrove trees invade the main channel between the confluence and R102 Bridge.
1:10	0.030	0.045	0.030	
1:20	0.200	0.045	0.200	
1:50	0.200	0.045	0.200	
1:100	0.200	0.060	0.200	
1:2	0.025	0.030	0.025	**Middle floodplain** is an extensively large area where on the left bank is privatised sugar cane plantations with the canal to drain access flow. The right bank plain is sub-divided into different vegetation (woody plants, old sugar farming fields, salt marsh, mangroves, and reeds)
1:10	0.035	0.035	0.030	
1:20	0.060	0.045	0.200	
1:50	0.150	0.045	0.200	
1:100	0.150	0.045	0.200	
1:2	0.025	0.030	0.025	The **lower floodplain** is 4km long and bounded by dunes and sub-tropical forest. The presence of a sand berm at the mouth increases the roughness.
1:10	0.030	0.030	0.030	
1:20	0.100	0.030	0.100	
1:50	0.100	0.030	0.100	
1:100	0.120	0.060	0.120	

During flood events, the main estuary channel is assumed to remain steady and experience minor roughness, although there could have been changes that increased flow velocities in the larger storms (Figure 5.3). However, the mangrove colony's presence in the upper estuary's

main channel and the sand berm at the mouth, is assumed to increase the channel roughness as they would impact flow with a rising stage. The drainage canals systems on the sugar cane plantation allow the excess groundwater flow and overland flow from Q_{10yr} storm events to be quickly channelled into the main estuarine channel.

As explained in Chapter 4: Section 4.2, it was difficult to determine the surface roughness on the left and right bank/floodplain below the Railway Bridge due to the variation of vegetation types. The Q_{10yr}-flood return did inundate this area due to high soil moisture from groundwater flow (old sugar cane field) and flood tide in the salt marsh. The hydraulic roughness at this stage was controlled by the dominant vegetation pattern, as shown in Table 5.1.

The expansion or contraction loss coefficient (C) within the Mlalazi Estuary is applicable during high flows at hydraulic structures (bridges). The flow can change from the sub-critical upstream to super-critical downstream. Therefore, the construction values were adjusted from 0.1 to 0.3 upstream of the main bridges crossing the estuary and expansion values from 0.3 to 0.5 downstream.

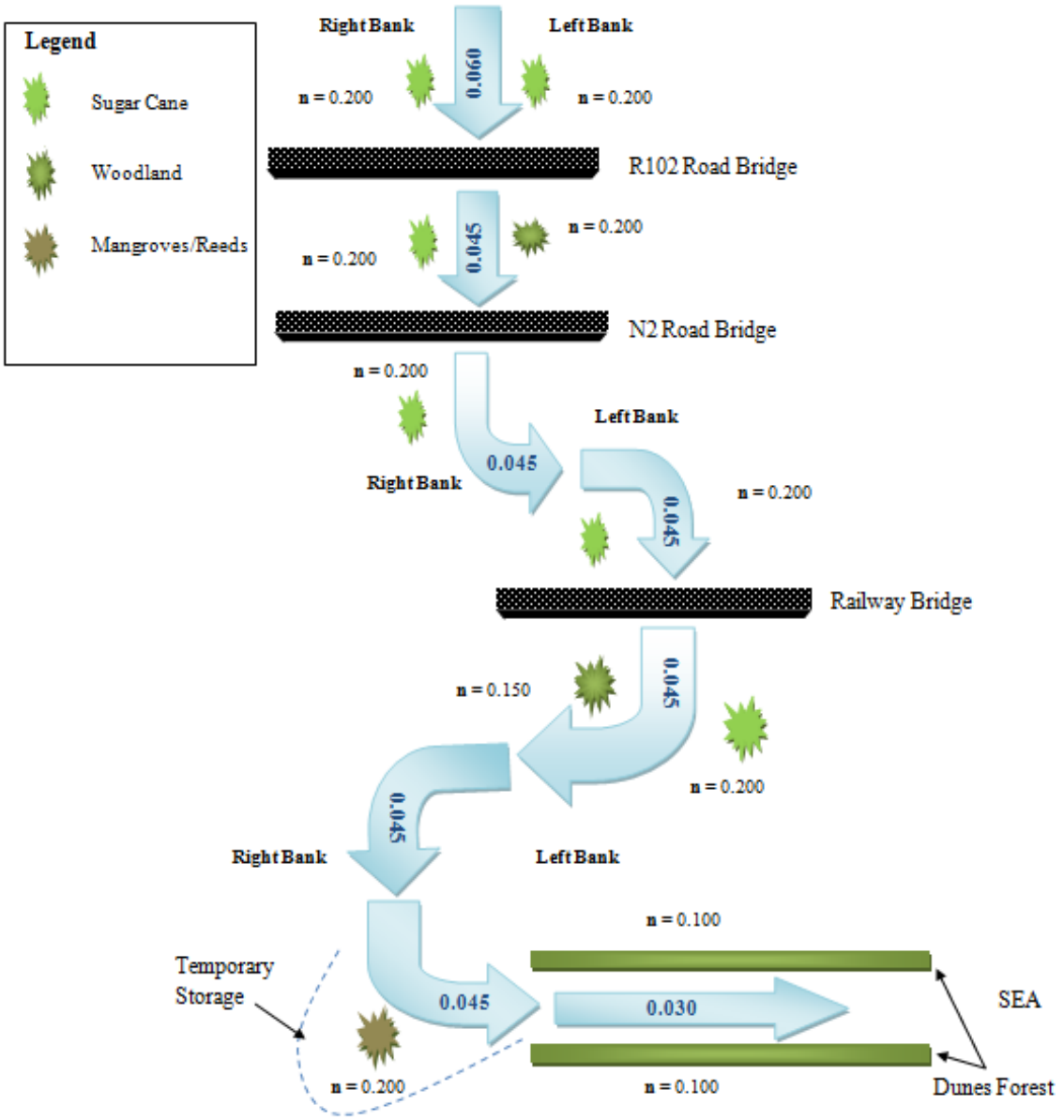

Figure 5.3: The calibration values of the Manning roughness coefficient (n) on the main channel and floodplain along the Mlalazi Estuary for Q_{100yr} flood event (as per vegetation patterns adapted from Hill, 1966)

5.1.2 Continuous-based approach (unsteady flow)

The unsteady flow model set-up and simulation used the same Manning 'n' coefficients values in the steady flow simulation. This was due to the constant flow model being well-calibrated. However, it was difficult to obtain the correct computation time and hydrograph output interval. For this reason, a time-step of 6-minute computation intervals and 6 hours for

hydrograph output intervals was used to successfully run the estuary's continuous or unsteady flow analysis (Table 5.2). During the unsteady flow, more interval space between the river cross sections was required for the model to successfully run. Therefore, some of the interpolated cross sections in the upper and middle estuary (low-lying areas with flat slope) had to be removed for the unsteady flow model to run successfully.

Table 5.2: Simulation parameters of the HEC-RAS flow model for the Mlalazi Estuary

No.	Description of Simulation Parameters	Steady Flow Condition	Unsteady Flow Condition	Remarks
1	Manning's 'n'	Figure 5.3	Figure 5.3	Table 5.1
2	Contraction coefficient of c/s At all bridges u/s & d/s	0.1 0.3	0.1 0.3	HEC-RAS Reference Manual (2016)
3	Contraction coefficient of c/s At all bridges u/s & d/s	0.3 0.	0.3 0.5	HEC-RAS Reference Manual (2016)
4	Upstream boundary conditions	Figure 4.4: frequency distribution curve	Flow hydrograph (01 Jan 70, 24:00 to 11 Mar 18, 24:00)	From the catchment model (hec-hms)
5	Downstream boundary conditions	Bed slope = 0.001 (for normal depth)	Bed slope = 0.001 (for normal depth)	Table 4.2
6	Spacing of c/s (Δx)	60 – 200 m	60 – 200 m	For unsteady flow, interpolated c/s were removed
7	Time step (Δt)	-	Computation interval = 6 mins Hydrograph = 6 hrs	-
9	Initial condition	-	Flow at u/s c/s = 0.32 m^3/s (01 Jan 70, 24:00)	Corresponding values at the confluences (HEC-HMS model)

c/s: cross section d/s: downstream section u/s: upstream section

5.2 Steady Flow calibration evaluation

Table 5.3 shows the simulated water surface elevation and velocity values for different storm events for this project's steady flow analysis. The hydraulic model estimated the water surface elevation (Y_2, Y_1) at each cross section. The velocity component was derived from the component of the energy equation ($\frac{a_2 V_2^2}{2g}$) (Equation 4.1) at each river section through the process called the standard step method (STM). The simulated surface water elevation and

velocity for each event were used to calibrate/validate the hydrodynamic condition within the Mlalazi Estuary.

Table 5.3: Simulated steady flow output for various storm size events at strategic cross-section profiles in the Mlalazi Estuary

Measured Sites	Distance downstream (km)	Flood Events	[1]Flow (m^3/s)	E.G. Slope (m/m)	W.S. Elevation (m)	Average velocity ($m.\ s^{-1}$)
Confluence (*12156. 4)	0.00	1:10	221	0.000205	4.10	0.56
		1:50	767	0.000140	7.10	0.64
		1:100	1175	0.000121	8.62	0.72
N2 Bridge (*10449. 74)	2.00	1:50	767	0.000682	5.95	0.82
		1:100	1175	0.000666	8.36	0.80
D/S of N2 Bridge (*8439. 04)	4.00	1:100	1175	0.000483	5.99	0.75
Railway Bridge (*7595. 656)	5.30	1:2	47	0.000048	0.78	0.22
		1:50	767	0.000223	4.60	0.37
		1:100	1175	0.000226	5.73	0.34
D/S of Railway Bridge (*7118. 423)	6.05	1:100	1175	0.000068	5.67	0.14
Middle Estuary (*5015. 724)	7.92	1:100	1175	0.000038	5.55	0.23
Lower Estuary at the bend (*4767. 722)	9.29	1:2	47	0.000094	0.58	0.21
		1:20	372	0.000027	2.93	0.16
Mouth (*1448. 347)	12.0	1:2	47	0.000894	0.81	0.55

*** HEC-RAS cross-section number D/S: downstream [1]Upstream boundary condition**

5.3 Event-based Calibration

The event calibration was based on how well the important features of a simulated water level fitted the observed water level. An event-based calibration was done on different storm sizes (Q_{2yr}, Q_{10yr}, Q_{20yr}, Q_{50yr} and Q_{100yr}) which resulted in significant flooding and sediments production within the Estuary.

5.3.1 Flow calibration for the 1:2 (Q_{2yr}) year flood condition

The average flow (Q_{2yr}) for this project was considered to be a flow in terms of level and velocity required to sustain the hydrodynamic conditions within the estuary. The measured water levels at several sites that were favourable for monitoring have been compared to the model predictions during the calibration process (Figure 5.4 & 5.5). Table 5.4 shows the disagreement between the average simulated and measured water levels at the Railway Bridge, the Channel Bridge (lower bend), and DWS tidal stations. The HEC-RAS flow model underestimated the flow levels from the Railway Bridge downstream towards the mouth channel. The prediction error and *PBIAS* between the observed and simulated water elevation values varied between 0.37 (32%), 0.20 (26%) and 0.47 (37%).

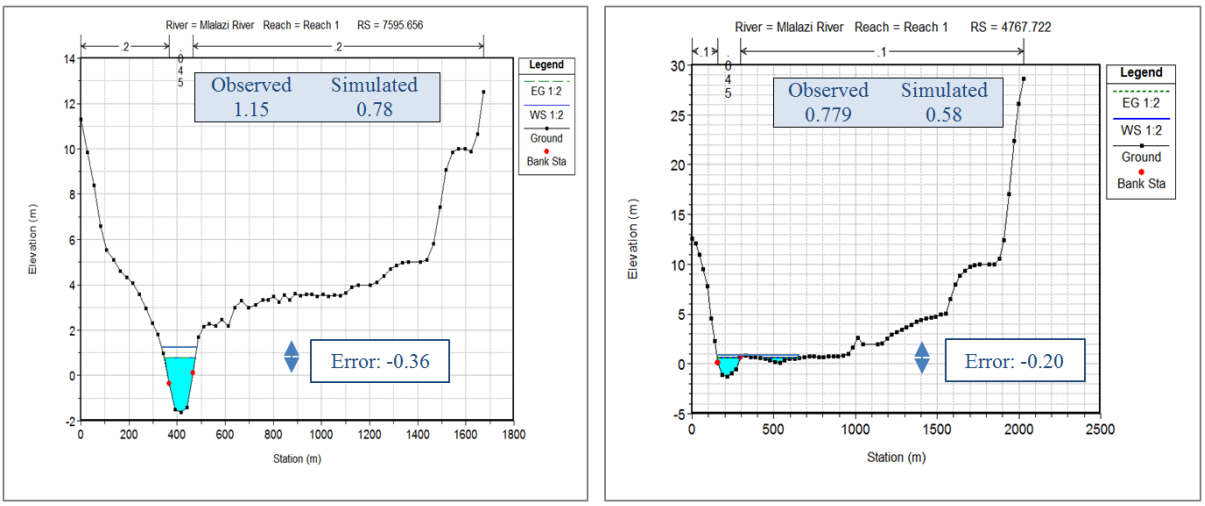

Figure 5.4: Comparisons between the measured (blue line) and simulated river stage for a 1:2 (Q_{2yrs}) run-off event at the Railway Bridge (left) and Channel Bridge (right)

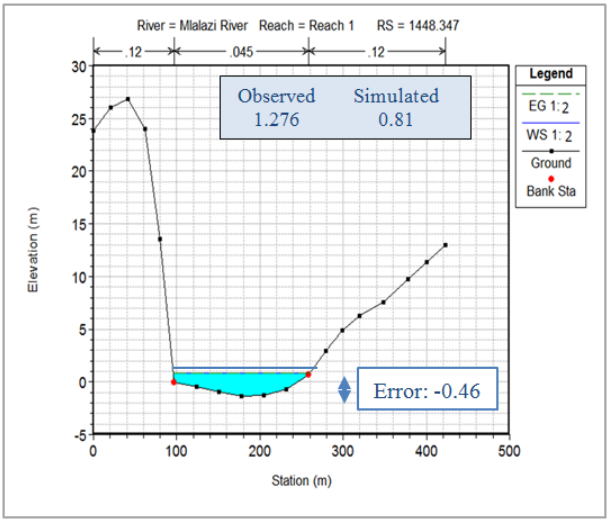

Figure 5.5: Comparisons between the measured (blue line) and simulated river stage for a 1:2 (Q_{2yrs}) run-off event at the Estuary Mouth

The variation is due to several conditions that can mask the influence of the average fluvial event. These include the following conditions:

a) Tidal (flood & ebb tide) influence is dominant during the average flow regime. It can exceed the water level in the lower estuary under average fluvial conditions, especially during spring high.

b) The water level can continuously rise during the period leading to mouth closure when there is still some overtopping at the mouth

c) The mouth breaches and becomes mainly tidal.

It can be seen from the hydrography in Figure 5.6 from Kelbe *et al.,* (2019) that the tidal and mouth conditions influence ultimately dominates the average fluvial events at the estuary mouth. The model results were compared to several examples of the measured tidal motion at the estuary mouth for several months during 2014. During this period, several small fluvial events of approximately median amplitude ($Rainfall_{2yrs}$ = 20 mm & 27 mm) interrupted the basic tidal pattern, as illustrated in Figure 5.6. The fluvial event is assumed to raise the estuary high and low tides at the locations. It is also assumed that the larger fluvial events may change the mouth through sediment scouring, causing a lowering of the minimum neap tides.

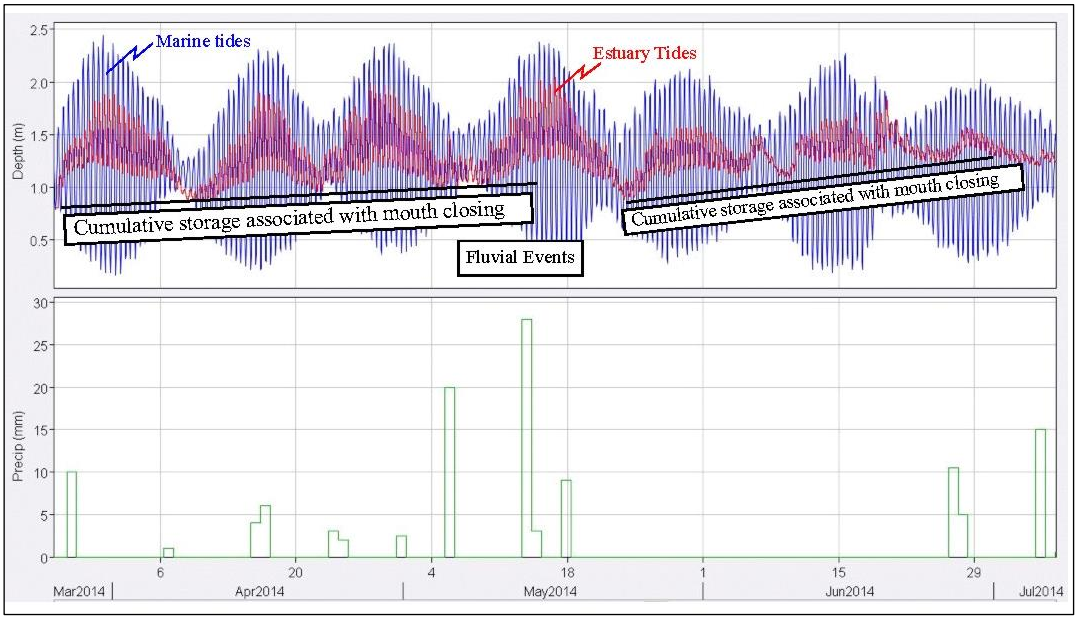

Figure 5.6: Observations of the marine (blue line) and estuary (red line) tidal interaction during 2014 showing the trends in estuary storage, resulting in rising levels of the minimum low tide that is assumed to be associated with the mouth elevation. The rising trend in storage (mouth elevation) is interrupted by fluvial events shown by the lower graph's rainfall record (Kelbe *et al.,* 2019).

Figure 5.7 shows the extent of the floodplain inundation for a 1:2-year run-off event without a tidal component. This event does not normally over-top the riverbanks of the main channel. The inundation map indicated that the average flood could extend into some of the small streams connected to the main channel in the low-lying areas, particularly in the middle estuary below the railway line and the low-lying salt marshes.

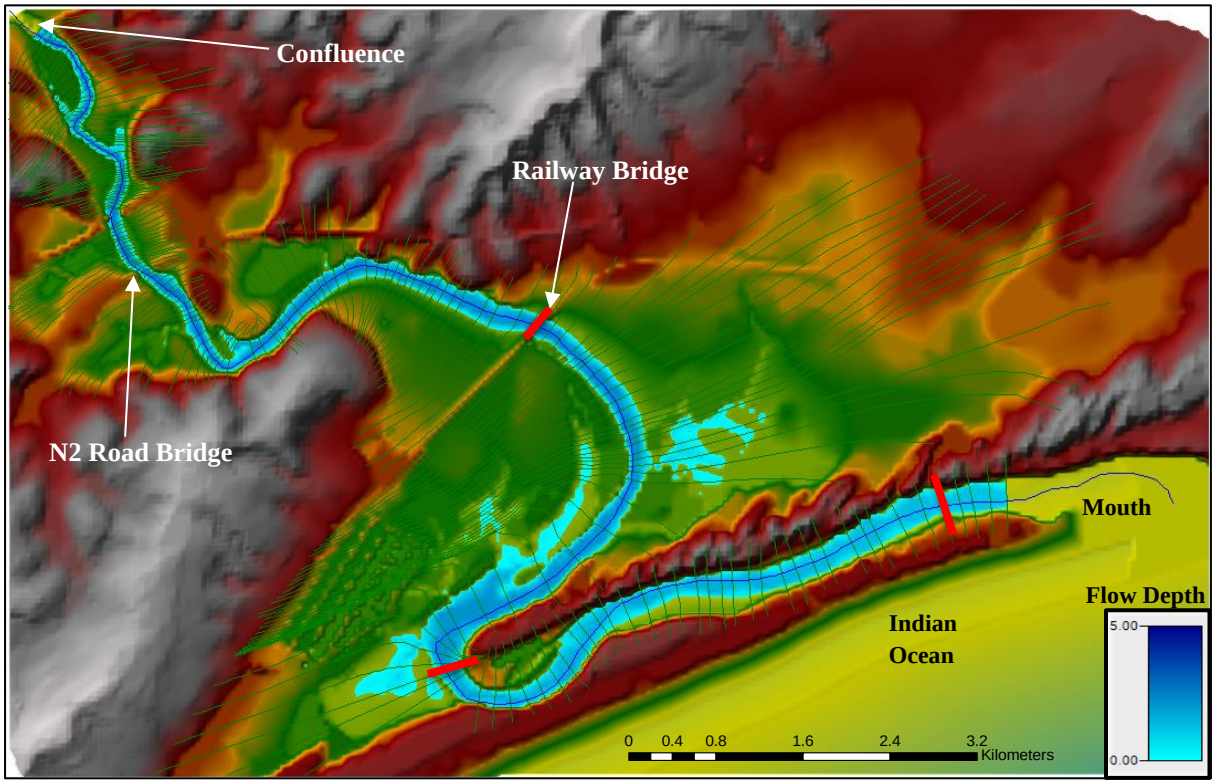

Figure 5.7: The simulated spatial extent of the inundation map for a 1:2 (Q_{2yrs}) run-off event in the Mlalazi Estuary. The bold red lines represent river sections where the water level was observed for this event.

5.3.2 Flow calibration for the 1:10 (Q_{10yr})-year flood return

A 1:10-year storm event was only monitored in February 2018 when the storm was predicted to produce over > 60 mm of rainfall recorded along the coastal areas over a 48-hour (19 - 20 Feb 2018) period. This event created significant flooding within the Mlalazi Estuary and floodplain. The flood hydrograph at the estuary's upper channel is shown by the 1:10-year flood-wave together with a marine tidal range in Figure 5.8. There was no significant marine tidal motion in the upper reaches of the estuary during this monitoring period. At the confluence of the Mlalazi River and Ntuze River, the fluvial river stage reached a peak level of 3.88 m during the storm that lasted for about 48 hours.

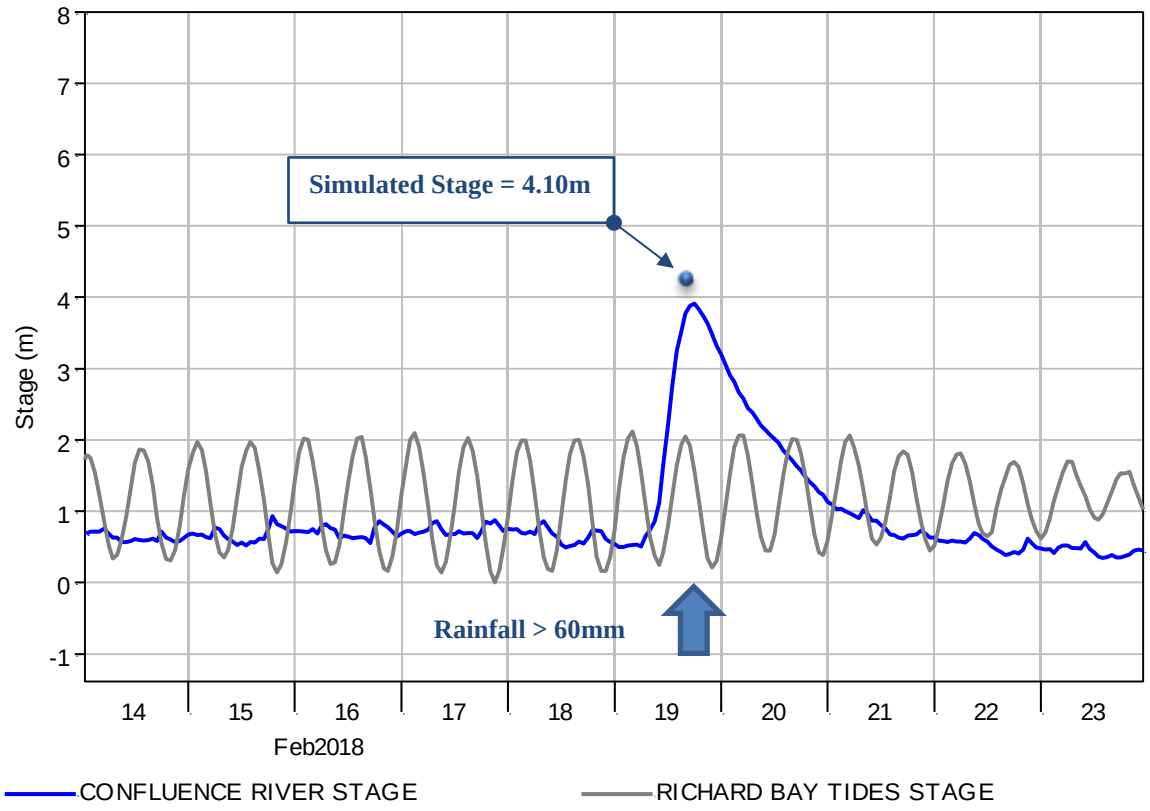

Figure 5.8: Observations of the river stage (blue) and marine (grey) tidal interaction during the February 2018 storm event at the two rivers' confluence in the upper estuary

The hydraulic flow model simulated the flood peak of the Q_{10yrs} event in February 2018 from the simulated river discharge of 221 m^3/s generated from the rainfall-run-off (HEC-HMS) model (Rasifudi, 2019). The simulated flood peak level reached 4.10 mMSL after model calibration, and it was then compared with the observed peak level at the confluence (Figure 6.6). The hydraulic model gave an acceptable agreement between the predicted and the measured water level, where the prediction error and *PBIAS* values were 0.22 and 5.67%, respectively (Figure 5.9). According to Kelbe *et al.*, (2019), the flood-wave of major events starts to overtop most of the active channel (river banks) at a stage level of about 2 mMSL and starts to inundate the upper reaches of the floodplain. It can be seen from Figure 5.9 that the simulated Q_{10yrs} storm event was over-topping (confluence overflow) above 2 mMSL onto the adjacent floodplain.

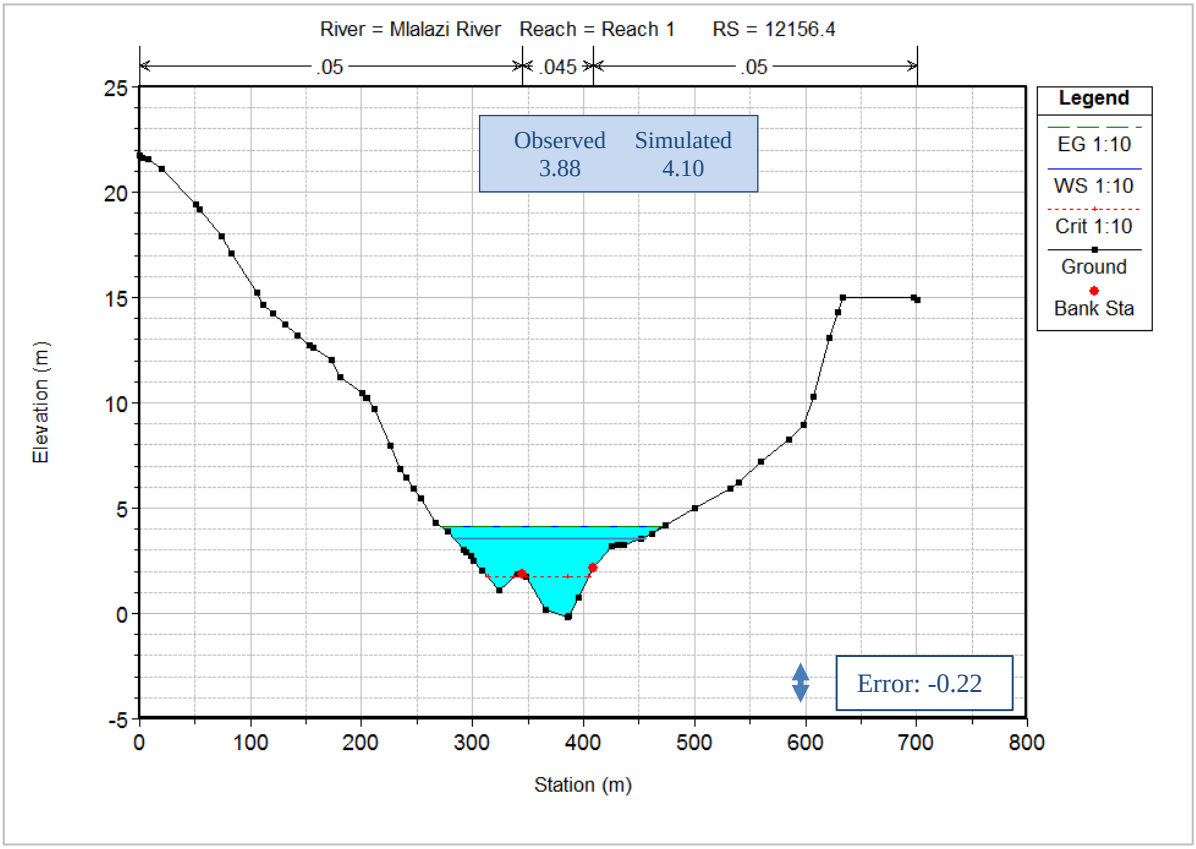

Figure 5.9: Comparisons between the measured (blue line) and simulated river stage for a 1:10 (Q_{10yrs}) run-off event at the confluence of the Mlalazi River and Ntuze River on the February 2018.

5.3.3 Flow calibration for the 1:20 (Q_{20yr})-year flood return

A Q_{20yrs} storm event was only measured in May 2017. This storm produced over > 100mm of rainfall along the coastal area (Mtunzini) over a 48 hour (14 - 15 May 2017) period. The flood hydrograph at the estuary's railway channel is shown by the 1:20-year flood-wave and tidal stage in Figure 5.10. The fluvial water level reached a peak stage of 2.73 m at the lower estuarine channel (toward the U-shape bend). The storm event lasted for five days.

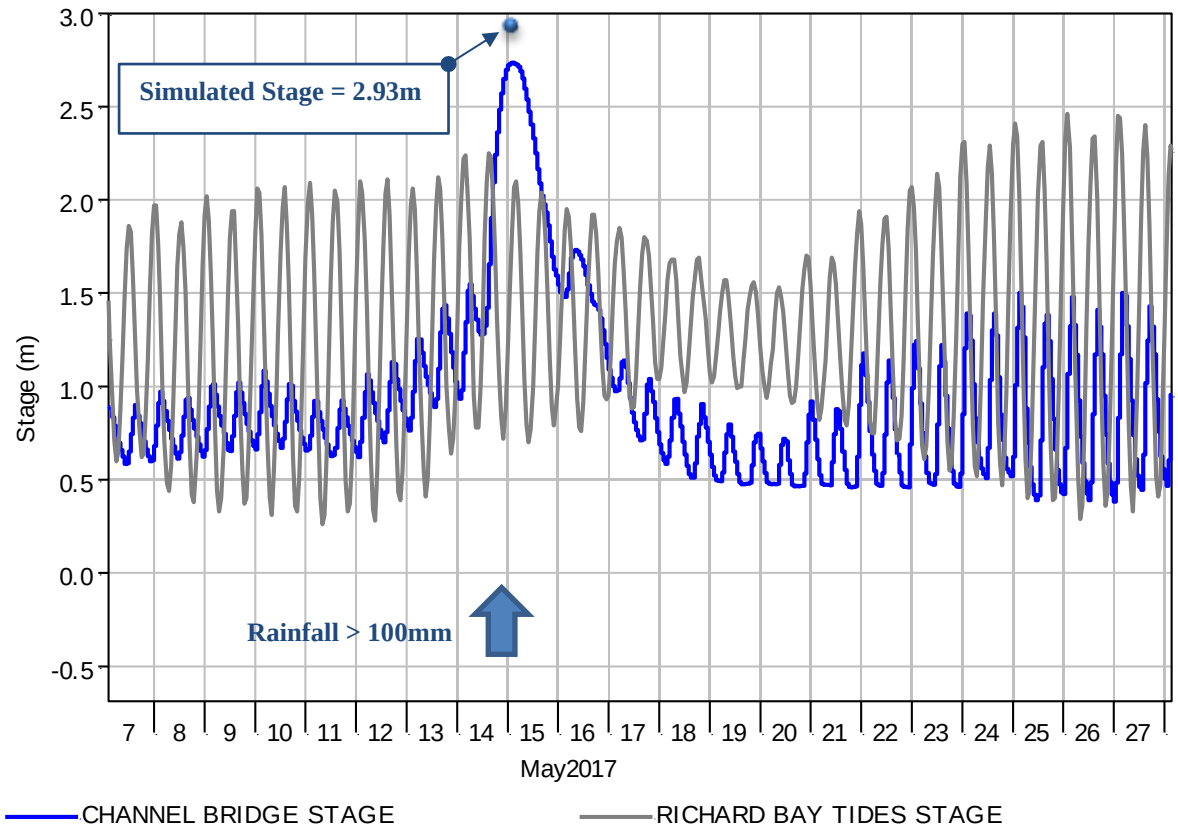

Figure 5.10: Observations of the river stage (blue) and marine (grey) tidal interaction during the February 2018 storm event at the two rivers' confluence in the upper estuary

The HEC-RAS flow model predicted the propagation of the Q_{20yrs} flood event in the estuary from the simulated river run-off of 371 m^3/s, acquired from Rasifudi (2019). The model gave reasonable agreement between the simulated and measured flood peaks after model calibration. The statistical tests showed satisfactory results for this event, where the prediction error and *PBIAS* values are 0.20 and 7.33%, respectively, at the selected river section (Figure 5.11).

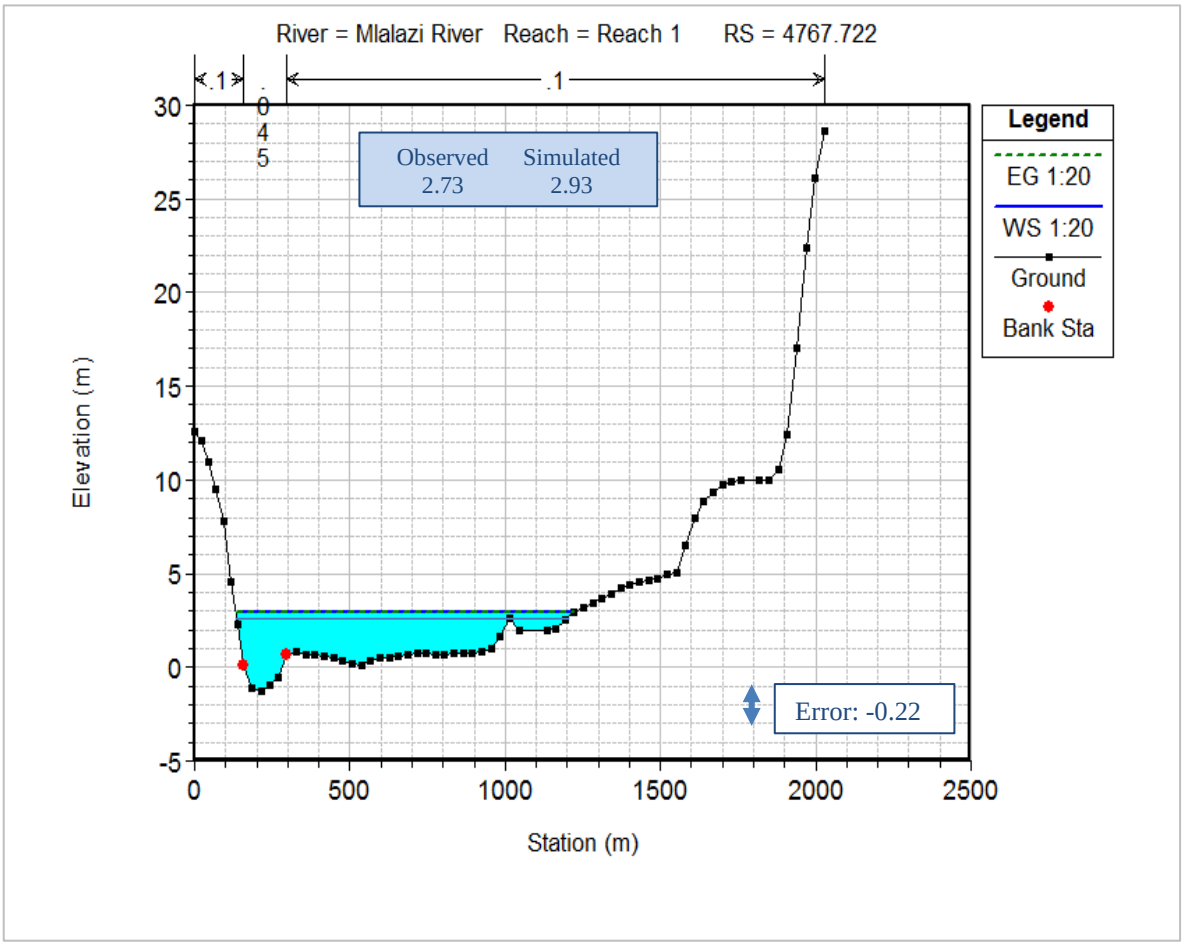

Figure 5.11: Comparisons between the measured (blue line) and simulated river stage for a 1:20 (Q_{20yrs}) run-off event at the Channel Bridge (Lower bend).

5.3.4 *Flow calibration for the 1:50 (Q_{50yr})-year flood return*

As noted in Chapter 3, Section 3.6, a Q_{50yrs} year flood return was documented for the estuary for the 1969 flood-survey by Badenhorst *et al.* (1989). The flood peak reached 6.40 mMSL at the old N2 Bridge and 3.70 mMSL at the Railway Bridge (Badenhorst *et al.*, 1989). It is unknown how much rainfall was produced in the 1969 flood event since the available rainfall archives by Rasifudi (2019) did not show any major rainfall event in 1969.

Another estimated Q_{50yrs} storm event, recorded in May 2018, produced over 200 mm of rainfall over a 48-hour (16 - 17 May 2018) period in the Mlalazi Catchment. A significant flood event was created in the estuary which caused some floodplain erosion and deposition (Schumann, 2013). The river stage at the confluence peaked at 7.28 mMSL which receded to pre-storm levels only over 48 hours (Figure 5.12). The HEC-RAS flow model simulated the flood peak of Q_{50yrs} event from a river inflow of 767 m^3/s obtained from the rainfall-run-off (HEC-HMS)

model by Rasifudi (2019). The model gave an acceptable agreement between the simulated and the measured Q_{50yrs} flood event after model calibration.

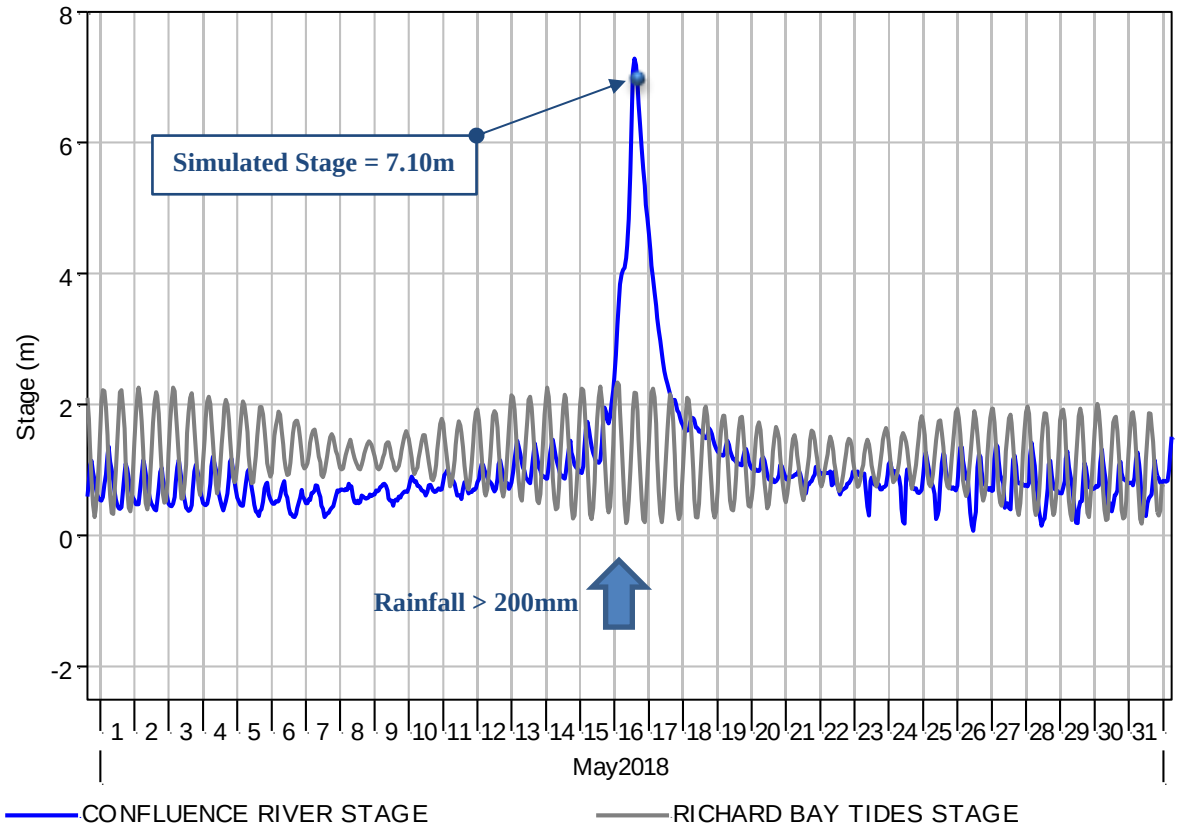

Figure 5.12: Observations of the river stage (blue) and marine (grey) tidal interaction during the February 2018 storm event at the two rivers' confluence in the upper estuary

The statistical model tests gave satisfactory results, with the prediction error and *PBIAS* values ranging from (0.18 and 2.47%), (0.45 and 7.03%) and (-0.90 and 24.3%) at the confluences, N2 Road Bridge and Railway Bridge, respectively (Figures 5.13 & 5.14). The area of inundation for the 1:50-year flood event is illustrated in Figure 5.15. The field observation revealed that the prawn farm and parkland downstream of the Railway Bridge were not entirely flooded, as the model indicated in Figure 5.15. However, the canalised floodplains adjacent to the prawn farm were all flooded.

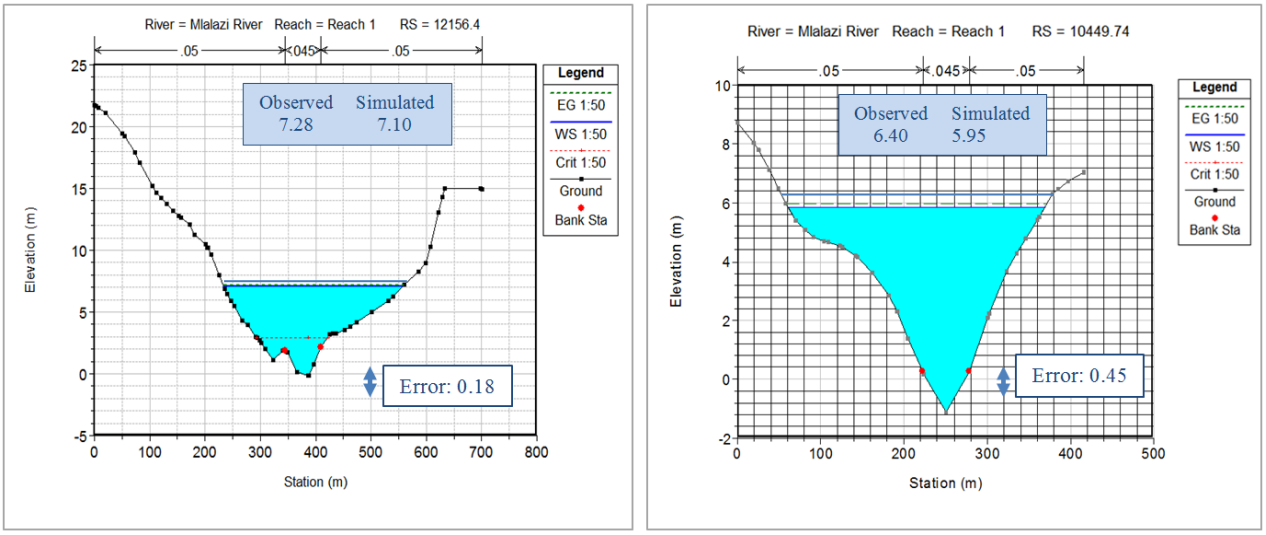

Figure 5.13: Comparisons between the measured (blue line) and simulated river stage for a 1:50 (Q_{50yrs}) run-off event at the confluence (left) and N2 Road Bridge (right).

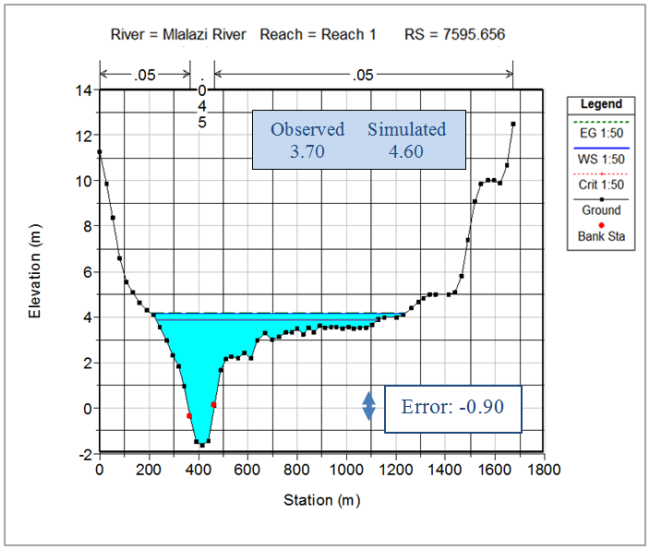

Figure 5.14: Comparisons between the measured (blue line) and simulated river stage for a 1:50 (Q_{50yrs}) run-off event at the Railway Bridge

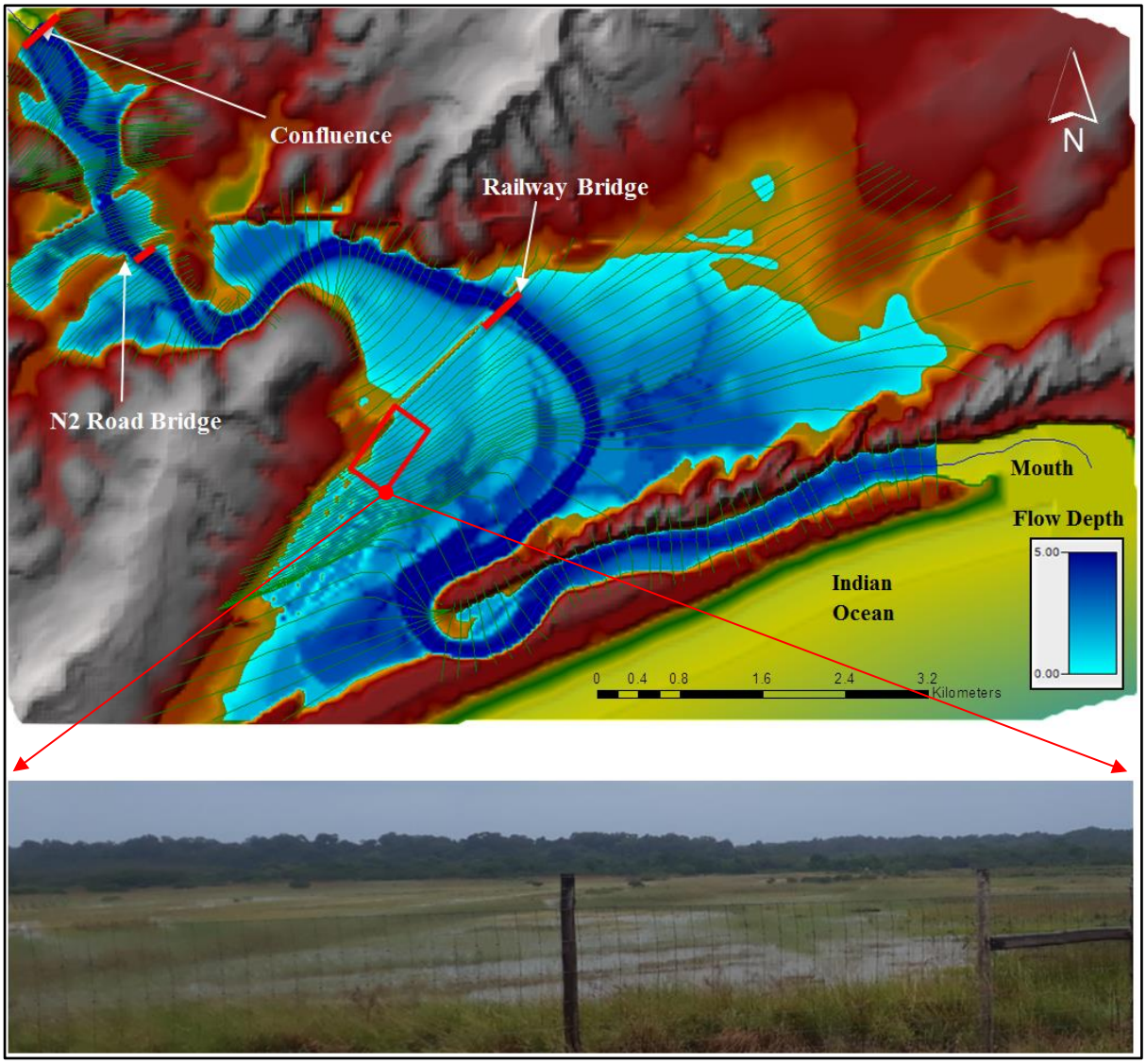

Figure 5.15: The simulated spatial extent of the flooding along the Mlalazi Estuary during a 1:50 (Q_{50yrs}) -flood event (upper). The flooded canalised floodplain adjacent to the prawn farm (photo by Kelbe)

5.3.5 *Flow calibration for the 1:100 (Q_{100yr})-year flood return*

The HEC-RAS flow model simulated the flood peak of Q_{100yrs} event from a fluvial event of 1175 m^3/s in September 1987 (Rasifudi 2019). The model prediction for this 1:100-year flood event gave acceptable agreement between the simulated and measured water levels at various sections and the estuary's full extent, based on the survey by Badenhorst *et al*. (1989). The surveyed water level helped in the calibration of this flood event. The simulated longitudinal flow profile of the simulated Q_{100yrs} flood event along the Mlalazi Estuary (Figure 5.16) did illustrate varying agreement levels in the simulated and observed peak stage heights. The stage

was slightly over predicted in the upper half of the estuary and possibly under-predicted in the lower sections of the estuary, above and below the railway bridge. The model simulations could have been improved with further calibrations but the level of uncertainty in the accuracy of the observations may not have improved the reliability of the prediction to any significant level.

It can be seen from Table 5.4 that the 1:100-year flood event prediction error and *PBIAS* values vary from 0.34 (15%), 0.11 (1.8%), 0.22 (3.7%), 0.38 (6.3%) and 0.60 (12.6%), respectively, from upper to middle estuary. The scatter diagram for comparison between the simulated and observed water levels within the Mlalazi Estuary for the Q_{2yr}, Q_{10yr}, Q_{20yr}, $Q_{50yr,}$ and Q_{100yr} flood returns is presented in Figure 5.17. The correlation coefficient value of 0.98 indicates a very close relationship between the simulated and observed water levels.

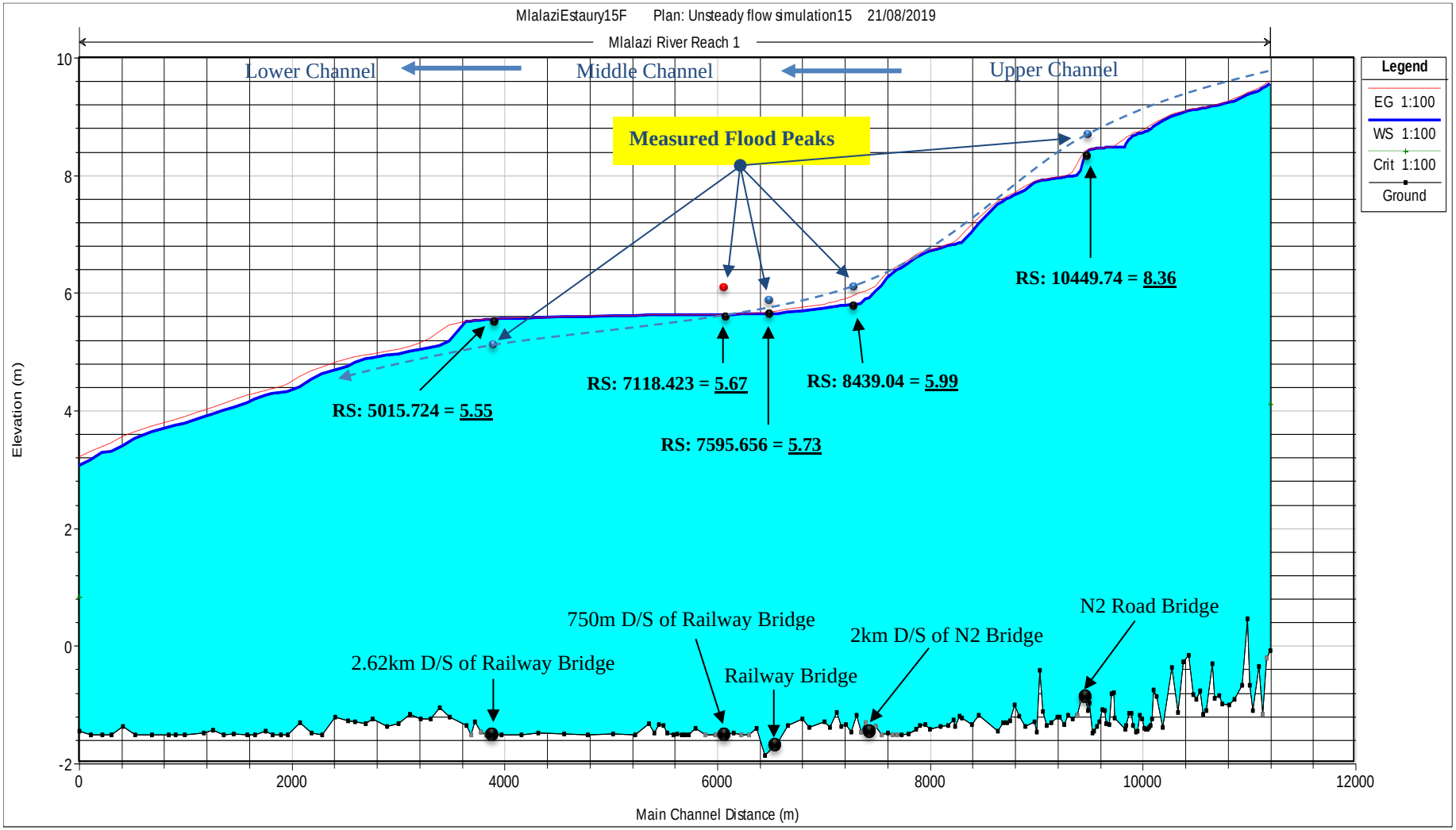

Figure 5.16: Simulated surface water elevation longitudinal profile and measured surface water elevation at various locations surveyed along the Mlalazi Estuary during a 1:100 (Q_{100yrs}) extreme flood event

Table 5.4: Summary of event-based model calibration results in the Mlalazi Estuary

Measured Sites	**Distance (km)**	**Flood Events**	**[1]Flow (m^3/s)**	**Observed WL (m)**	**Simulated WL (m)**	**Prediction error**	**PBIAS (%)**
Confluence (*12156. 4)	0.00	1:10	221	3.88	4.10	-0.22	-5.67
		1:50	767	7.28	7.10	0.18	2.47
		1:100	1175	9.00	8.62	0.38	4.22
N2 Bridge (*10449. 74)	2.00	1:50	767	6.40	5.95	0.45	7.03
		1:100	1175	8.70	8.36	0.34	15.06
D/S of N2 Bridge (*8439. 04)	4.00	1:100	1175	6.10	5.99	0.11	1.80
Railway Bridge (*7595. 656)	5.30	1:2	47	1.15	0.78	0.37	32.17
		1:50	767	3.70	4.60	-0.90	-24.32
		1:100	1175	5.95	5.73	0.22	3.70
D/S of Railway Bridge (*7118. 423)	6.05	1:100	1175	6.05	5.67	0.38	6.30
Middle Estuary (*5015. 724)	7.92	1:100	1175	4.95	5.55	-0.60	-12.12
Lower Estuary at the bend (*4767. 722)	9.29	1:2	47	0.779	0.58	0.20	25.55
		1:20	372	2.73	2.93	-0.20	-7.33
Mouth (*1448. 347)	12.0	1:2	47	1.276	0.81	0.47	36.71

* HEC-RAS, River Transects D/S: downstream [1]Upstream boundary condition

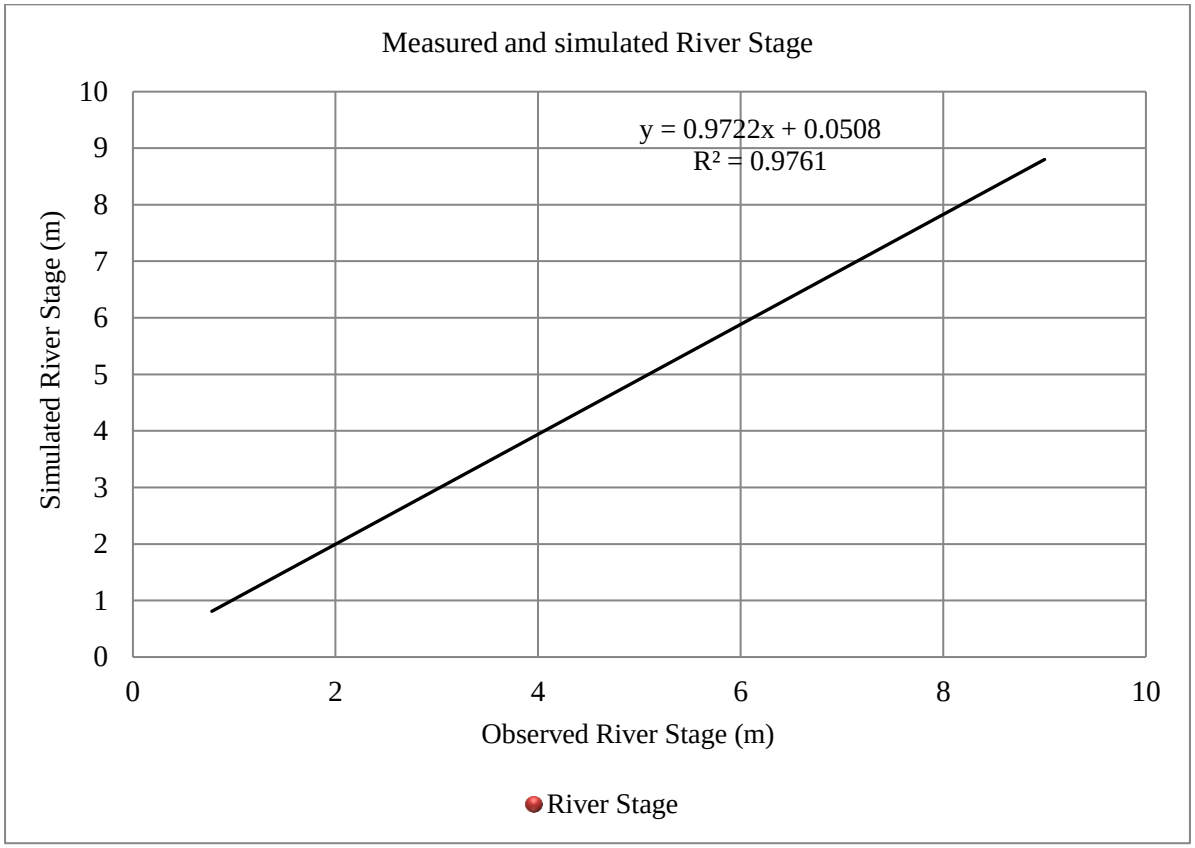

Figure 5.17: The scatter plot of the measured and simulated water levels for different storm sizes (Q_{2yrs}, Q_{10yrs}, Q_{20yrs}, $Q_{50yrs,}$ and Q_{100yrs})

5.4 Summary of the event-based model calibration

The calibration results indicated an acceptable goodness of fit for the entire range of storm events examined, with the possible exception of the Q_{2yr} run-off simulation in the middle and lower part of the estuary where the marine tidal effect is dominant. The model results for the Q_{2yr} run-off event differed from those observed at the Railway Bridge, Channel Bridge, and Mouth by *Percent bias* (*PBIAS*) of 32%, 26%, and 37%, respectively. The calibration runs for high flows were within acceptable limits in all the strategic locations in the estuary, showing that the *PBIAS* is within < 25% of the observed data. However, the hydraulic model slightly overestimated the Q_{50yrs} flood event at the Railway Bridge since the result differed by almost a meter (0.90 and 24%) compared to the measured peak level. The scatter plot diagram also shows a perfect correlation (R^2 = 0.98) between the observed and simulated fluvial peaks of different storm sizes in the estuary.

5.5 Continuous-based Calibration

The continuous-based calibration was done on two storm events that would have resulted in significant erosion and deposition of fluvial sediments. The flow routing simulations were done at a six-hour time-step for the estuary, using the simulated run-off series predicted by Rasifudi (2019). The HEC-RAS continuous model calibration was carried out by comparing daily simulated water levels with an observed river stage at the upper and lower estuary. During the calibration period, the model's performances were assessed by comparing the simulated hydrograph with the measured hydrograph pre and post the flood events (Figure 5.18 & 5.19). Three statistical methods: *Percent Bias Error* (*PBIAS*), correlation coefficient (R^2) and RMSE were used to evaluate or rate the performance of the hydraulic model for these events (Table 5.5).

The simulated *PBIAS* for the upper estuary's calibration is 14.18 %, and -31.25 % in the lower estuary. The *PBIAS* value obtained for the upper estuary suggested a good result for the calibration of the water level, and the *PBIAS* value for the lower estuary gave a poor result (as discussed in detail in Chapter 5). The simulated R^2 of calibration for the upper estuary was 0.54 to and 0.24 for the lower estuary. The R^2 value $\geq$ of 0.5 on the upper estuary was considered acceptable, as outlined by Makungo *et al.*, (2010). The simulated RMSE of calibration for the upper estuary was 0.21m and 0.39m in the lower estuary. The RMSE for the calibration period tended to be reasonably close to zero (Loliyana and Patel, 2012); it was reasonable for the upper and lower estuary. These results obtained are considered satisfactory and acceptable for water level simulations.

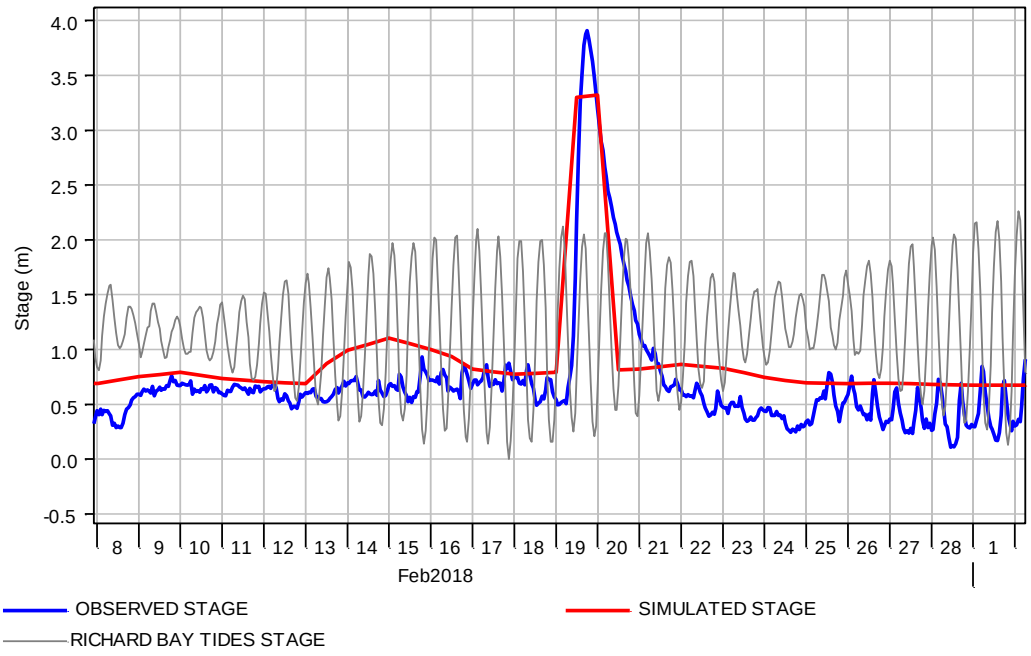

Figure 5.18: Comparison of the simulated stage, tidal stage and observed stage hydrograph for the calibration run of the upper channel of the Mlalazi Estuary. It should be noted that the logger was not secured, so the datum is not accurately known and may have undergone some changes during significant storm events.

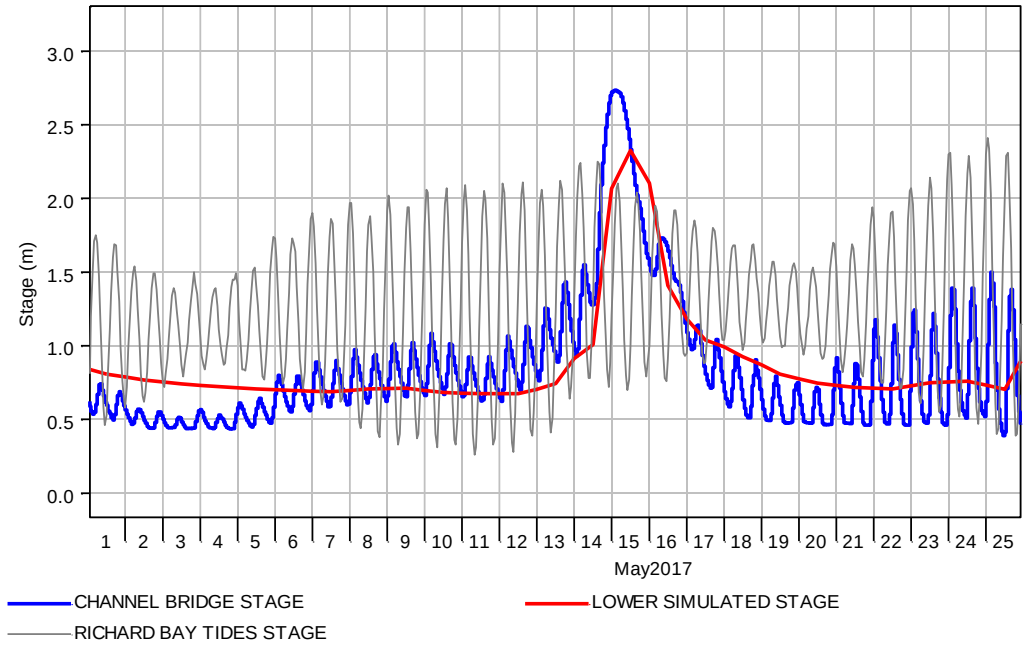

Figure 5.19: Comparison of the simulated stage, tidal stage and observed stage hydrograph for the calibration run of the lower channel of the Mlalazi Estuary. It should be noted that the logger was not secured, so the datum is not accurately known and may have undergone some changes during significant storm events.

The study area was characterised by limited observed data where the data loggers were not secured, so the datum was not accurately known and may have undergone some changes during significant storm events. The minimum simulated stage represented the residual storage. The minimum logger stage should also have described the residual storage. The simulated run-off time series did not accurately capture each event (Rasifudi, 2019). The HEC-RAS did not simulate the tidal motion because it is a one-dimensional (1D) flow model. The model did simulate the fluvial component at the upper and lower estuary. The logger data showed a similar magnitude and hydrograph to many small fluvial events and the large storm event. However, it slightly underestimated the extent of the large storms' peak water level (May 2017 and Feb 2018). All these factors could have affected the *PBIAS*, R^2 and RMSE values for the continuously-based calibration.

Table 5.5: Model performance rating for continuous calibration period (Statistical analysis is from 10 to 20 May 2017 - Lower Estuary and 16 to 22 Feb 2018 - Upper Estuary)

Performance measure	Measured Sites		Acceptable ranges
	Upper Estuary	Lower Estuary	
PBIAS (%)	14.18	-31.25	±25% – Acceptable[a]
R^2	0.535	0.235	>0.5 – Acceptable[b]
RMSE	0.207m	0.390m	0 = Perfect c

[a]Moriasi *et al.* (2007) [b]Makungo *et al.* (2010) [c]Loliyana and Patel (2012) ± over/underestimation

5.6 Event-based Validation

5.6.1 Flow validation for the Imboa (Q_{50yr}) flood event

The rainfall run-off (HEC-HMS) model by Rasifudi (2019) predicted flow values of 291 m^3/s and 367 m^3/s for the Domoina and Imboa cyclones, respectively. The continuous simulations were done at a six-hour timestep for the estuary and the results of these two independent storm events, Domoina (Jan 1984) and Imboa (Feb 1984). The hydrologic model simulated peak flow of the Imboa event was considered acceptable, even though it was higher than the Domoina event, with a much higher rainfall magnitude (Rasifudi, 2019). This was because on the arrival of the Imboa, the soil moisture on the ground surface was saturated by the Domoina flood event. There was also rainfall of roughly 10mm recorded on the coast just before the Imboa

event's arrival, contributing to the soil moisture content. The HEC-RAS flow model continuously routed the two events and generated flood peaks of 5.99 mMSL and 6.83 mMSL, respectively, at the confluence (Figure 5.20).

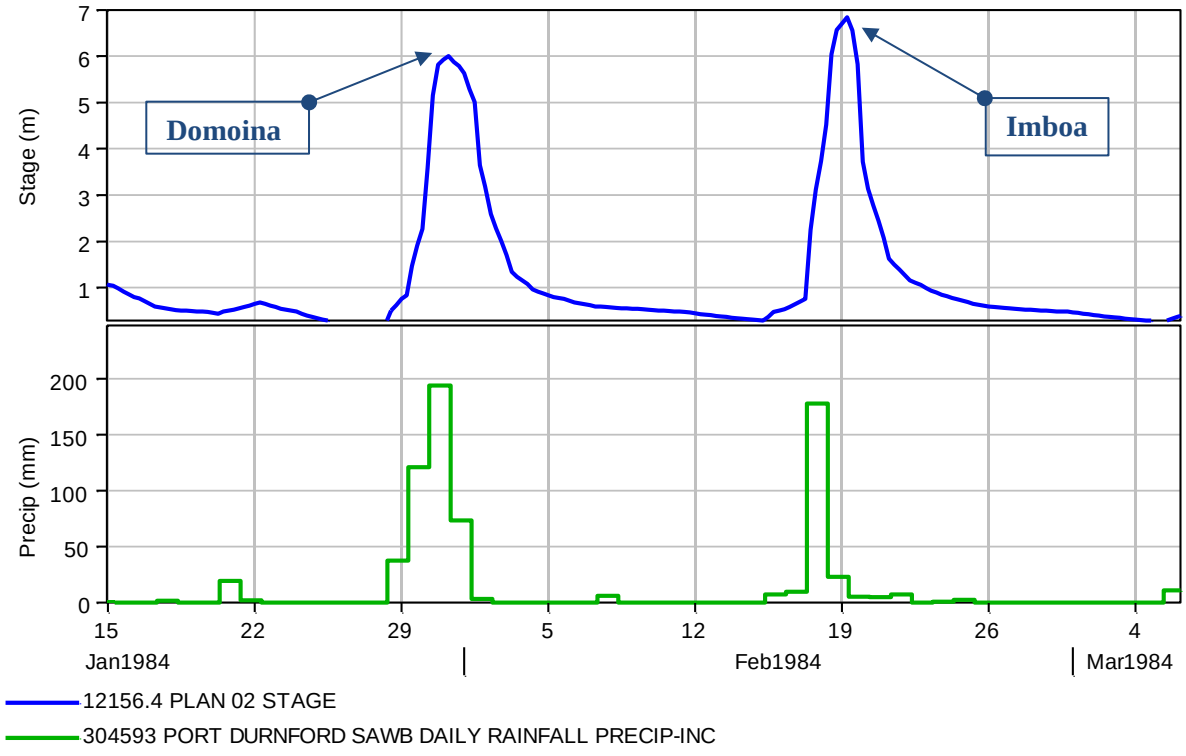

Figure 5.20: The continuous stimulation of major fluvial events (upper graph) at the confluence (blue line) of the Mlalazi River and Ntuze River. The lower graph shows rainfall recorded along the coastal region (green line).

The February 1984 validation simulated storm event showed a good agreement between the predicted and observed storm event at the estuary's strategic locations. The model validation test at the Mlalazi River's confluence and its tributary Ntuze River gave satisfactory results compared with the measured peak of 7.28 m, where the prediction error and *PBIAS* values were 0.45 and 6.18%. The model evaluation of the old N2 Bridge also gave values of 0.47 and 7.34%. The model validation test showed results whose values ranged from 0.47 (7.34%), 0.32 (8.65%) and 0.26 (8.13%) at the old N2 Road Bridge, Railway Bridge, and Bridge channel in the lower estuary, respectively (Figure 5.21, Figure 5.22 and Figure 5.23).

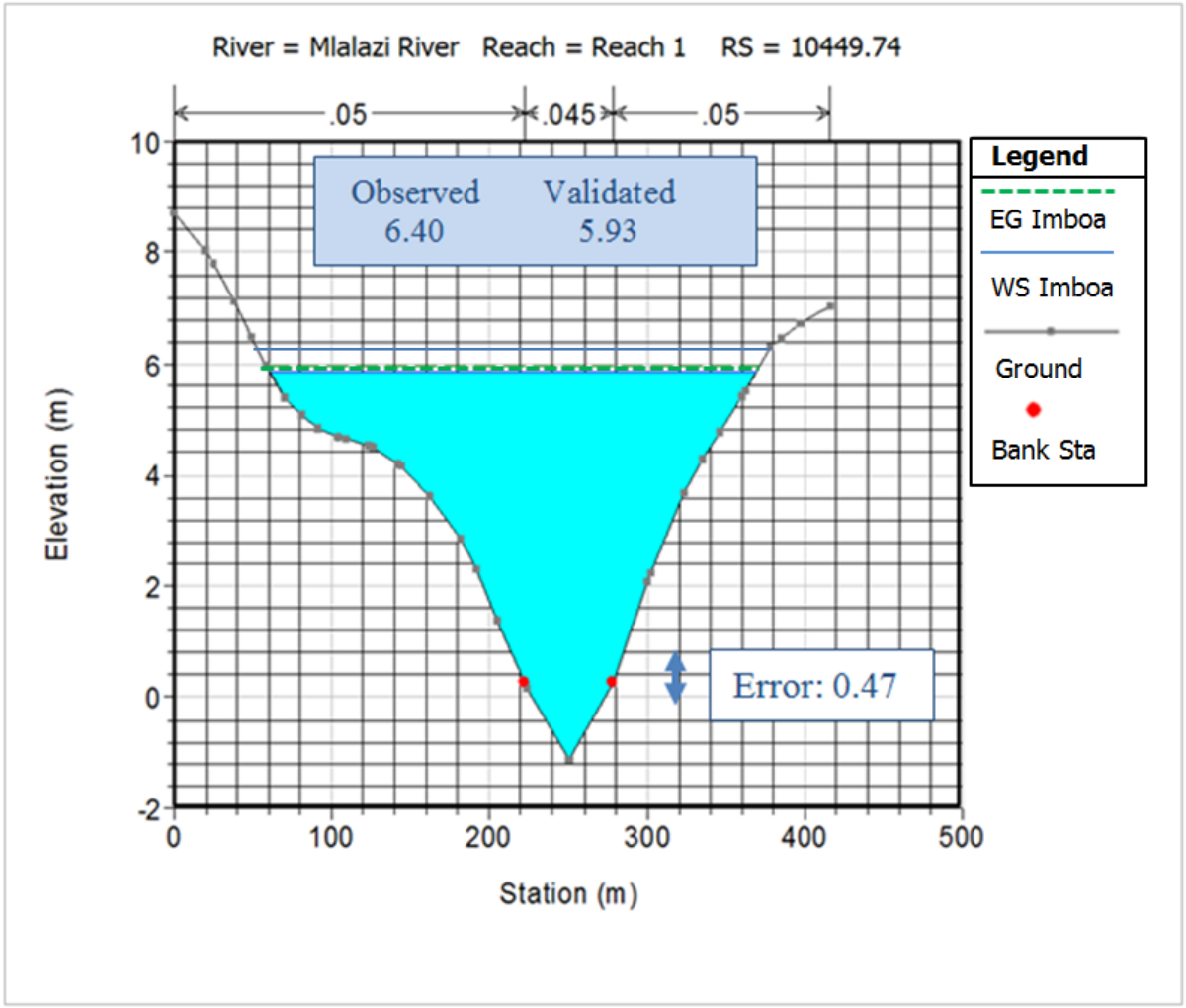

Figure 5.21: Comparisons between the measured (blue line) and simulated peak for the Imboa storm event on the N2 Bridge

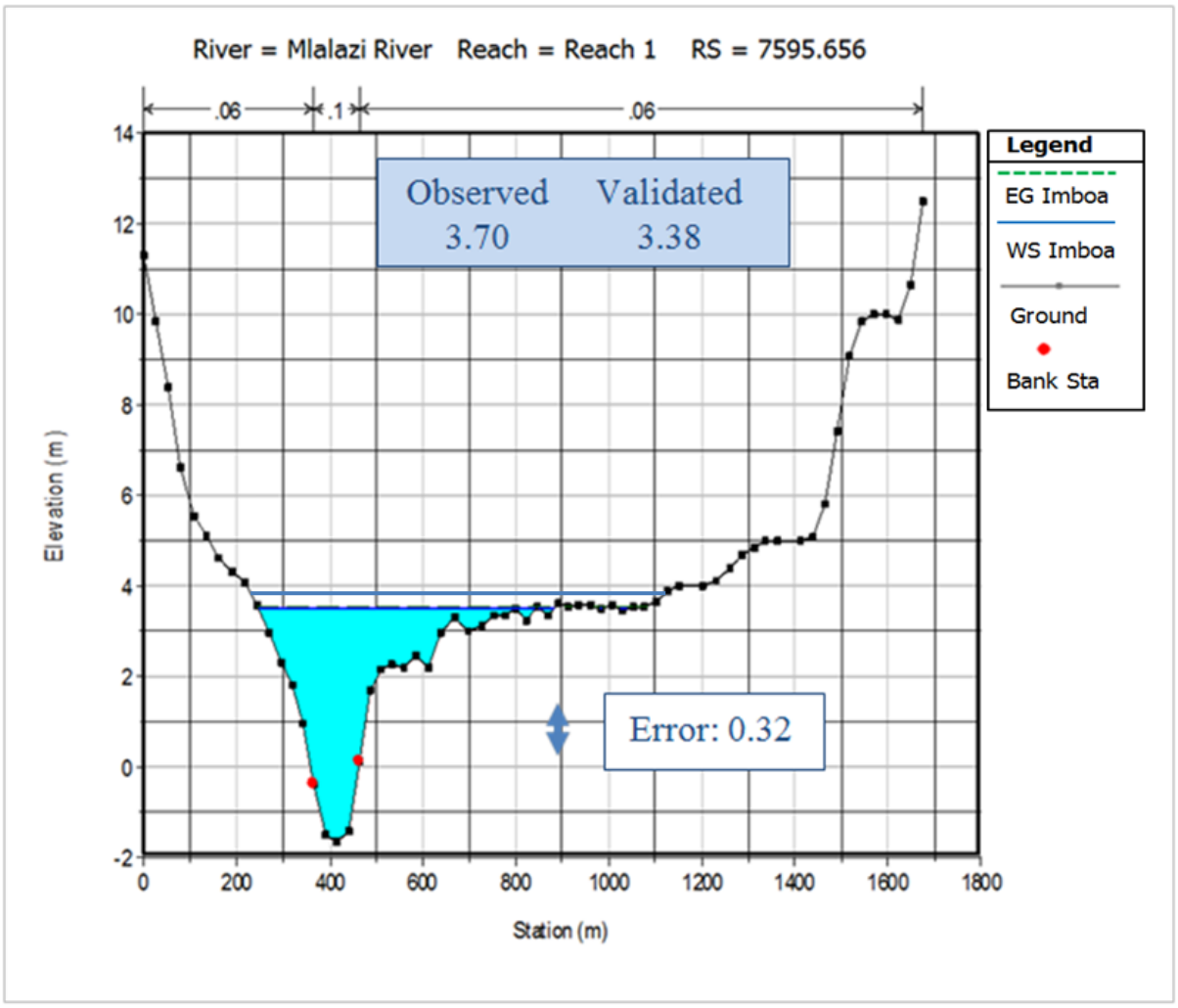

Figure 5.22: Comparisons between the measured (blue line) and simulated peak for the Imboa storm event at the Railway Bridge

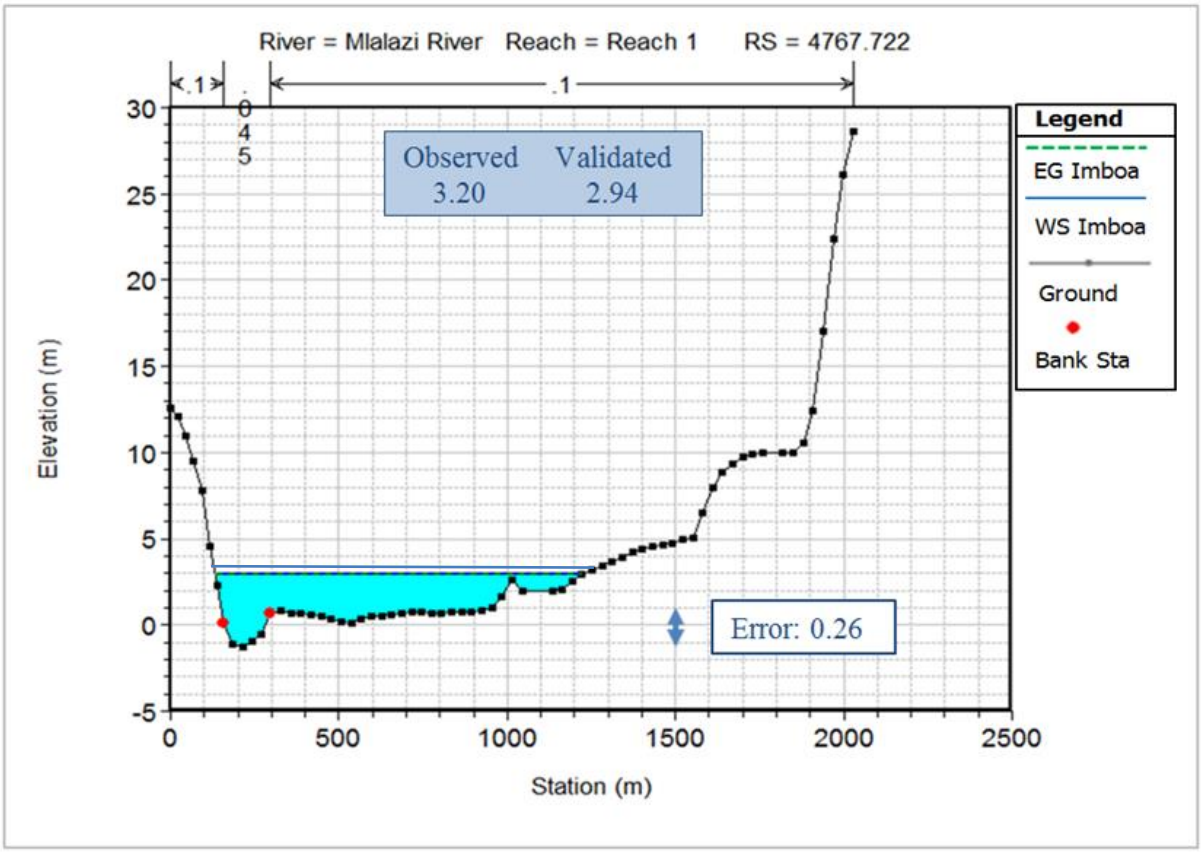

Figure 5.23: Comparisons between the measured (blue line) and simulated peak for the Imboa storm event at the lower estuary bridge channel

The area of inundation for the Imboa flood event in the estuary and floodplain is illustrated in Figure 5.24. This flood event extended from the main channel onto the adjacent floodplain. It did not rise above the significant hydraulic structures (bridges) in the estuary, as shown in the photograph (Figure 5.24). The observed peak level was approximately 0.3 m below the R102 Road Bridge during the May 2018 flood event. The field observation revealed that the prawn farm and parkland downstream of the railway bridge were flooded, as the model indicated in Figure 5.24. The drainage canals in the sugar cane fields in the estuary did overflow onto the floodplain and hydraulic roughness increased.

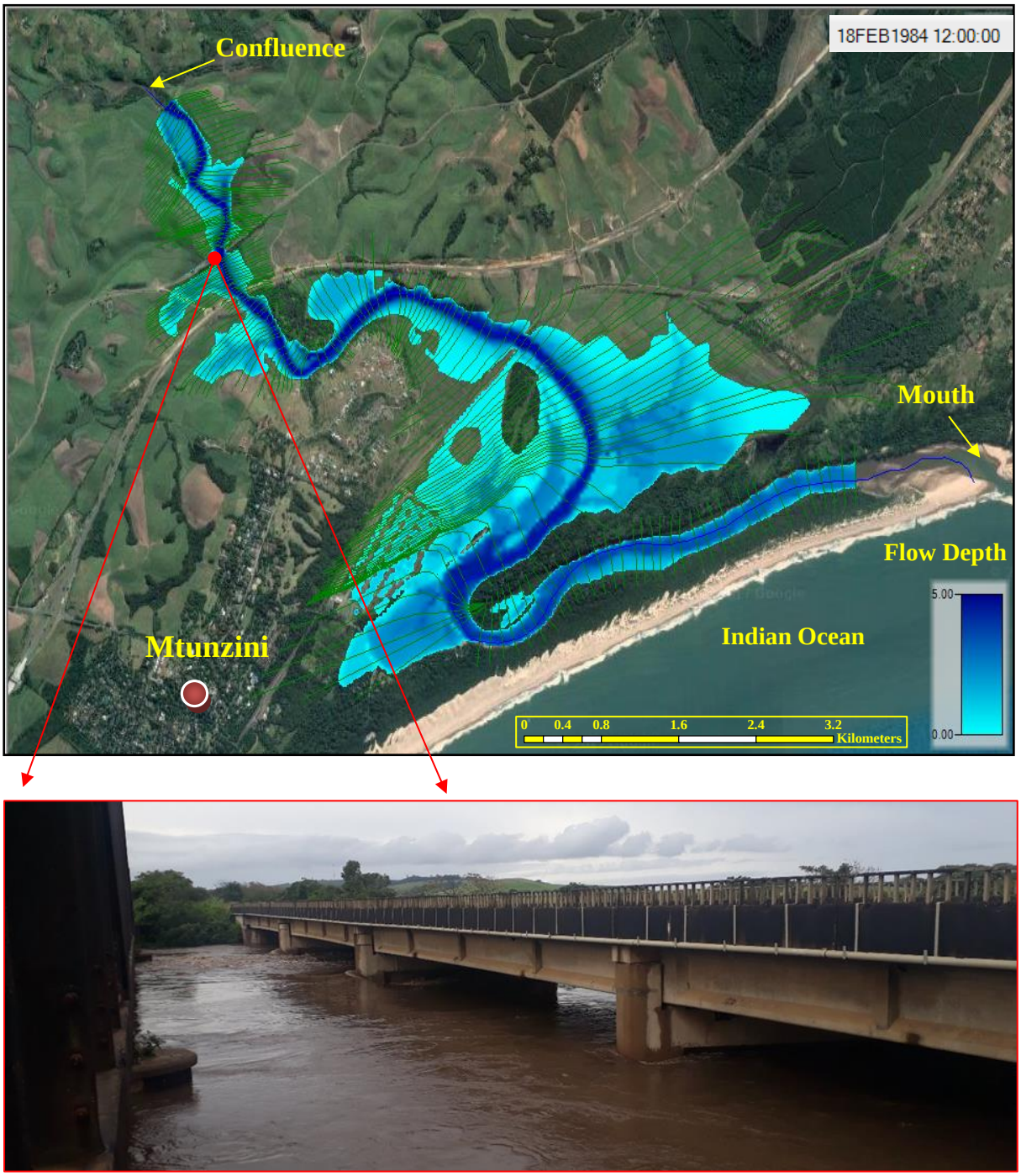

Figure 5.24: The simulated spatial extent of the flooding along the Mlalazi Estuary during a 1984 Imboa flood event. The photograph shows the May 2018 storm event's maximum peak level at the old N2 Road Bridge (photo by Kelbe).

5.6.2 *Flow validation for the Q_{10yr} flood event*

The rainfall run-off (HEC-HMS) model by Rasifudi (2019) predicted flow values of 220 m^3/s and 215 m^3/s for the May 1971 and October 1999 flood events, respectively. The HEC-RAS flow model continuously routed the two events in the estuary and produced a fluvial stage of 4.13mMSL (May 71) and 3.90 mMSL (Oct 99) confluence, as shown in Figure 5.25 and 5.26. There was a simulation difference of 0.23 m between the two events, which could be attributed to rainfall variation. A significant amount of rainfall was recorded before the May 1971 event, whereas little rainfall was observed before the October 1999 flood event. The model results correlated very well with the observed flood peaks of these independent events. The validation run gave stage differences of 0.25 (*PBIAS* of 6%) and 0.12 (*PBIAS* of 0.5%) for May 1971 and Oct 1999 flood events, respectively (Table 5.6).

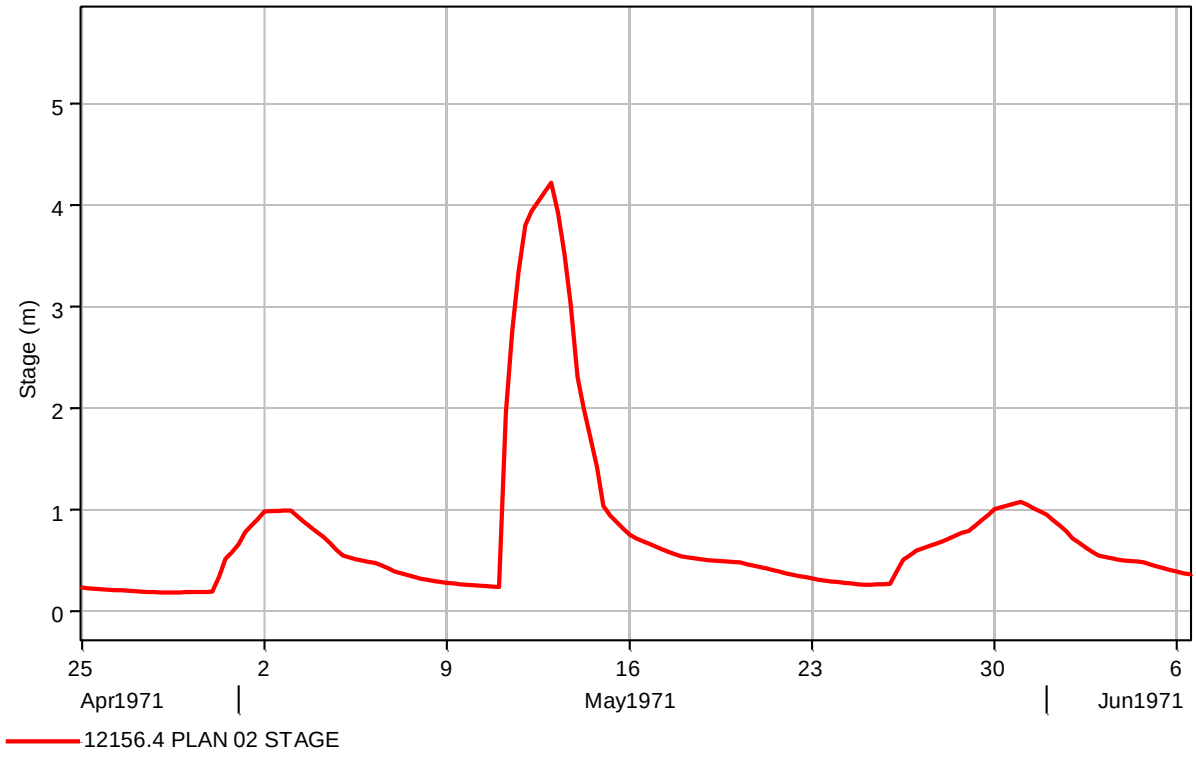

Figure 5.25: The continuous simulation of May 1971 storm events (upper graph) at the confluence of the Mlalazi River and Ntuze River

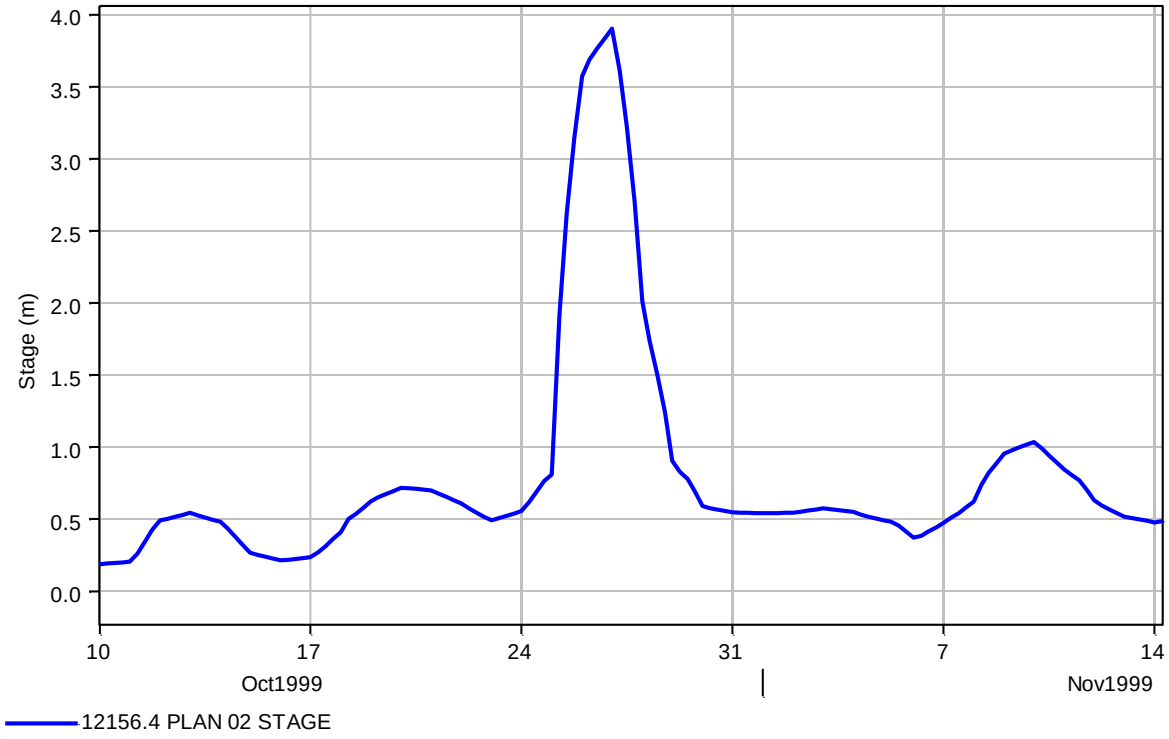

Figure 5.26: The continuous simulation of October 1999 storm events (upper graph) at the confluence of the Mlalazi River and Ntuze River

The area of inundation for the May 1971 flood event in the estuary and floodplain is illustrated in Figure 5.27. It was observed that the occurrence of this magnitude did not entirely overflow onto the floodplain where the land use was predominantly used for sugar cane cultivation. As noted in Chapter 3: Section 3.3, some sugar cane plantations have many drainage canals (Figure 5.27) that increased the flow rates and thus minimised the fluvial erosion and deposition on the floodplain (Kelbe *et al.,* 2019). The inundation map shows the quick overland flow from the May 1971 event onto the drainage canals, then into the estuary's main channel. This is an indication that the adjusted parameters during model calibration were successful.

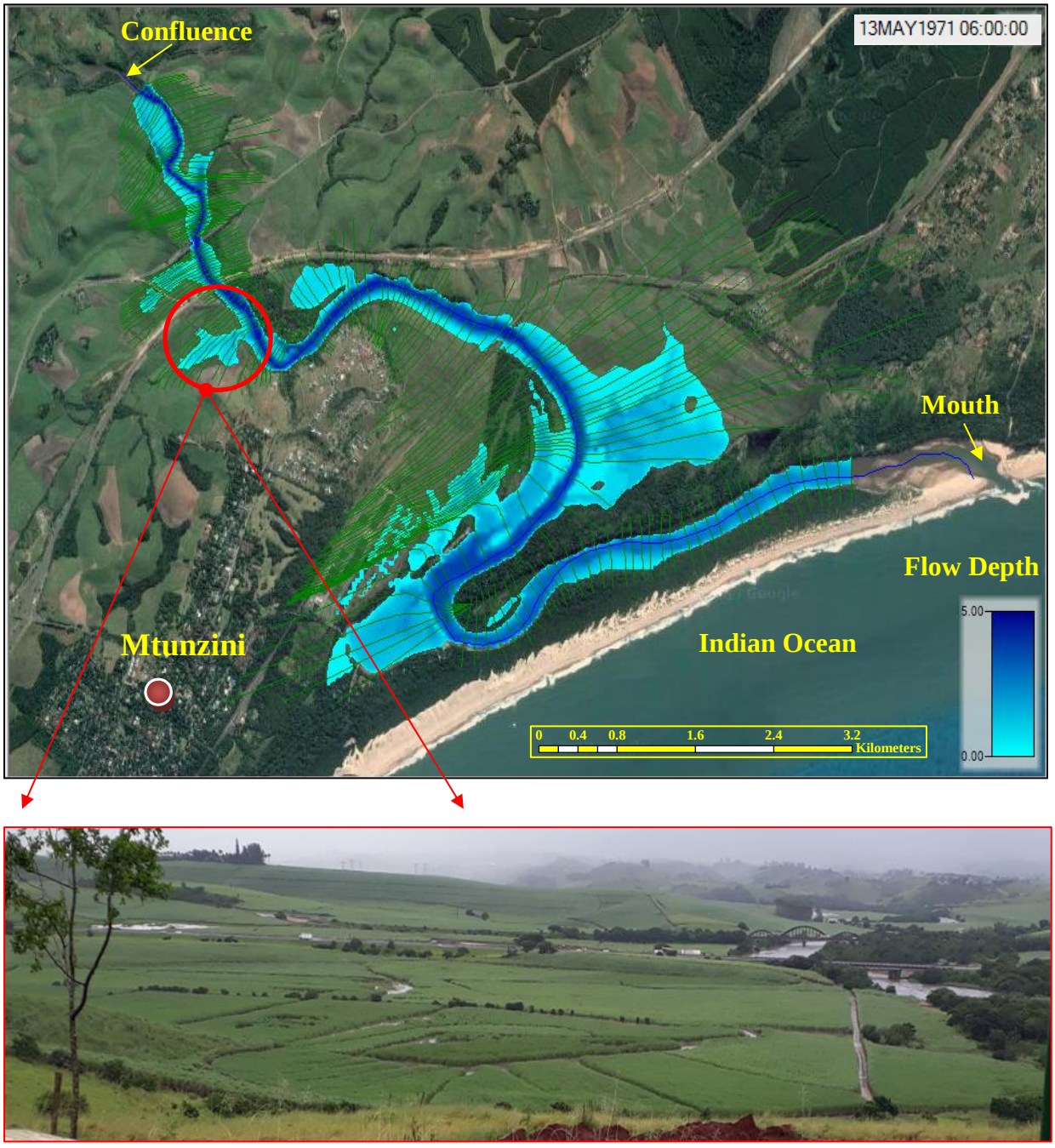

Figure 5.27: The simulated spatial extent of the flooding along the Mlalazi Estuary during a May 1971 flood event. The photograph shows the flooded sugar cane field during the February 2018 storm event at the old N2 Road Bridge (photo by Kelbe).

The floodplain inundation for the Q_{10yrs} flood event would have attenuated the flood hydrograph along the estuary to varying extents. This event moderately flooded the upper estuary and slightly flooded the spatial area downstream of the railway bridge in the north-eastern portion. This is due to the fact that the land use in this portion is predominantly sugar

cane plantations with artificial canals running parallel to the elevation contours and perpendicular to the surface flow lines. This flood event did not entirely inundate this section since the drainage canals quickly channelled the overland run-off by increasing the flow rate due to decreased roughness from the floodplain (Figure 5.27). This flood management practice also reduced the floodplain erosion and deposition.

5.7 Summary of the event-based model validation

The event-based model validation task was performed to test the calibration parameters for specific storm events observed within the Mlalazi Estuary. There were a few significant differences between the simulated and the observed data. The validation ran well, with all the strategic locations in the estuary showing results within 0.5m of the experimental measurements. The percent bias (*PBIAS*) performance was also very satisfactory since the values were within 10% of the experimental data (Table 5.6). Although the experimental data from the HEC-RAS flow model could simulate a medium to high fluvial stage and future flood events, good run-off data (boundary conditions) was not available from the Mlalazi River.

Table 5.6: Summary of model validation results in the Mlalazi Estuary

Location	Flood Events and Date		Simulated Peak Stage (m)	Observed Peak Stage (m)	Prediction error	PBIAS (%)
Upper Estuary	Q_{10yrs}	May 71	4.13	3.88	-0.25	-6.44
	Q_{10yrs}	Oct 99	3.90	3.88	-0.12	-0.52
	Q_{50yrs}	Feb 84	6.83	7.28*	0.45	6.18
	Q_{50yrs}	Feb 84	5.93	6.40#	0.47	7.34
Middle Estuary	Q_{50yrs}	Feb 84	3.38	3.70	0.32	8.65
Lower Estuary	Q_{50yrs}	Feb 84	2.94	3.20	0.26	8.13

* Peak Observed at Confluence # Peak Observed at Old N2 Bridge

CHAPTER 6. RESULTS AND DISCUSSION

This chapter uses the HEC-RAS (version 5.0) flow model as a predictive tool to analyse floods and aspects of their dynamic characteristic zones and duration of flooding within the Mlalazi Estuary for different size storm events (Q_{2yr}, Q_{10yr}, Q_{20yr}, Q_{50yr} and Q_{100yr}). The model simulations were used to analyse flow velocity further to identify the potential erosion and deposition sites in the estuary and floodplain and to analyse the particle sizes (clay, silt, sand, etc.) likely to be transported downstream by different flood events.

6.1 Spatial Flow Velocity Distribution for a Q_{2yrs} Fluvial Event

The Q_{2yrs} run-off simulation on the upper estuary indicated the depth-averaged velocity for this fluvial event when there is no tidal interaction between 0.51 m/s in the narrow sections and 0.22 m/s towards the wider channel. Figure 6.1 illustrates the depth-averaged velocity distribution across an area of the floodplain and main channel on a section with a straight channel and a floodplain inundated during these events. It can be observed that the maximum velocity was concentrated in the main channel for the straight channel as the depth of inundation in the floodplain is shallow with high surface friction, causing the flow to almost cease and allow significant deposition of suspended sediments. In contrast to the velocity distribution in a cross section through a left-hand bend shown in Figure 6.2, there was a stagnant inundation area, with sediment deposition on the inner bank floodplain and a higher velocity across the outer bank floodplain.

The averaged flow velocity further decreased gradually downstream of the Railway Bridge. It rarely exceeded 0.2 m/s (Figure 6.3) due to the active channel, which gets wider towards the lower bend with increased water storage in the adjacent floodplains. At the U-shape bend on the lower estuary, the flow rate rose to more than 0.5 m/s (Figure 6.4) in the main channel and some sections on the lower channel, narrowed by the deposition of the marine sediments brought in during flood tides.

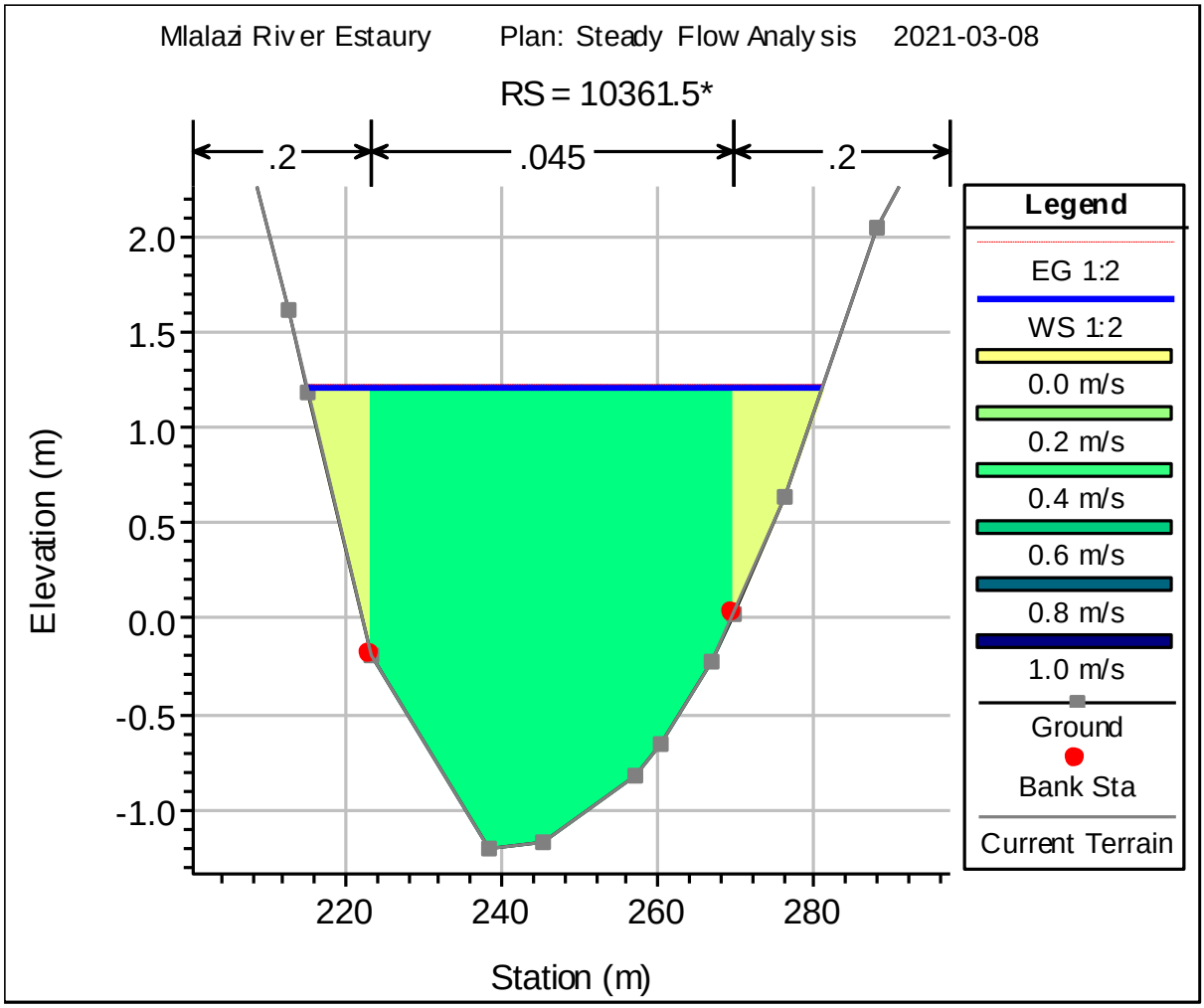

Figure 6.1: The flow velocity distribution on a straight river section roughly 100m downstream of the N2 Road Bridge for Q_{2yrs} flood event. The EG represents the energy guideline for a given water surface elevation. The WS represents the calculated water surface from the energy equation.

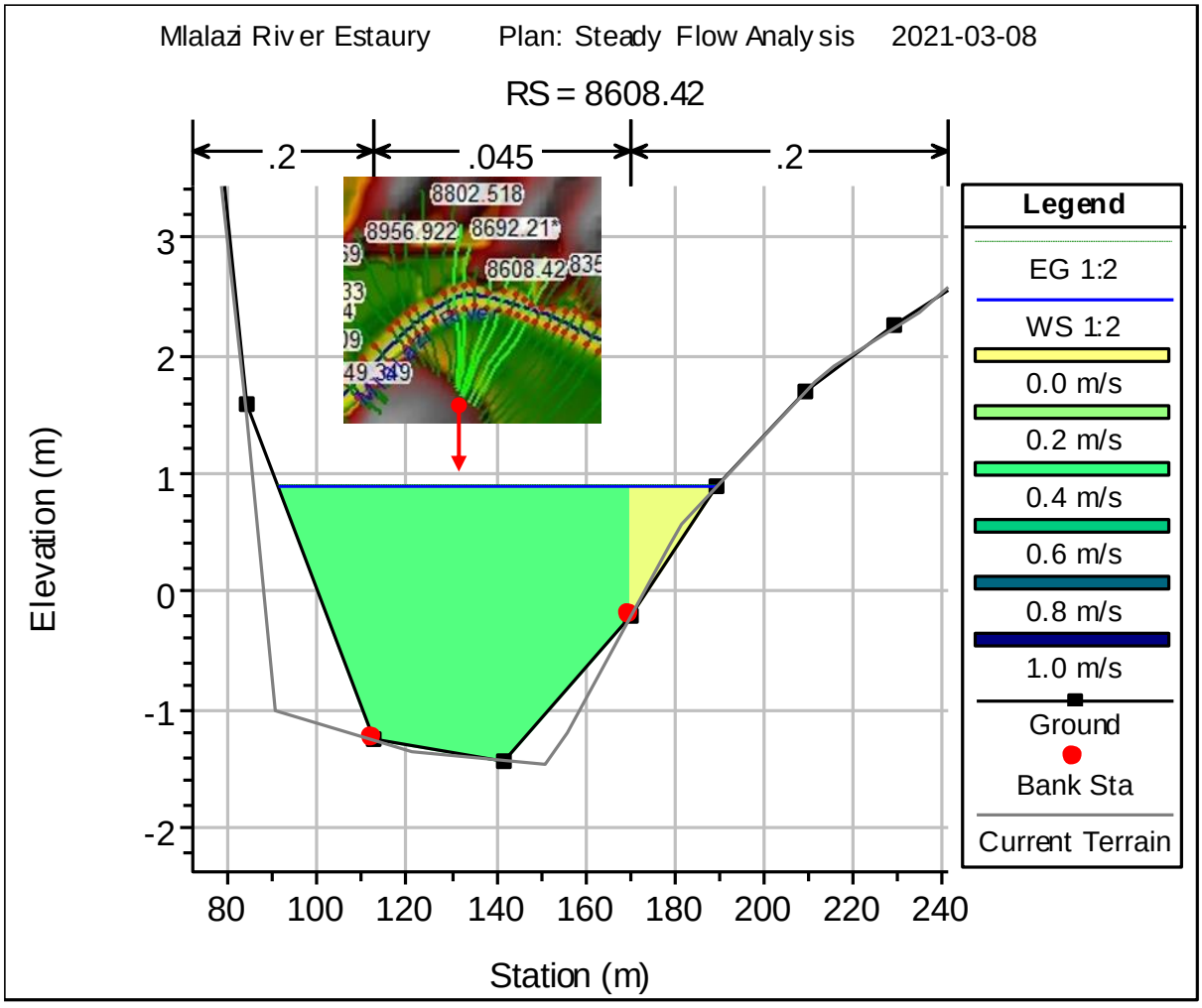

Figure 6.2: The flow velocity distribution on a left-hand bend river section roughly 1 km downstream of the N2 Road Bridge for Q_{2yrs} flood event. The RS represents the river cross section number on the HEC-RAS flow model.

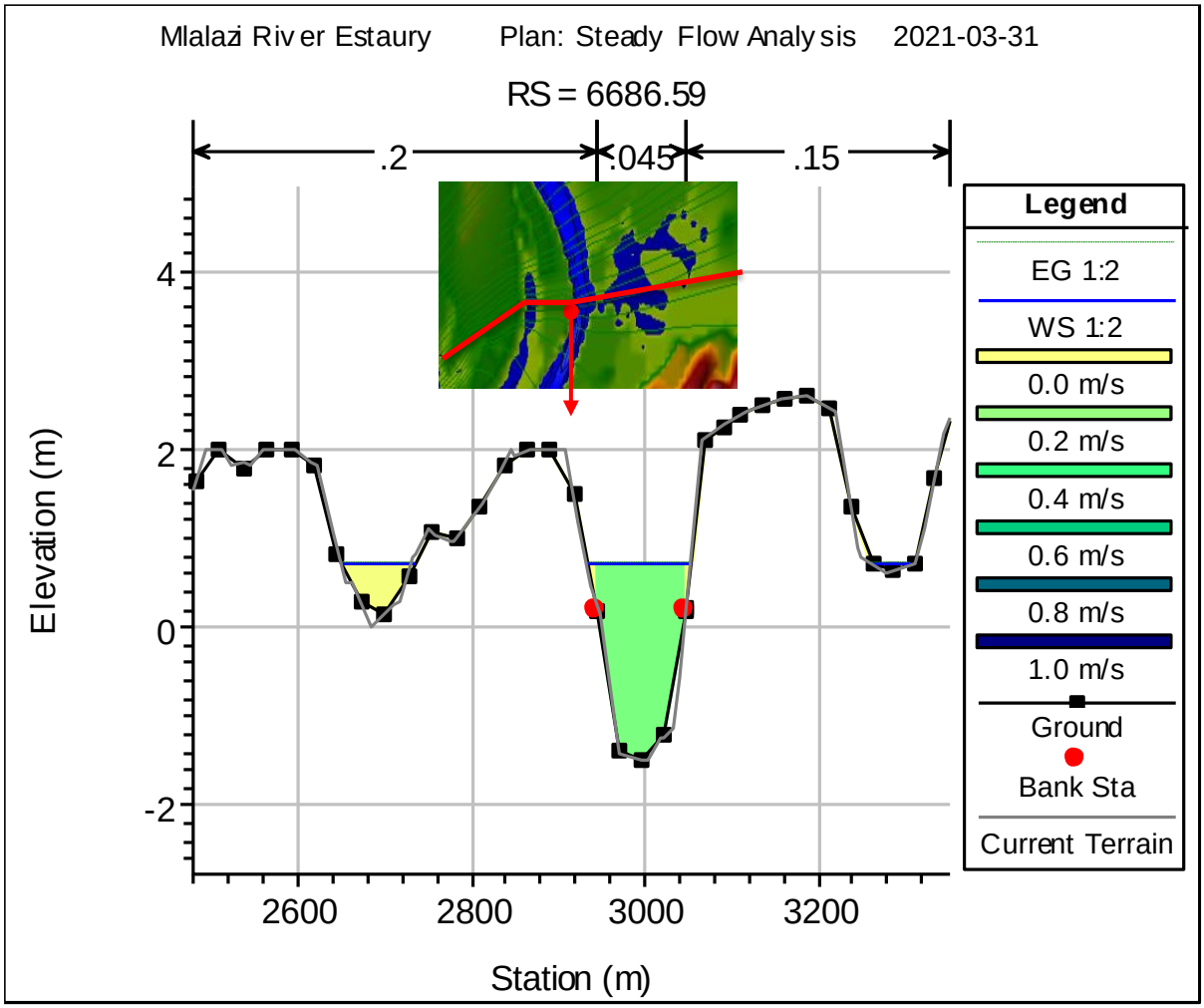

Figure 6.3: The flow velocity distribution of a cross section through the extensive floodplain/marsh area roughly 500 m downstream of the Railway Bridge for Q_{2yrs} flood event. The RS represents the river cross section number on the HEC-RAS flow model.

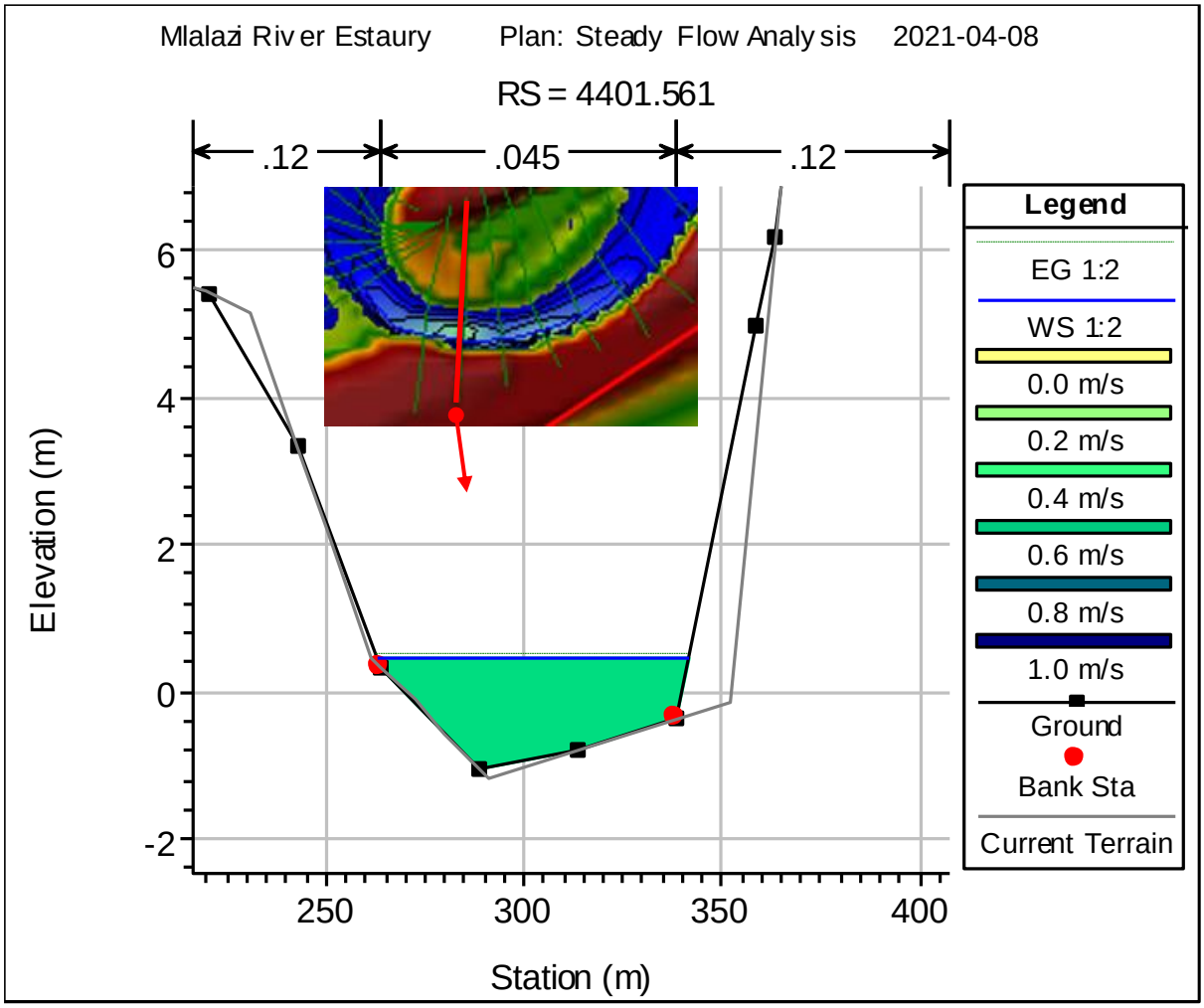

Figure 6.4: The flow velocity distribution profile at the U-shape bend on the lower estuary for Q_{2yrs} flood event

It should be noted that the HEC-RAS flow model underestimated the Q_{2yrs} fluvial event on the middle channel and lower channel of the estuary during calibration which was attributed to the tidal dynamics not included in the model. However, the flow velocity distribution pattern for the Q_{2yrs} event was important for providing knowledge on the alluvial sediment transport and deposition in the estuary during average flow conditions when the tidal motion dominates for more than 50% of the time. Figure 6.5-A shows the contour lines of the depth-averaged spatial velocity distribution within the Mlalazi Estuary. The model simulations indicated that the estuary generally has a depth-averaged velocity of < 0.5 m/s (Figure 6.5-B) but showed several sections in the upper channel and mouth channel where the velocity can reach almost 1 m/s.

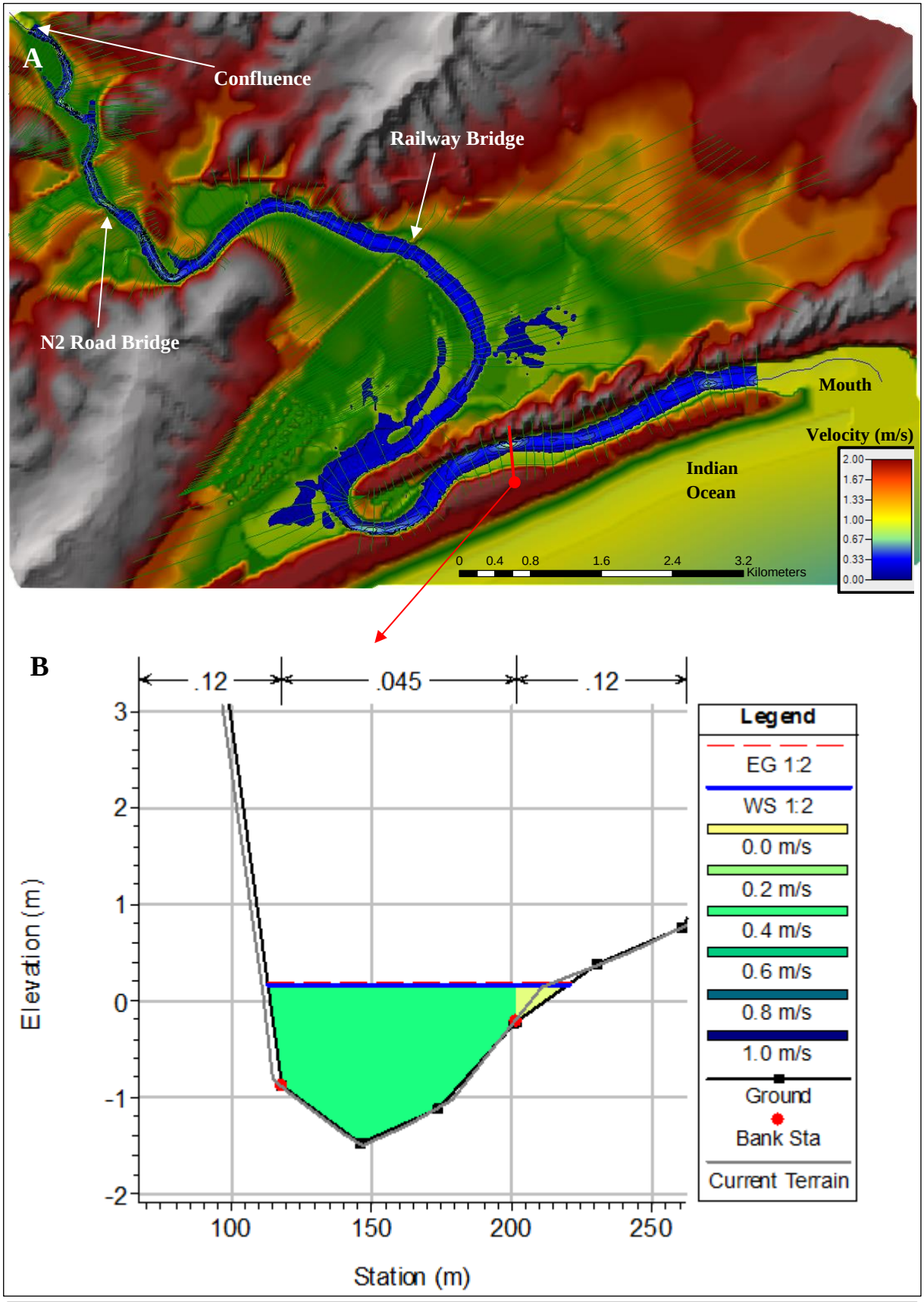

Figure 6.5: A - horizontal flow distribution for Q_{2yrs} flood event along the topographical terrain of the Mlalazi Estuary. B - a narrow river section on the lower channel where the flow velocity rises to 0.5 m/s

Using the Hjulström-Sundborg diagram explained in Section 2.2 of Chapter 2, the depth-average velocity of 0.51 m/s (510 mm/s) in the upper estuary is capable of eroding silt particle (0.01 m) and sand particle (1 mm). This velocity is however not significant enough to erode fine clay particles (< 0.01 mm) that are bound by cohesive forces. However, once these particles have been eroded in the channel or inflow from the upstream catchment, the velocity is enough to keep clay sediments in suspension and transport them along the estuary until the settling velocity is reached in sections further downstream. For the sand particle to remain in suspension and transported downstream, the settling velocity should be > 0.1 m/s (>100 mm/s). The Q_{2yrs} flow event could only erode and transport sediment particles between 0.01mm and 1.0mm. The simulated depth-averaged velocity obtained was > 0.50 m/s at the lower bend and some constricted area in the estuary. This event could not erode and transport the fluvial sediment particle > 1.0 mm (e.g. gravel, pebbles, etc.), but this velocity of 0.50 m/s would allow such sediments to be deposited from the upstream catchment.

The simulated depth-averaged fluvial flow velocity at the mouth was 0.29 m/s (290 mm/s). The alluvial clay, silt and fine sand sediment particles would remain in suspension and be transported into the Indian Ocean. The fluvial depth-averaged velocity of 0.29 m/s would also be able to scour some fine loose marine sediments (< 0.10 mm) brought in during the flood tide in the estuary floodplain.

6.2 Spatial Flow Velocity Distribution for a Q_{10yrs} Flood Event

The peak spatial distribution of the estuary area underwater during the Q_{10yrs} flood event is shown in Figure 6.6. It illustrates the contour lines of the depth-averaged velocity along the Mlalazi Estuary for a predicted inflow rate of 221 m^3/s. There is minimal change across the floodplain, but the main channel shows that the flow rate varied significantly in certain sections. The Q_{10yrs} flow simulation for the upper part of the estuary showed that the depth-averaged flow velocity varied between >0.6 m/s and <0.5 m/s in the narrow river sections >0.5 m/s <0.25 m/s near the expansive floodplain sections in the middle part of the estuary. The expansion resulted from the accumulated flow storage upstream of the U-shape bend in the lower part of the estuary. The depth-averaged velocity rose to >1 m/s as flow was restricted through the narrow section of the lower estuary towards the mouth.

The hydraulic model for the Q_{10yrs} simulated peak depth-averaged velocity of < 0.5 m/s occurred just upstream of the Railway Bridge where flow is confined by steep embankments and rose to > 0.5 m/s immediately downstream. This was mainly due to the narrow river sections below the Railway Bridge (Figure 6.7) and extended approximately 200 m downstream. The model also predicted a higher velocity (< 0.8 m/s) near the mouth.

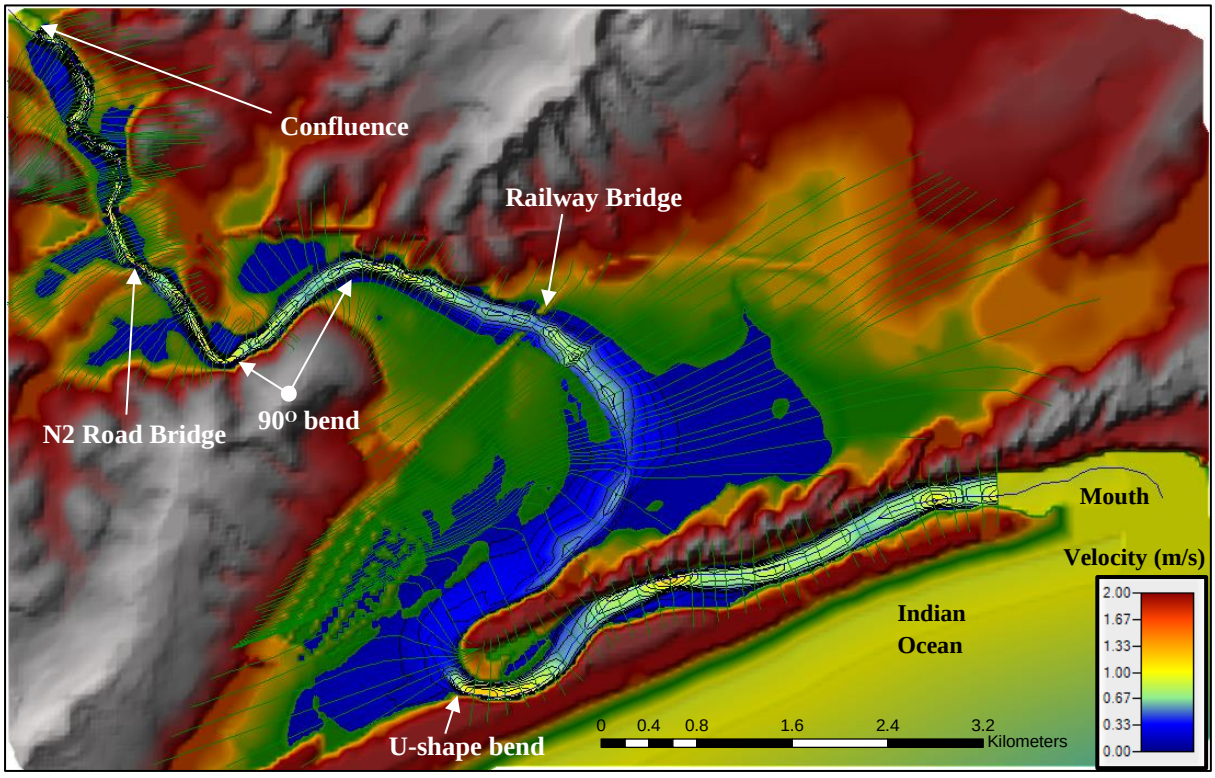

Figure 6.6: The horizontal flow velocity distribution for Q_{10yrs} flood event along the topographical terrain of the Mlalazi Estuary

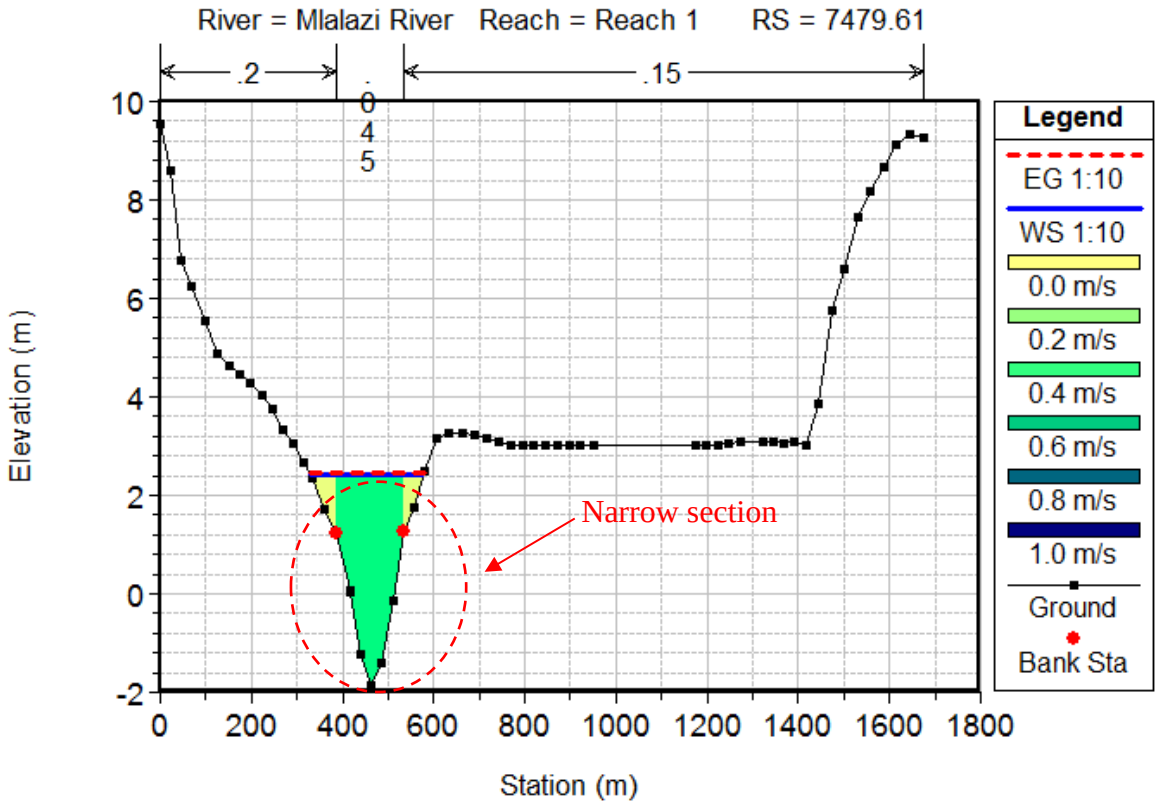

Figure 6.7: A narrow river section below the Railway Bridge where the flow velocity on the main channel rises to > 0.6 m/s for Q_{10yrs} flood event.

The flow model at several constricted channel cross sections near the confluence showed a peak velocity reaching almost 1.6 m/s on the main channel for the Q_{10yrs} flood event (Figure 6.8-A). This section's channel bathymetry revealed a lightly deeper narrow channel towards the left river bank where the only elevation value was surveyed (Figure 6.8-B).

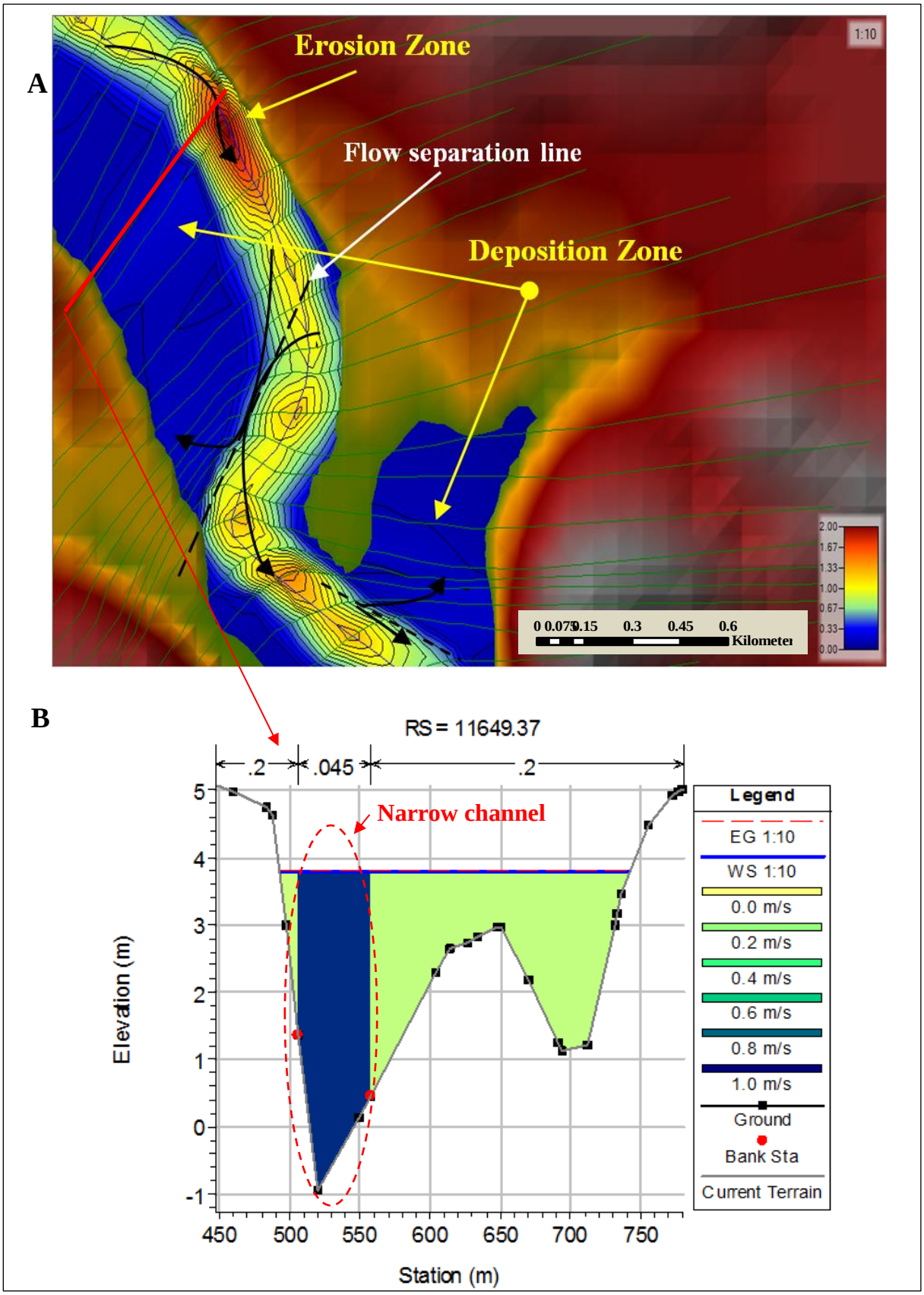

Figure 6.8: A - flow velocity direction at a curved channel on the upper estuary near the confluence. Note the flood lines (blue shaded area) of low velocity conducive to the fine-grained sediments deposition, with nearly high velocities in the main channel. B – a narrow river section on the flow velocity rises to 1.8 m/s (dark blue area) for Q_{10vrs} storm event.

Despite these significant errors from the bathymetry data where one point was taken in the main channel, the hydraulic model show the separation lines between the flow in the main channel and floodplains. This was caused by some water flowing downstream, which was then pushed back or reserved upstream outside the river bend. The deposition of fine-grained alluvial sediments, such as clay, silt or medium-grained sand particles (> 1 mm in diameter), primarily occurred on the floodplain where the velocity was < 0.3 m/s. The deposition also incorporated organic matter such as leaves and twigs brought down in the main channel.

A peak velocity of <1 m/s (1000 mm/s) on the main channel is capable of eroding and transporting sediment particles up to 10mm in diameter (gravel) from the upper catchment to the middle estuary. The fine-grained sediments particles (> 1 mm in diameter) will remain in suspension, and large particles (> 10 mm in diameter) will move along the riverbed through the process of saltation or traction where the velocity > 0.3 m/s. The Q_{10yrs} event is not significant enough to cause substantial erosion on the riverbanks but will bring in much needed fluvial deposit on to the floodplain.

6.3 Spatial Flow Velocity Distribution for a Q_{20yrs} Flood Event

Figure 6.9 illustrates the simulated horizontal flow velocity variation associated with an inflow rate of 372 m^3/s in the Mlalazi Estuary, representing the Q_{20yrs} flood event. The depth-averaged velocity at this flow rate in the upper channel varied between > 0.8 m/s to > 0.5 m/s. The mid-channel section varied between > 0.6 m/s and < 0.25 m/s due to the expanded area of inundation. The model simulation showed that the average velocity profile generally remained the same on the plain upstream of the U-shape curve in the lower estuary, even though the floodplain storage level rose by 1 m between the Q_{20yrs} and Q_{10yrs} storm event. As the water level increased, more flow was confined to a sub-critical condition in the storage, and thus most fluvial sediments deposited on the floodplains due to the decline in flow velocity. However, there is a slight variation on the main flow channel due to deposited marine sediments brought in by flood tide.

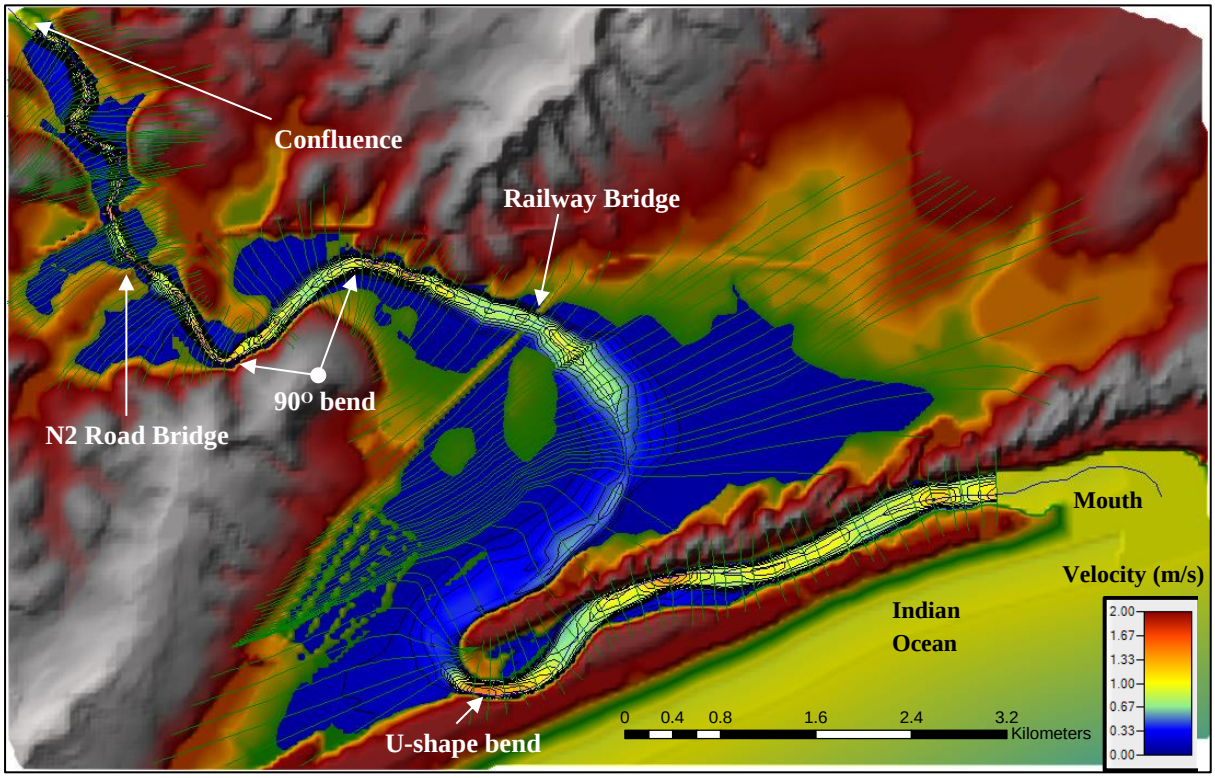

Figure 6.9: The horizontal flow velocity distribution for Q_{20yrs} flood event along the topographical terrain of the Mlalazi Estuary

The flow velocity on the active or main channel reached more than 1.20 m/s in the deep narrow channel near this storm event's confluence. This flow rate can overcome some of the stronger cohesion forces between tiny clay particle nodules. It can erode the silt and fine to medium-grained particles and transport them downstream, although particles > 5 mm will be deposited. Immediately downstream of the Railway Bridge, the active channel's velocity reached about 1m/s and dissipates below 0.5 m/s due to a broader channel path (wetted perimeter) about 500 m downstream. This could have been due to increased levels on the back-up floodplain storage further downstream..

The depth-average velocity at the lower 180° bend reached more than 1.30 m/s as the estuary (channel and floodplain) narrows towards the estuary mouth, where the flow is capable of eroding and transporting sediment particles up > 10 mm (Figure 2.5) along the frontal dune. This event could mobilise the marine sediments brought in by the flood tide since the simulated velocity at the mouth was < 1 m/s (1100 mm/s). This velocity could have caused significant erosion of the larger particle (Figure 2.6). The effect of this Q_{20yrs} flood event is illustrated by

the scouring that occurred at the mouth shown in the image in Figure 6.10, about five (5) days after this event due to movement of sediment and simultaneous increase in water level at the mouth.

Figure 6.10: Google image showing a mouth breaching of the Mlalazi Estuary after the Q_{20yrs} flood event in May 2017

6.4 Spatial Flow Velocity Distribution for a Q_{50yrs} Flood Event

The simulated peak Q_{50yrs} flood event of 767 m^3/s that occurred on 19 February 1984 was estimated to be the second-largest event observed in the Mlalazi Estuary. The horizontal flow velocity distributions through the estuary and floodplain for the Q50yrs flood event are plotted in Figure 6.11. The flow rates for this event varied along the estuary and floodplain, as did the stage, but the researcher observed turbulent flows through major hydraulic structures (e.g. Bridge), as was noted in Photograph 3.15. The HEC-RAS model simulated the depth-averaged flow velocity of 0.64 m/s on the floodplain at the confluence for this flood event (Table 5.2) and peaked at over 2.0 m/s 1.5m/s in some constricted channel in the upper estuary.

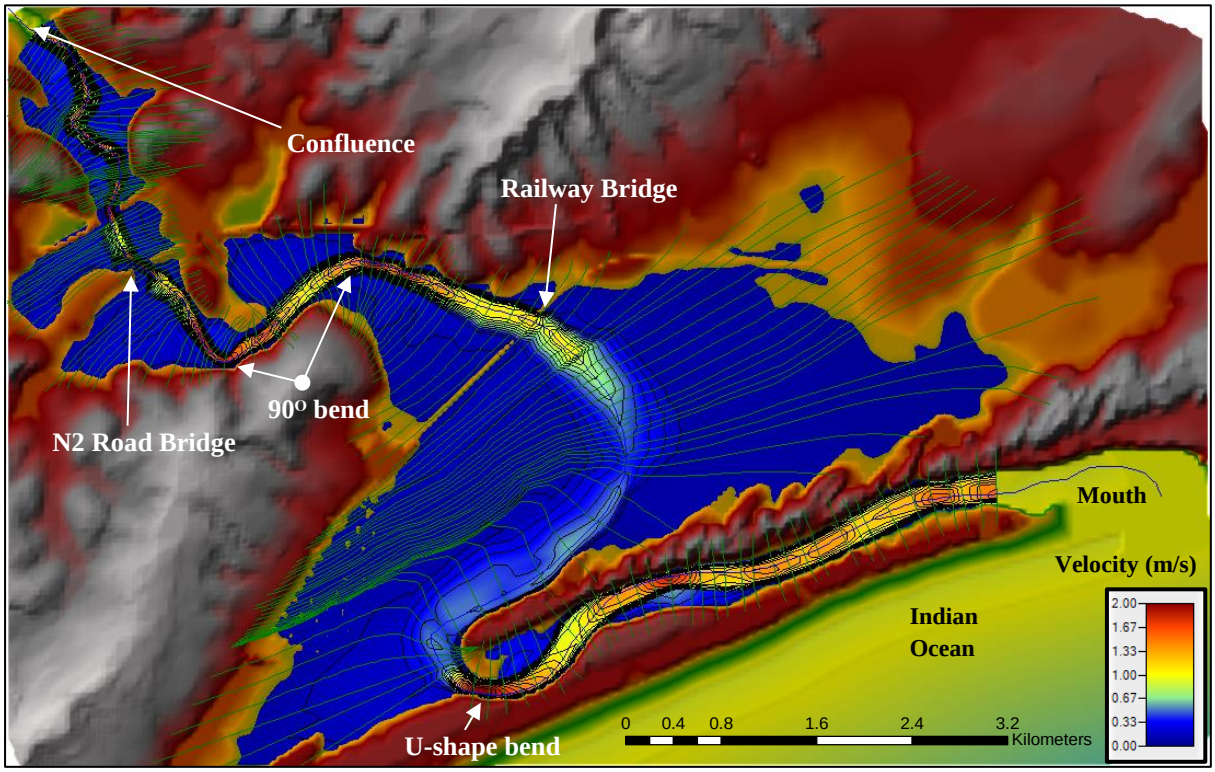

Figure 6.11: The horizontal flow velocity distribution for a Q_{50yrs} flood event along the topographical terrain of the Mlalazi Estuary

The flow velocity of 1.5 m/s (1500 mm/s) on the main channel can erode and transport fluvial sediment particles up to 50 mm in diameter, according to the Hjulström-Sundborg diagram. The large particle sizes (e.g. pebbles, cobbles, etc.) would experience less resistance during transportation in the main channel from the confluence along the estuary until it approached the embankment storage upstream the Railway Bridge, where the velocity dropped below the settling velocity of 1.0 m/s. These particles would either be deposited on the river banks' edges, remain stationary on the riverbed or become blocked by the Railway Bridge's pillars as the flow velocity decreased rapidly into the floodplain, as shown by the velocity contours in Figure 6.11. However, the finer particles would have been transported and deposited further up the cross section into the floodplain.

The depth-averaged flow velocity was 0.37 m/s downstream of the Railway Bridge, whereas, in the main channel, it propagated from 1.0m/s to 0.6 m/s at less than 600 m. The gravel-sized particles (20 mm in diameter) were channelled around pillars and moved along the riverbed until the settling velocity fell below 0.1 m/s (100 mm/s) further downstream. The fine-grain sediment was deposited on the floodplains and supplied much-needed nutrients to sugarcane

fields and vegetation. It is important to note that the flood levels were not enough to cause significant damage because the flow velocity was less than 0.3 m/s over most of the floodplains. However, the event would have causes an agricultural loss by submerging the crops if the flooding persisted for too long.

The depth-averaged velocity increased to 1.8 m/s at the U-shaped bend of the lower Mlalazi Estuary. This flow rate was significant to scour even large marine sediment particles transported on the lower floodplain during high flood tides. The event had the energy to considerably reduce the height of the sand berm, widen and deepen the mouth channel and stop the tidal cycle for several days. A large amount of sediment would have been carried into the ocean since the simulated velocity at the mouth was < 1.4 m/s and provided nutrients and shelter for marine species.

6.5 Spatial Flow Velocity Distribution for a Q_{100yrs} Flood Event

The simulated peak Q_{100yrs} flood event during the extreme events of September 1987 of 1175 m^3/s was the most significant event measured in the Mlalazi Estuary and gave a good correlation between observed data during model calibration. Figure 6.12 illustrates the horizontal peak flow velocity contour lines for this extreme flood event in the estuary. This flood event rose above major hydraulic structures and flooded the entire estuary and floodplains. The extent of flooding at the fish farm was gauged from the debris line leading to the Parks Board gate, where boats were ferrying people during the peak flood height. The model simulated the depth-averaged flow velocity of 0.72 m/s on the floodplain at the confluence for the Q_{100yrs} flood event (Table 5.2).

This stream velocity varied along the river sections' length, reaching peaks of < 2.0 m/s in sections of the channel while indicating velocities slightly above 0.30m/s on the floodplains. The flow velocity of 2.0 m/s (2000 mm/s) on the main pathway could have eroded and transported fluvial sediment particles up to 10 mm in diameter from the Hjulström-Sundborg conceptual model (Figure 2.6). The large particle sizes (e.g. pebbles, cobbles, etc.) from the upstream catchment would easily have been transported from the confluence to downstream, where the velocity dropped below the settling velocity of 1.0m/s for the large particles. The velocities of up to 0.3 m/s on the floodplain were generally capable of eroding and transporting

the exposed silt and fine sand particles. The area would however have experienced deposition of the coarse sand particles.

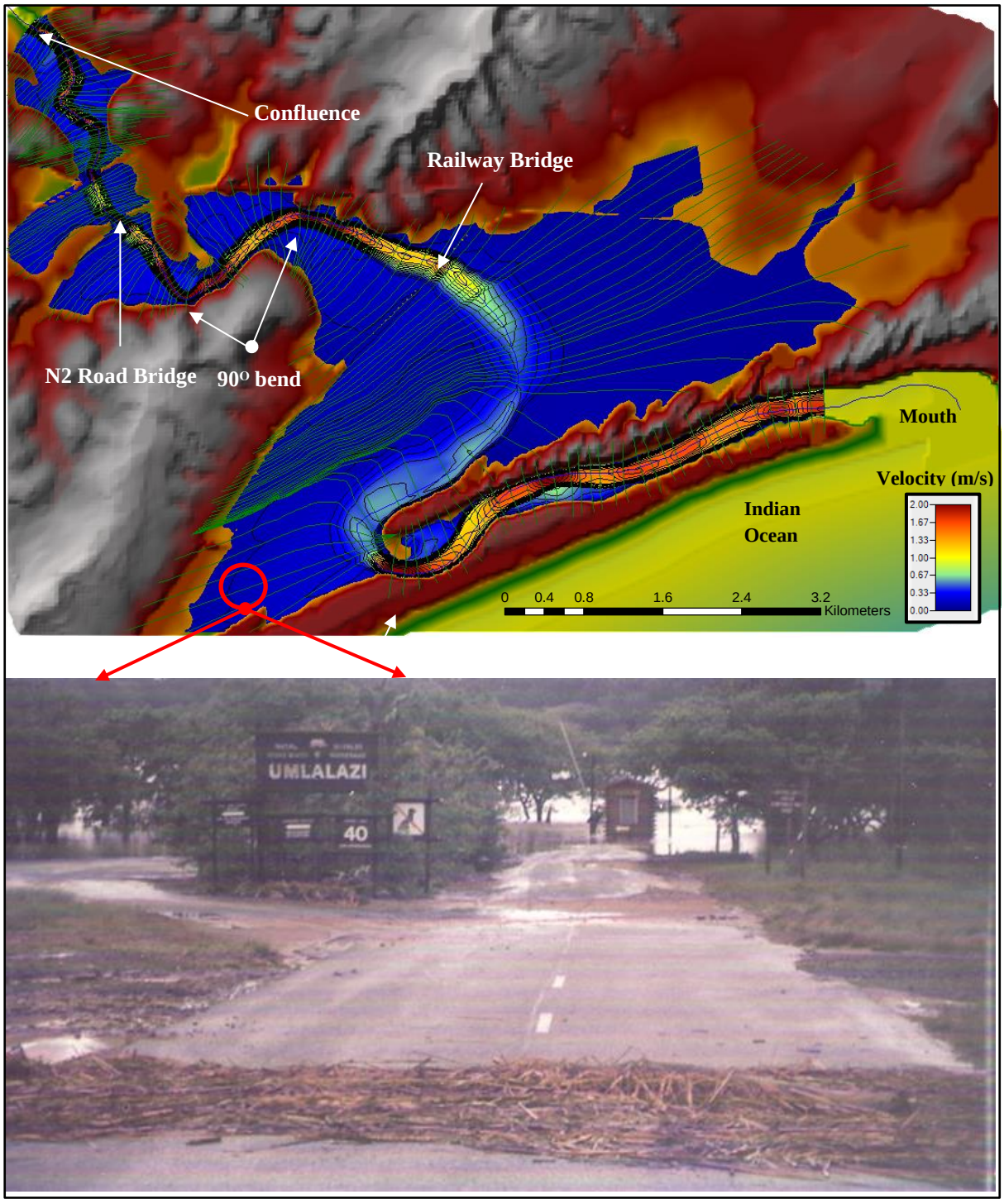

Figure 6.12: The simulated spatial extent of the flooding along the Mlalazi Estuary during a Q_{100yrs} extreme flood event. The maximum height of the 1987 flood event shown by the debris on the road at approximately the same height as the farm ponds (photo by Kelbe).

The inundation map for the Q_{100yrs} flood event indicates that the flow velocity generally remained below 0.3 m/s on the floodplains upstream of the N2 Road Bridge (Figure 6.13). But the flow velocity on the main channel was < 2.0 m/s. However, the depth-averaged flow velocity of 0.82 m/s was simulated at the N2 Road Bridge for the Q_{100yrs} flood event, which correlated well with the calculated 0.87 m/s average velocities from the 1987 survey data (Table 3.1). The statistical evaluation for the average velocity gave a net error and *PBIAS* values of 0.05 and 5.74%, respectively. Satisfactory performance was also achieved for the Q_{50yrs} flood event, where the net error and *PBIAS* values were -0.17 and -26.2%, respectively (Table 6.1).

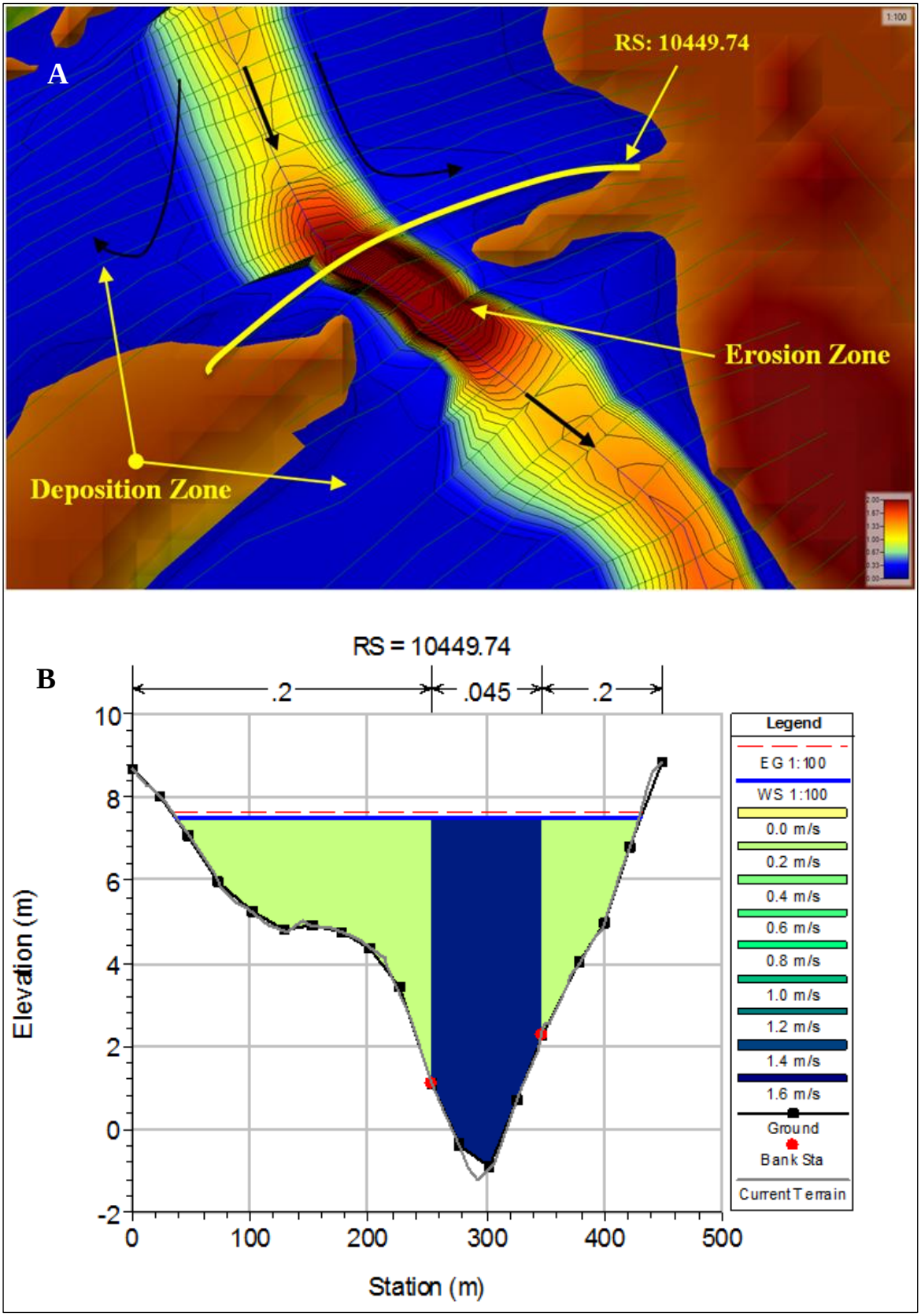

Figure 6.13: Inundation map (A) and cross-sectional velocity distribution profile (B) at the N2 Road Bridge for Q_{100yrs} flood event

The surveyed cross-section profile near the lower bend in the mid-estuary after a significant flood in 1987 showed very little erosion taking place (Chapter 3: Section 3.7). The hydraulic model simulated the depth-averaged velocity of 0.23 m/s at this river section (RS: 5015.724) which differed significantly from the 0.62 m/s estimated velocity from the 1987 survey data. The statistical evaluation for the model in this event gave a net error and PBIAS values of 0.39 and 62.9%, respectively (Table 6.1), indicating model uncertainty.

The flow velocity increased above < 2.0 m/s at the U-shaped bend at the start of the channelled narrow section of the lower floodplain. Figure 6.14 illustrates the flow velocity distribution at the U-shape bend for the Q_{100yrs} flood event. This flow rate was sufficient to scour even large marine sediment particles and transport them along the lower floodplain. The event would have ultimately reduced the height of the sand berm, widened and deepened the mouth channel and stopped the tidal cycle for several days. A large amount of sediment would have been carried to the ocean since the simulated velocity at the mouth was < 1.7 m/s and provided fluvial nutrient and shelter for coral/marine species. There was no observation or other data on the extent of the scouring in the estuary mouth during these extreme events.

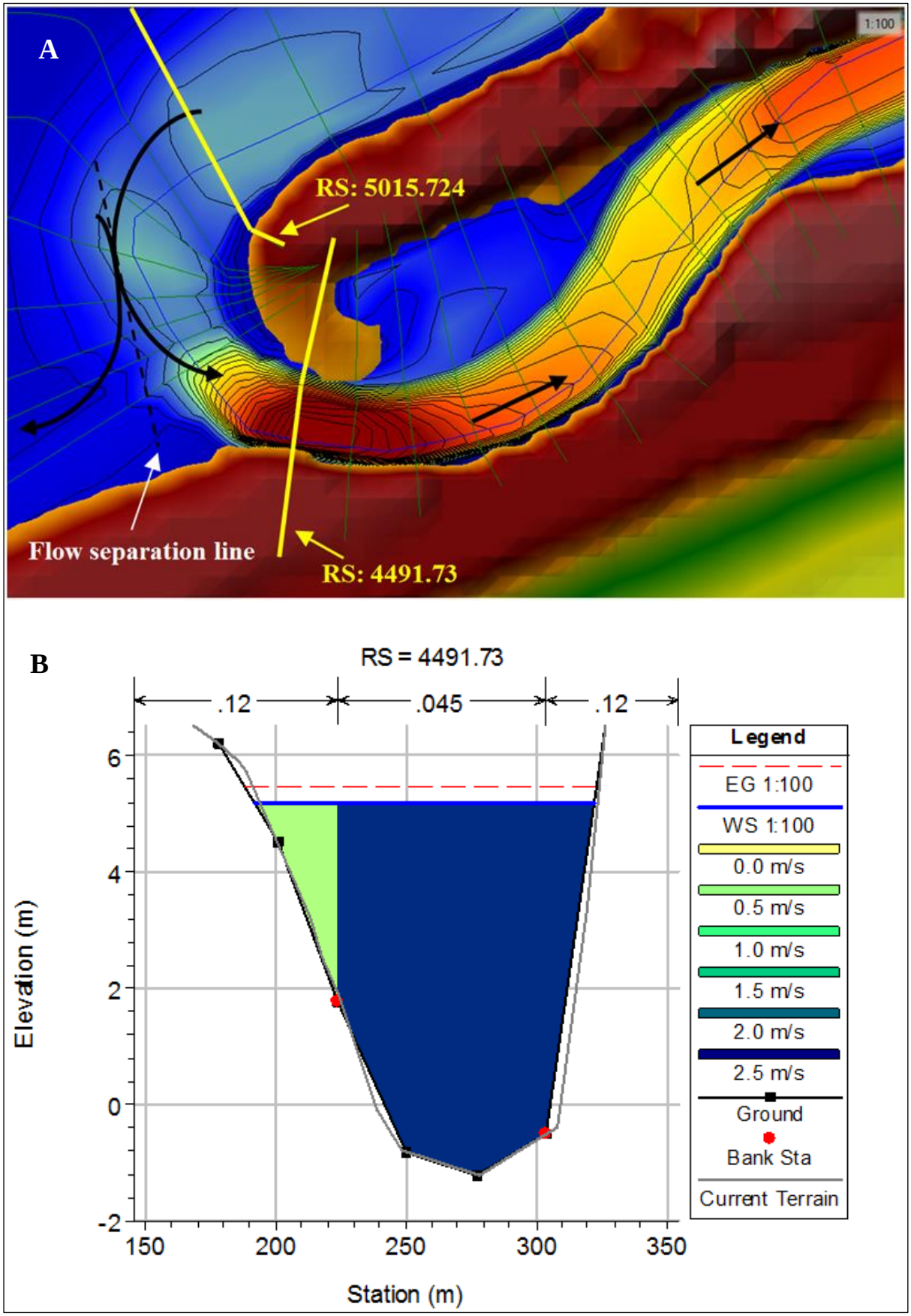

Figure 6.14: Inundation map (A) and cross-sectional velocity distribution profile (B) at the lower bend for Q_{100yrs} flood event

Table 6.1: Simulated and estimated depth-average peak flow velocity at selected river sections for Q_{50yrs} and Q_{100yrs} flood events

Location	Event	*Flow (m^3/s)	Velocity (m/s)	#Flow (m^3/s)	Velocity (m/s)	Prediction error	PBIAS (%)
N2 Bridge (10449.74)	Q_{50yrs}	522.46	0.65	767.36	0.82	-0.17	-26.2
	Q_{100yr}	930	0.87	1174.90	0.82	0.05	5.74
D/S of N2 Bridge (8439.04)	Q_{100yr}	930	1.51	1174.90	1.01	0.50	33.11
Railway Bridge (7595.656)	Q_{50yrs}	522.46	0.90	767.36	0.37	0.53	58.9
	Q_{100yr}	930	1.12	1174.90	0.34	0.31	69.6
D/S of Railway Bridge (7118.423)	Q_{100yr}	930	1.18	1174.90	0.34	0.84	71.2
Middle Estuary (5015.724)	Q_{100yr}	930	0.62	1174.90	0.23	0.39	62.9

***RMF: Slope Area Method** **# HEC-HMS model simulation**

6.6 Summary

The model identified critical areas where the flow velocity varied significantly along the channel. This played a vital role in fluvial and marine sediments distribution within the estuary. In the upper channel, the velocities were high due to steep terrains and constricted channels. The flow velocities were generally much lower due to flat landscapes, wider channels, and an expansive floodplain that holds more storage during medium to high flows downstream of the Railway Bridge. Figure 6.15 shows the depth-averaged flow velocity profile along the Mlalazi Estuary for Q_{2yr}, Q_{10yr}, Q_{20yr}, Q_{50yr}, and Q_{100yr} flood returns. The more significant fluvial events could cause flooding to occur for several days in the Mlalazi Estuary, giving enough time for fluvial sediments to settle on the floodplains. Table 6.2 shows the observed and simulated transient times for peak waves of various events in the estuary.

Table 6.2: Observed and simulated transient times from confluence to estuary mouth for the Q2yrs, Q50yrs and Q100yrs flood events

No.	Event	Measured travel time	Simulated travel time	Differences
1	Q_{2yrs}	1h20	2h00	40min
2	Q_{50yrs}	2h00	3h00	1h00
3	Q_{100yrs}	2h30	4h00	1h30

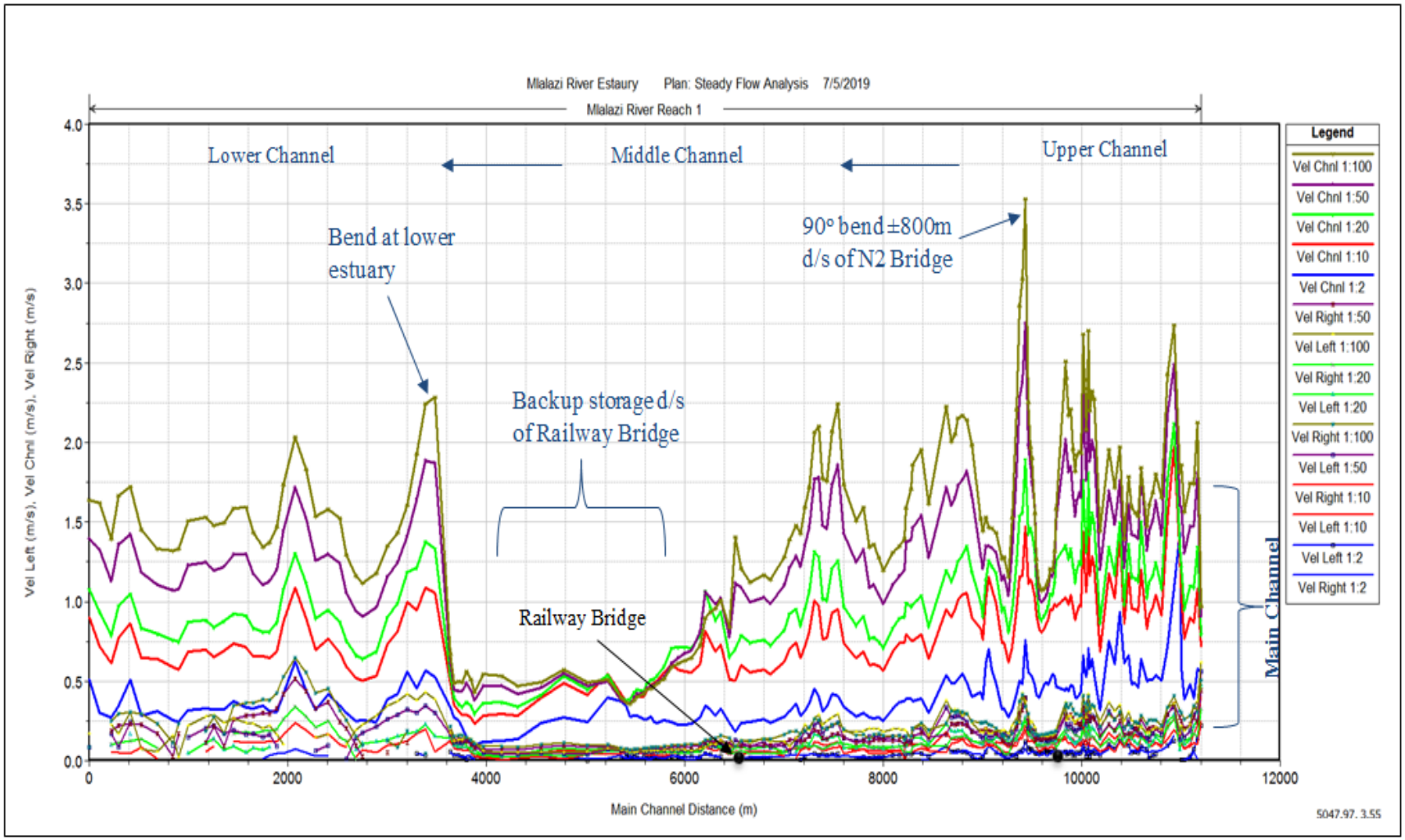

Figure 6.15: The flow velocity distribution profile along the main channel and floodplain of the Mlalazi Estuary for different storm sizes (Q_{2yrs}, Q_{10yrs}, Q_{20yrs}, Q_{50yrs} and Q_{100yrs})

CHAPTER 7. CONCLUSION AND RECOMMENDATIONS

7.1 General Conclusions

The key aim of this project was to derive estimates of the hydrodynamics and sediment transport within the Mlalazi Estuary that could influence the mouth dynamics that lead to open and closed states, using a suitable hydraulic (estuarine) model. To achieve this aim, the following objectives were addressed:

a) The conceptual flow and sediment model(s) were developed using various publications, fieldwork data (water level & tidal), and simulated flow/sediment data from the catchment model (Rasifudi 2019). The goal was to identify and establish the main features that significantly affect the hydrodynamic process of the Mlalazi Estuary and to populate the numeric model(s) parameters. The conceptual flow model identified the confluence as the upstream boundary and the estuary mouth as the downstream boundary. The sand berm at the mouth is conceptualised as a broad crest weir that varies in hydraulic characteristics due to marine and fluvial impacts on the sediment scour and deposition. The mouth closes occasionally, and it is frequently breached artificially as part of management interventions that have a direct influence on the marine dynamics. It frequently exists in a partially closed state that has not been well documented. Hence the actual marine contributions to the estuary dynamics are not sufficiently known to reliably establish the downstream boundary conditions. Consequently, this study focused on the fluvial contribution to the estuary hydrodynamics that need to be superimposed on the marine contributions.

b) The HEC-RAS estuarine model, which is the product of the US Army Corp of Engineers (USACE), was selected to route 1D steady and unsteady flow simulation of the Mlalazi Estuary floods.

c) The 1m Digital Elevation Model (DEM) and the main channel bathymetry data were used to set up and generate 174 river cross sections at different interval spaces (60m - 200m) from upstream channel to downstream channel of the Mlalazi Estuary. The channel bathymetric survey in the upper half of the channel was insufficient to

accurately capture the channel profile and would have introduced significant errors at strategic locations such as the bridges (Figure 7.1).

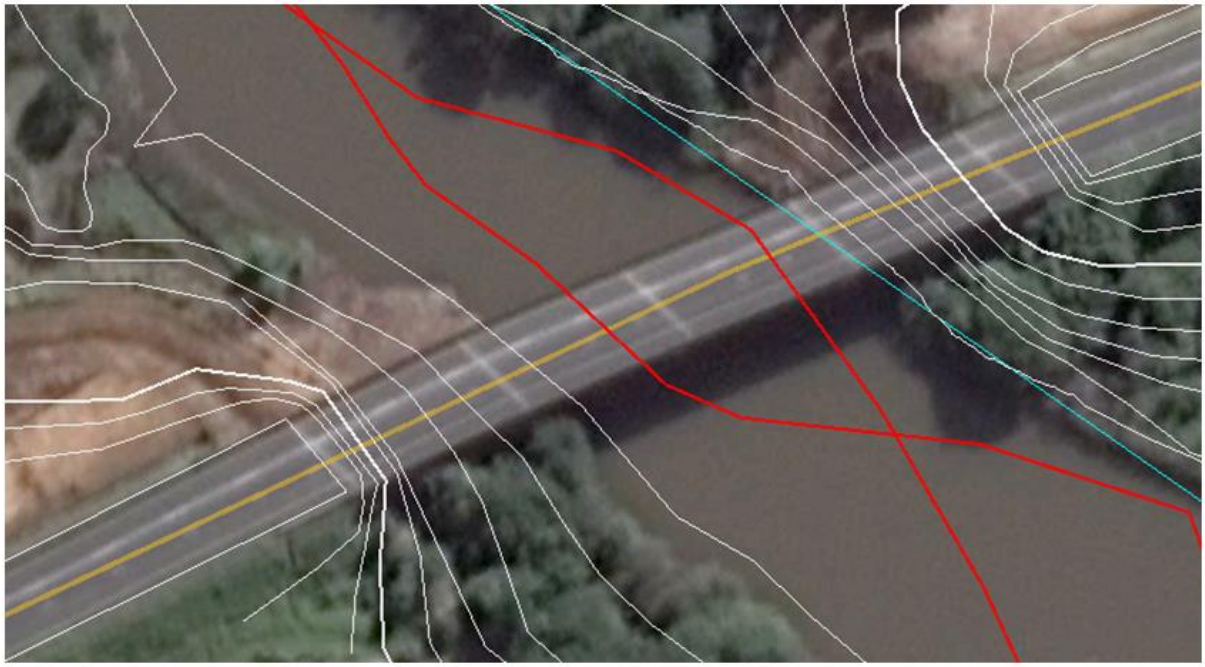

Figure 7.1: The path of the bathymetric survey (red lines) and derived elevation contours (white lines) used to specify the topography at the location of the N2 road bridge

d) The continuous flow and sediment data from the Mlalazi Catchment were obtained from the HEC-MHS model (Rasifudi, 2019) and were used as upstream boundary conditions. The historical water level data from the flood survey by Badenhorst *et al.* (1987) and flood events recorded using loggers from 2014 to 2018, were used to calibrate the steady and unsteady flow model. The Manning's roughness (n) coefficient was the main parameter used in the calibration of the flow model.

The steady flow simulation of Q_{2yrs} run-off event was underestimated by the model at the observed station within the middle and lower channels of the estuary. This was due to the fact that the HEC-RAS flow model did not consider the presence of the sand berm and the seepage of groundwater flow into the main channel. The effort was made to introduce the tidal data as a downstream boundary condition, using the tidal record from Richards Bay, but these did not

represent the estuary tidal regime correctly and the unsteady flow was unable to run due to model instabilities.

The HEC-RAS model slightly overestimated the spatial inundation area downstream of the Railway Bridge during the Q_{10yrs} flood event. It was observed that during this event the overland flow did not inundate the sugarcane fields but was quickly channelled into the artificial canals' networks. However, this was due to the fact that the DEM lacked detailed survey data of these drainage canal systems. It was also observed that the prawn farm and old sugarcane fields downstream of the Railway Bridge were partially flooded during the Q_{20yrs} simulated flood event, but it has been established that these were only flooded during larger events. The model also overestimated the spatial extent of flooding at these areas, which was primarily due to errors in the DEM. The hydraulic model was validated using the Imboa Cyclonic event, and the May 1971 and October 1999 flood events. The validation runs were very accurate, with all the strategic locations in the estuary showed results within 0.5 m of the observed measurements. The Percentage bias (*PBIAS*) performance was also very satisfactory since the values were within 10% with the observed data.

The model gave satisfactory performance predictors between the simulated and observed water level data during the simulation of the Q_{100yrs} flood event. This event was well calibrated using the 1987 flood survey data (Badenhorst *et al.,* 1989). The model highlighted critical areas within the Mlalazi Estuary where the flow velocity varies and plays a vital role in mobilising fluvial and marine sediments. During these flood events, the hydraulic model illustrated flow separation lines between the estuary channel and floodplains. The inundation maps show that in the upper channel the flow velocities in the main channel were high (< 1.0 m/s) whereas on the floodplains they were much lower (> 0.30 m/s), even during an extreme flood event. The deposition of fine-grained sediment particles (> 1- mm in diameter) took place on the floodplain and provided much needed fluvial nutrients. The model also indicated that only alluvial fine-grained sediment particles entered the Indian Ocean, as larger particles (< 1.0 mm in diameter) fell behind as the backup storage in the middle of the estuary.

7.2 Recommendations

A major challenge identified for this study was the lack of geometric data, especially in the upper channel bathymetry and in sections of the low-lying areas downstream of the Railway

Bridge. There was also a lack of suitable long-term continuous water level data within the estuary for calibrating and validating the model results. There is a need to strengthen the monitoring in the Mlalazi Catchment and Estuary, particularly for flow (water level and velocity), rainfall, groundwater and tides. The following recommendations for future research are highlighted in this project for improving the hydrodynamics information in the estuary:

a) For **Q_{2yrs} average run-off events** - the bathymetric data conducted by DWS (le Roux, 2018) should be expanded from the railway to the confluence and be incorporated into the current 1m DEM. This original bathymetric data was performed using the latest technology of Acoustic Doppler Profiler (ADP) with detailed cross sections and 3D river topography. The HEC-RAS model has the option to install or insert the lateral structure (broad crest weir) at the mouth which would act like a sand berm. The weir would confine the flow and enable the water stage in the estuary channel to rise to acceptable levels. The average condition could be improved by employing other numeric solutions such as MIKE11 that uses the Chezy's equation. The Chezy's coefficient roughness (n) will enable low flows to be calibrated to the acceptable level in contrast to Manning's coefficient roughness (n) which was created for medium to high flow situations. Groundwater seepage into the main estuary channel should be investigated numerically (e.g. MUDFLOW) for improving the simulation of average flow condition.

b) For **medium to high flow events** – the latest survey data for low-lying areas downstream of the Railway Bridge by Tembe (2018) should be incorporated into the DEM in order to improve the model simulation, especially during Q_{10yrs} and Q_{20yrs} year flood events. A full control survey of the drainage canals in the sugarcane fields should be done in order to improve the current DEM for the floodplains.

c) Data for **model calibration and validation** – flood surveys should be conducted after major flood events within the estuary by the DWS regional office since they have capacity and equipment. The DWS tidal station at the mouth should be revived in order to monitor long-term changes in the estuarine tides. The Ezemvelo logger should also be re-instated to monitor the water level fluctuation in the middle estuary channel. The DWS should also establish a permanent monitoring site in the upper channel (e.g. N2

Bridge) in order to provide river inflow data from the Mlalazi River where a rating curve or table is generated using the current meter gauging at different flow levels.

d) HRU should establish sediment sampling points in the estuary. Important samples for collection include bed samples for determination of its characteristics (texture, shape, cohesion, etc.), suspended water samples for determining the concentration of fine sediments and sediment layer thickness along the floodplain. Bed-load meters (Helley-Smith) equipment can be installed in the main channel for determining the sediment transport rates.

REFERENCES

Abbott, M. and Ionescu, F. (1967). On the numerical computation of nearly-horizontal flows. J. Hydraul. Res., 5, pp. 97-117.

Adams, J., Cowie M. and van Niekerk, L. (2016). Assessment of completed Ecological Water Requirement Studies for South African Estuaries and responses to changes in freshwater inflow. WRC Report no: KV 352/15, pp. 6-11.

Adamson, P.T. (1981). Southern African Storm Rainfall. Technical Report (TR) No. 102. Department of Water Affairs (DEA), Division of Hydrology.

Ackers, P. and White, W.R. (1973). Sediment transport: new approach and analysis. *Journal of Hydraulics Division, American Society of Civil Engineers*, Vol. 99, No. HY11, pp. 2040 - 2060.

Ambrose, R.B., Wool, T.A., and Martin. J.L. (1993). The Dynamic Estuary Model Hydrodynamics Program, DYNHYD5 Model Documentation and User Manual, U.S Environmental Protection Agency (USEPA), Georgia, USA.

Azarang, F. and Bajestan, M.S. (2015). Simulating the Erosion and Sedimentation of Karun Alluvial River in the Region of Ahvaz (Southwest of Iran). *American Journal of Engineering Research (AJER)*, Volume 4, pp. 233-245.

Badenhorst, P., Cooper, J.A.G., Crowther, J., Gonsalves, J., Grobler, N.A., Illenberger, W.K., Laubsher, W.I., Mason, Moller, J.P., Perry, J.E., Reddiering, J.S.V. and van der Mere (1989). Survey of September 1987 Natal Floods. Report No 164, FRD (CSIR) Pretoria. 105 – 110 pp.

Bate, G., Kelbe, B.E., and Taylor, R. (2016). Draft Final Report. Mgobeleni Linkages between Hydrological and Ecological Drivers. WRC Report No K5/2259/1/1, Water Research Commission, Pretoria, South Africa, pp 39.

Bathe, K.J. and Wilson, E. L. (1976). Numerical Methods in Finite Element Analysis. Prentice-Hall, Englewood Cliffs, New Jersey.

Beck, J.S., Theron. A.T., Kemp, A., Huisinga, P. and Basson, G.R. (2004). Hydraulics of Estuarine Sediment Dynamics in South Africa: Implications for Estuarine Reserve Determination and the Development of Management Guidelines. WRC Report No 1257/1/04. Water Research Commission, Pretoria, South Africa.

Beck, J.S. and Basson, G.R. (2008). Klein River Estuary (South Africa): 2D numerical modelling of estuary breaching. University of Stellenbosch, Stellenbosch, South Africa. Available on: *http://www.wrc.org.za*

Berger, R.C., Tate, J.N., Brown, G.L. and Savant, G. (2010). Adaptive Hydraulics User Manual, A Two-Dimensional Modeling System Developed by the Coastal and Hydraulics Laboratory, US Army Engineering Research and Development Centre. *http://chl.erdc.usace.army.mil* and *http://adh.usace.army.mil*.

Brito, D., Braunschweig, F. and Fernandes, L. (2016). MOHID Studio Quick Start Guide for MOHID Water. User Guide for setting up MOHID Water Projects with MOHID Studio Professional Edition.

Brunner, G.W. (2008). Calibration of Unsteady Flow Models. Presentation L-10(188-04)/May 2008/GWB.

Climate. Eshowe: Temperature, Climate Graph, Climate table for Eshowe, Climate-Data.Org

https:// en.climate-data.org/ location/12807/ and https:// www.windfinder.com/ windstatistics/ Richards Bay

Chikoore, H. (2005). Vegetation feedback on the boundary layer climate of Southern Africa. Msc Thesis, University of Zululand (UZ), KwaDlangezwa, KZN, South Africa.

Chow, V.T. (1959). Open Channel Hydraulics. PhD thesis in Hydraulics Engineering, University of Illinois.

Cooper, J.A.G. (2001). Geomorphological variability among microtidal estuaries from the wave-dominated South African coast, Geomorphology, Chapter 40, pp. 99-122.

Cooper, J.A.G. (2002). Coastal Zones and Estuaries: Anthropogenic Impact on Estuaries. School of Environmental Studies, University of Ulster, UK.

Deltares. (2014). Delft3D-Flow, Simulation of multi-dimensional hydrodynamic flows and transport phenomena, including sediments, User Manual, Version 3.15.34158, May 2014, 684 pp.

Danish Hydraulic Institute (DHI). (2013). MIKE 21 & MIKE 3 Flow Model FM. Hydrodynamic Module – Short Description.

Danish Hydraulic Institute (DHI). (2014). MIKE 11: River and Channel Modelling - Short Introduction - Tutorial, 44 - 46 pp.

Department of Water and Sanitation (DWS). (2014). Resource Directed Measures: Reserve determination study of selected surface water and groundwater resources in the Usutu/Mhlathuze Water Management Area. Pongola Floodplain – EWR Report _ Hydrodynamic Modelling. Report produced by Tlou Consulting (Pty) Ltd. Report no: RDM/WMA6/CON/COMP/1213.

Department of Water and Sanitation (DWS). (2015). Chief Directorate – Water Ecosystems: Reserve determination study of selected surface water and groundwater resources in the Usutu/Mhlathuze Water Management Area. Mlalazi Estuary Rapid Environmental Water Requirements Determination. Prepared by Tlou Consulting (Pty) Ltd and CRUZ Environmental. Report no: RDM/WMA6/CON/COMP/1313.

Department of Water and Saniattion (DWS). (2018). Hydrological Services. Viewed on 20th August 2018, http://www.dws.gov.za/Hydrology/.

Earle, S. (2015). Physical Geology Chapter 13.3: Stream Erosion and Deposition. https://courses.lumenlearning.com/physicalgeology/chapter/13-3-stream-erosion-and-deposition/

Engelbrecht, F. (2019). Green Book – Detailed Projections of Future Climate Change over South Africa. Technical report, Pretoria: CSIR.

EPA, (2000). Estuarine and Coastal Marine Waters: Bioassessment and Biocriteria Technical Guidance. United States Environmental Protection Agency.

Fleenor, W.E. and Jensen M.R. (2003). Evaluation of Numerical Models ... HEC-RAS and DHI-MIKE 11. *Journal of Hydraulic Engineering*.

Gupta, H.V., Sorooshian, S., and Yapo, P.O. (1999). Status of Automatic Calibration for Hydrologic Models: Comparison with Multilevel expert Calibration. *Journal of Hydrologic Engineering* 4(2), pp. 57 – 64.

Haghiabi, A.H. and Zaredehdasht, E. (2012). Evaluation of HEC-RAS Ability in Erosion and Sediment Transport Forecasting, Lorestan University and Islamic Azad University, Iran, pp. 1490 – 1497.

Hill, B.J. (1966). The Ecology of the Umlalazi Estuary. Department of Zoology, Rhodes University, Grahamstown, South Africa.

Hinwood, J.B. and McLean E.J. (2001) Monitoring and Modelling Tidal regime changes following Inlet Scour. *J. Coastal Research.* Special Publn. 34, 449-458.

Huizinga, P. and van Niekerk, L. (2005). Coastal Engineering Course. University Stellenbosch,

September 2005. Mouth dynamics and Hydrodynamics of Estuaries. Unpublished notes.

Hydrologic Engineering Centre (HEC). (2016). River Analysis System Hydraulic Reference Manual U.S. Army Corps of Engineers. Davis CA. Chapter 2: pp 2 – 21 and Chapter 3: pp 11 – 16. (*http://www.hec.usace.army.mil/software/*).

Hydrologic Engineering Centre (HEC). (2018). HEC-RAS Verification and Validation Tests. Chapter 3: One-Dimensional Unsteady Flow, pp 17 - 29. (*http://www.hec.usace.army.mil/software/*).

Kane, S., Sambou, S., Leye, I., Diedhiou, R., Tamba, S., Cisse, M.T., Ndione, D.M., and Sane, M.L. (2017). Modelling of Unsteady Flow through Junction in Rectangular Channels: Impact of Model Junction in the Downstream Channel Hydrograph. Computational Water, Energy and Environmental Engineering, 304-319 pp.

Kelbe, B.E. (1988) Features of westerly waves propagating over Southern Africa during summer. *Mon. Wea. Rev.*, Vol 116, 60-70

Kelbe, B.E., Snyman, N., and Germishuyse, T. (2002). The Development of a Hydrological Decision Support System for the Mhlathuze River Catchment Area in Kwazulu-Natal. WRC Project K5/906. Published on http://water.hru/uzulu.ac.za/dss

Kelbe, B.E., and Germishuyse, T. (2010). Groundwater/surface water relationships with specific references to Maputaland (WRC Report No 1168/1/10), Pretoria.

Kelbe, B.E. and Germishuyse, T. (2010). Surface and Groundwater Interaction with particular reference to the Maputaland Coastal Plain. WRC report K5/1168/10.

Kelbe, B.E. and Taylor, R.H. (2016). The development of a Bayesian Model of the ecosystem and mouth dynamics for Temporary Open/Closed Estuaries (TOCEs). WRC Proposal Number: 1004377, Hydrological Research Unit (HRU), University of Zululand, KwaDlangezwa, South Africa.

Kelbe, B.E., Taylor, R.H., Rasifudi, K.J., and Mmako, L.V., (2019). Mlalazi Estuary and Floodplain: Hydrology and Vegetation Dynamics. Hydrological Research Unit (HRU), University of Zululand, KwaDlangezwa, South Africa. WRC report K5/2541.

Kelbe, B.E. – pers comm.

Kovacs, Z.P., Du Plessis, D.B., Bracher, P.R., Dunn, P. and Mallory. G.C.L. (1985). Documentation of the 1984 Domoina Floods. Technical Report (TR) No. 122. Department of Water Affairs, Pretoria.

Kovacs, Z.P., (1988). Preliminary hydrological assessment of the Natal floods, Civil Engineer in South Africa, VOL 30(1), p. 7-13.

Kovacs, Z.P., (1988). Regional Maximum Floods Peaks in Southern Africa. Technical Report (TR) No. 137. Department of Water Affairs (DWA), RSA.

Leitão, P.C., Mateus, M., Braunschweig, F., Fernandes, L. and Neves, R. (2008). Modelling Coastal Systems: The MOHID Water Numerical Lab. Perspectives on Integrated Coastal Zone Management in South America.

Le Roux, F. (2018). Mlalazi Estuary Experimental Bathymetry Survey. Department of Water and Sanitation (DWS). 108pp

Loliyana, V.D. and Patel, P.L. (2012). Calibration and Performance of HEC-RAS Based Hydrodynamic Model for Stage Predictions in Lower Tapi River. Hydraulics and Water Resources (Hydro 2012), 1 - 11 pp.

Makungo, R., Nditítu, J. and Odiyo, J.O. (2010). Rainfall-run-off modelling approach for ungauged catchments: A case study of Nzhelele River sub-quaternary catchment. Physics and Chemistry of the Earth 35, 596 – 607 pp.

Masih, I., Maskey, S., Mussa, F.E. and Trambauer, P. (2014). A review of droughts on the African continent: Ageospatial and long-term perspective. Hydrology and Earth System Sciences 18 (*www.hydrol-earth-sys-sci.net/18/3635/2014/)*, 3635 – 3649 pp.

Mashriqui, H.S. (2003). Hydrodynamic and Sediment Transport Modeling of Deltaic Sediment Processes. Agricultural and Mechanical College, Louisiana State University, USA, Chapter 2 pp 14-16.

Mashriqui, H.S. (2010). Toward Modeling of River-Estuary-Ocean Interactions to Enhance Operational River Forecasting in the NOAA National Weather Service. 2nd Joint Federal Interagency Conference, Las Vegas (NV), USA.

May, D.R., Lopez, A. and Brown, L. (2000). "Validation of the Hydraulic-Open Channel Flow Model HEC-RAS with Observed Data," Department of Physics and Engineering, Fort Lewis College, Durango, CO.

McNally, W.H. and Mehta, A.J. (2006). Coastal Zones and Estuaries – Sediment Transport in Estuaries. EOLSS, USA. *http://www.eolss.net/Eolss-sampleAllChapter.aspx*

Meller, G., Hakkinen, S., Ezer, T. and Patchen, R. (2002). A Generalisation of a Sigma Coordinate Ocean Model and an Intercomparison of Model Vertical Grids. Ocean Foresting: Conceptual Basis and Applications, 55-72 pp.

Mensencal Y. (undated). Use of TELEMAC software system as a technical modelling tool for coastal zone development studies. SOGREAH Eau – Energie – Environnement, France.

Mkwananzi, N. (2003). Modelling Flood Inundation in the Mlazi River under Uncertainty. Master of Science in Engineering (MEng) thesis, University of Natal, Durban, South Africa.

Moriasi, D.N., Arnold, J.G., Van Liew, M.W., Bingner, R.L., Harmel, R.D. and Veith, T. (2007). Model evaluation guidelines for systematic quantifications. Transactions of the American Society of Agricultural and Biological Engineers 50 (3). 885 – 900 pp.

Ochiere, H.O., Onyando, J.O. and Kamau, D.N. (2015). Simulation of Sediment Transport in the Canal using the HEC-RAS (Hydrologic Engineering Centre – River Analysis System) in an Underground Canal in Southwest Kano Irrigation Scheme – Kenya. International Journal of Engineering Science Invention, Egerton University, Kenya.

Pameshwar, L.S., Steave, H.S., Scott, C.J., Philip, J.S., Macan, D., Clifford, E.F. and Carlie, T.T. (2014). Conceptual Site Model for Network Bay-Hydrodynamics and Sediment Transport. Journal of Marine Science and Engineering, CA, USA.

Pidwirny, M. (2006). "Erosion and Deposition". Fundamentals of Physical Geography, 2nd Edition. *http://www.physicalgeography.net/fundamentals/10w.htm*.

Pittaluga, M.B., Tambroni, N., Canestrelli, A., Slingerland, R., Lanzoni S. and Seminara, G. (2014). Where river and tide meet: The morhodynamic equilibrium al alluvial estuaries. *J.Gephys.Res..Earth Surf.* 120, 75-94. Doi: 10.1002/2014JF003233.

Prinos, P. (2016): Modelling coastal hydrodynamics. Available from *http://www.coastalwiki.org/wiki/*Modelling_coastal_hydrodynamics (accessed on 9-09-2016).

Putra, H.E., Putro, D.A., Hadi, T.W., Riawan, E., Junnaedhi, ID.G., Rojali A., Prasetyo, F.D., Pribadi, Y.S., Andarini, D.F., Khaerunisa, M. and Prakoswa, R.H. (2016). High Resolution Flood Hazard Mapping Using Two-Dimensional Hydrodynamics Model ANUGA: Case Study of Jakarta, Indonesia.

Rasifudi, K.J. (2019). Simulation of Catchment Run-off, Erosion and Sediment Transport using a Transient Numerical Model for Mlalazi Catchment. Msc. Thesis, University of Zululand (UZ), KwaDlangezwa, KZN, South Africa.

Rasifudi, K.J. – pers comm.

Roberts, S., Nielsen, O., Gray, D., Seaton, J. and Davies, G. (2015). ANUGA User Manual. Published by Australian National University and Geoscience Australia (ANUGA), Geoscience Australia. *anuga@ga.gov.au*

Schumann, E.H., Largier, J. and Slinger, J. (1999). Estuarine hydrodynamics. In Allanson BR and Baird D (eds.) *Estuaries of South Africa*, Cambridge University Press 289-321.

Schumann, E.H. (2003). Towards the Management of Marine Sedimentation in South African Estuaries with Special Reference to the Eastern Cape. WRC Report No. 1109/1/03. Water Research Commission, Pretoria, South Africa.

Schumann, E.H. (2013). Sea Level Variability in South Africa Estuaries. South African Journal of Science, http://sajs.co.za. Vol 109.

Sinha, P.C., Jena, G.K., Jain, I., Rao, A.D. and Husain, M.L. (2010). Numerical Modelling of Tidal Circulation and Sediment Transport in the Gulf of Khambhat and Narmada Estuary, West Coast of India, published by Pretanika J. Sc & Technol. Vol. 18 (2).

Sobey, R.J. (2001). Evaluation of Numerical Models of Flood and Tide Propagation in Channels. Journal of Hydraulic Engineering, ASCE, Vol. 127 No 10, pp 805-824.

Scott, S.H., Sharp, J.A., Gaurav, S., Johnson, C., and Ginter, D. (2012). Two Dimensional Hydrodynamic of the Moose Creek Floodway. US Army Engineering Research and Development Centre.

Soo, Chen-Lin., Ling, Teck-Yee. and Nyanti, Lee. (2018). Hydrodynamics Modeling of a Tropical Tidal River using the Dynamic Estuary Model (DYNHYD5): A Case Study in Sibu Laut River, Sarawak, Malaysia. https://www.hindawi.com/journals/mse/2018/8726752/

Steÿn, E.C., (2006). Basic Field Inspection of Gauging Stations: Hydrological Training Manual. Part 1: Flow Monitoring. Department of Water Affairs and Forestry (DWAF), Republic of South Africa (RSA).

Symonds, A.M., Vijverberg T. Post S., van der Spek B.J., Henrotte J. and Sokolewicz M. (2016). Comparison between MIKE21 FM, Delft3D and Delft3D FM Flow Models of Western Port Bay, Australia.

Tembe, S.S. (2018). Mapping the Mlalazi Floodplain section using DGPS. Hons Project, Department of Hydrology, University of Zululand.

Timbadiya, P.V., PremLal, Patel and Prakash, D. Porey (2011). "Calibration of HEC-RAS model on Prediction of Flood for Lower Tapi River, India." Journal of Water Resource and Protection, pp 805-811.

Taylor, R.H., (2017). Historical ecology: Insight into the past conditions and future trajectories of change in the Mlalazi Estuary. 2017 Symposium of Contemporary Conservation Practice, Fern Hill, Howich.

Taylor, R.H. – pers comm.

TELEMAC MODELLING SYSTEM (2000). Validation Document: TELEMAC-2D (2D hydrodynamics) Software (Version 5.0).

TELEMAC MODELLING SYSTEM (2014). User Manual: TELEMAC-2D (2D hydrodynamics) Software (Version 7.0). *www.telemacsystem.com*

Tetratech, Inc. (2007): The Environmental Fluid Dynamics Code Theory and Computation. Volume 1: Hydrodynamics and Mass Transport. Tetra Tech., Inc., Fairfax, Virginia.

Tetratech, Inc. (2007): The Environmental Fluid Dynamics Code User Manual USEPA Version 1.01. Tetra Tech., Inc., Fairfax, Virginia.

Torres-Bejarano, F., Padilla, J., Rodrĭguez-Cuevas. and Cantero, R. (2015). Hydrodynamics modelling utilising the EFDC Explorer model for the sustainable management of Canal del Dique-Guajaro hydrosystem, Colombia.

Turpie, J.K., Adams, J.B., Colloty, B.M., Joubert, A., Harrison, T.D., Maree, R.C., Taljaard, S., van Niekerk, L., Whitfield, A.K., Wooldridge, T.H., Lamberth, S.J., Taylor, R., Morant, P., Awad, A., Weston, B. and Mackay, H. (2002). Classification and Prioritization of South African estuaries on the basis of health and conservation priority

status for determination of the estuarine water reserve. Department of Water and Forestry, Pretoria.

Uzair, S. and Koran, J. (2017). Continuous Calibration. *Journal of Water Management Modelling* 25:C414.

Van Drie, V., Milevski P., and Simon M., (2016). Validation of a 2-D Hydrualic Model-ANUGA, to undertake Hydrologic Analysis.

Van Niekerk, L. (2005). Desktop assessment of the Wild Coast Estuaries: Sensitivity to Flow Reduction. CSIR Report ENV/S-C 2005-042.

Van Niekerk, L., Adams, J.B., James, N.C., Lamberth, S., MacKay, F., Rajkaran, A., Turpie, J., Weerts, S. and Whitfield, A.K. (2020). An estuary ecosystem classification that encompasses biogeography and a high diversity of types pin support of protection and management. African Journal of Aquatic Science 45. Pp 199 – 216.

Van Rijn, L.C. and Walstra, D.J.R. (2003). Modelling of Sand Transport in DELFT3D. RIKZ of Rijkwaterstaat and Delft Hydraulics, November 2003, 2-7 pp.

Webster, I.P., Ford, P.W., Robson, B.J., Margvelashvili, N. and Parslow, J. (2003). Conceptual Models of the hydrodynamics, fine sediments dynamics, biogeochemistry and primary production in the Fitzroy Estuary. Draft Final Report for Coastal CRC Project CM-2.

Whitfield, A., and Bate, G. (2007). A Review of Information of Temporarily Open/Closed Estuaries in the Warm and Cool Temperate Biogeographic Region of South Africa, with Particular Emphasis on the Influence of River Flow on these Systems. South African Institute for aquatic Biodiversity, Nelson Mandela Metropolitan University and University of KwaZulu-Natal. WRC Report No: 1581/1/07. Pp 6-18.

Whitfield, A.K., (1998). Biology and Ecology of Fishes in Southern African Estuaries. Ichthyological Monographs of the J.L.B. Smith Institute of Ichthyology No. 21-22.

Zhou, Z., Coc G., Jimenez, M., Olabarrieta M., van den Wegen, M. and Townsend, I. (2014) Morphodynamics of river-influenced back-barrier tidal basins: The role of landscape and hydrodynamic settings. *Water Resour. Res., 50*, doi:10.1002/2014/2014WR015891

Zungu, N.S. (2017). Phytosociology and Vegetation Ecology of Umlalazi Nature Reserve. Msc Thesis, University of Zululand (UZ), KwaDlangezwa, KZN, South Africa, pp 18-19.

APPENDIX

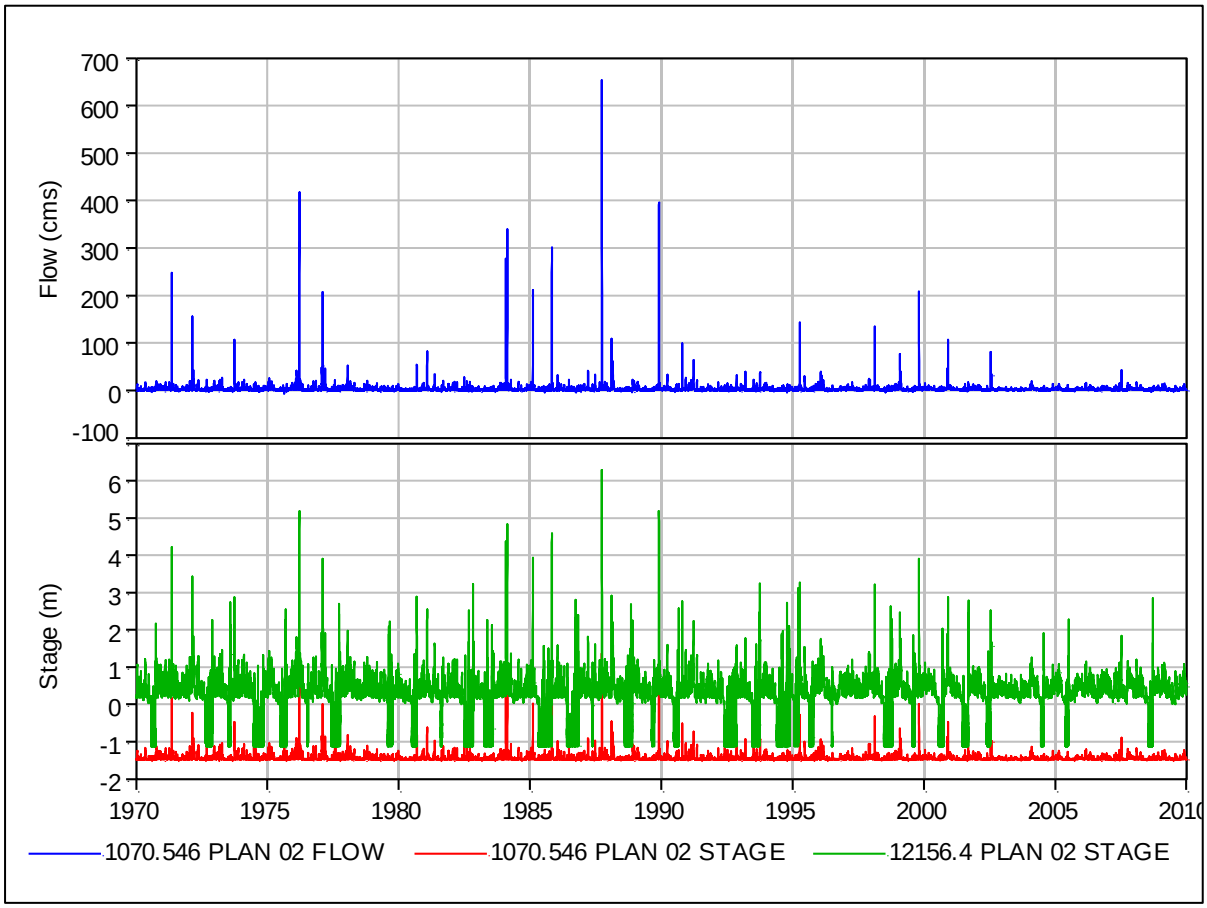

The simulated continuous flow (upper graph) and water level (lower graph) on the upper estuary (green line) and lower estuary (red line)

ANNEXURE C: CANDIDATE'S NOTICE OF INTENTION TO SUBMIT A DISSERTATION OR THESIS FOR EXAMINATION

The Head of Department
Department of Hydrology
Faculty of Science and Agriculture
University of Zululand

NOTICE OF INTENTION TO SUBMIT A MANUSCRIPT FOR EXAMINATION

I hereby give notice that I aim to submit my dissertation/ thesis for examination. I undertake to inform the University immediately in the event of a delay in submitting the manuscript by the date stipulated above.

Full Names and Surname	**Lesiba Vincent Mmako**
Student Number	**200959289**
Intended date of submission	**30 September 2021**
Degree	**Master of Science (Msc) in Hydrology**
Name of Supervisor	**Mr B.K. Rawlins**
Supervisor e-mail address	RawlinsB@unizulu.ac.za or bkrawlins@gmail.com
Name of Co-supervisor	**Prof B.E. Kelbe and Prof J.J. Simonis**
Co-supervisor e-mail address	bekelbe@gmail.com and simonismtz@yahoo.com
Title of dissertation/thesis	**The Flow and Sediment Dynamics of the Mlalazi Estuary in Kwa-Zulu Natal, South Africa**
Candidate's signature	
Date	**03 September 2021**

UNIVERSITY OF ZULULAND
RESEARCH ETHICS COMMITTEE
(Reg No: UZREC 171110-030)

RESEARCH & INNOVATION
Website: http://www.unizulu.ac.za
Private Bag X1001
KwaDlangezwa 3886
Tel: 035 902 6273
Email: MangeleS@unizulu.ac.za

ETHICAL CLEARANCE CERTIFICATE

Certificate Number	**UZREC 171110-030 PGM 2021/202**							
Project Title	**FLOW AND SEDIMENT DYNAMICS OF MLALAZI ESTUARY IN KWA-ZULU NATAL OF SOUTH AFRICA**							
Principal Researcher/ Investigator	L.V Mmako							
Supervisor and Co-supervisor	Mr B.K Rawlins		Prof B.E Kelbe					
Department	Hydrology							
Faculty	Science and Agriculture							
Type of Risk	Low Risk- Desktop, field work or laboratory							
Nature of Project	Honours/4th Year		**Master's**	x	Doctoral		Departmental	

The University of Zululand's Research Ethics Committee (UZREC) hereby gives ethical approval in respect of the undertakings contained in the above-mentioned project. The Researcher may therefore commence with data collection as from the date of this Certificate, using the certificate number indicated above.

SPECIAL CONDITIONS: **(1) This certificate is valid for 1 year from the date of issue.**
(2) Principal researcher must provide an annual report to the UZREC in the prescribed format [due date- 28 January 2023]
(3) The UZREC must be informed immediately of any material change in the conditions or undertakings mentioned in the documents that were presented to the meeting.
(4) Under the Protection of Personal Information Act, 04 of 2013 ("POPIA"), researchers have a general legal duty to protect information they process. They must ensure the security and protection of any personal information processed through the research and provide a compliant and consistent approach to data protection. The information collected via interviews must be for research purposes only. No personal information such as opinions, views and academic background may be linked to the respondents' identity or shared with anyone for marketing purposes or otherwise.

The UZREC wishes the researcher well in conducting research.

Prof. Nokuthula Kunene
Chairperson: University Research Ethics Committee
Deputy Vice-Chancellor: Research & Innovation
28 January 2022

STAMP

UNIVERSITY OF ZULULAND
RESEARCH ETHICS COMMITTEE
(Reg No: UZREC 171110-030)

RESEARCH & INNOVATION
Website: http://www.unizulu.ac.za
Private Bag X1001
KwaDlangezwa 3886
Tel: 035 902 6324/6374
Email: MangeleS@unizulu.ac.za/
MkwanaziMM@unizulu.ac.za

PROVISIONAL APPROVAL - ETHICAL CLEARANCE CERTIFICATE

Certificate Number	**UZREC 171110-030 PGM 2021/202**							
Project Title	**FLOW AND SEDIMENT DYNAMICS OF MLALAZI ESTUARY IN KWA-ZULU NATAL OF SOUTH AFRICA**							
Principal Researcher/ Investigator	L.V Mmako							
Supervisor and Co-supervisor	Mr B.K Rawlins		Prof B.E Kelbe					
Department	Hydrology							
Faculty	Science and Agriculture							
Type of Risk	Low Risk – Desktop, field work or laboratory							
Nature of Project	Honours/4th Year		**Master's**	x	Doctoral		Departmental	

The University of Zululand's Research Ethics Committee (UZREC) hereby grants provisional approval pending gatekeeper/permission letter from the following institution(s):

a) **Mlalazi Nature Reserve - Ezemvelo KZN Wildlife**

The Researcher may therefore NOT commence with data collection until gatekeeper/permission letter is obtained. The letter can be sent to MangeleS@unizulu.ac.za or MkwanaziMM@unizulu.ac.za so that final approval letter will be issued for data collection to commence.

SPECIAL CONDITIONS: **(1) Principal researcher must provide gatekeeper/permission letter of where the research will be conducted and submit to UZREC to acquire full approval certificate of 1- year.**

The UZREC wishes the researcher well in conducting research.

Prof. Nokuthula Kunene
Chairperson: University Research Ethics Committee
Deputy Vice-Chancellor: Research & Innovation
15 November 2021

CHAIRPERSON
UNIVERSITY OF ZULULAND RESEARCH
ETHICS COMMITTEE (UZREC)
REG NO: UZREC 171110-30

RESEARCH & INNOVATION OFFICE